KUOPION YLIOPISTON JULKAISUJA C. LUONNONTIETEET JA YMPÄRISTÖTIETEET 193
KUOPIO UNIVERSITY PUBLICATIONS C. NATURAL AND ENVIRONMENTAL SCIENCES 193

FERDINAND MOLNÁR

Structural Analysis of the Ligand-binding Domains of Human and Mouse CAR, Human VDR and Human PPARs

Doctoral dissertation

To be presented by permission of the Faculty of Natural and Environmental Sciences of the University of Kuopio for public examination in Auditorium L21, Snellmania building, University of Kuopio, on Saturday 4th March 2006, at 12 noon

Department of Biochemistry
University of Kuopio

KUOPION YLIOPISTO
KUOPIO 2006

Distributor:
Kuopio University Library
P.O. Box 1627
FI-70211 KUOPIO
FINLAND
Tel. +358 17 163 430
Fax +358 17 163 410
http://www.uku.fi/kirjasto/julkaisutoiminta/julkmyyn.html

Series Editors:
Professor Pertti Pasanen, Ph.D.
Department of Environmental Sciences

Professor Jari Kaipio, Ph.D.
Department of Applied Physics

Author's address:
Department of Biochemistry
University of Kuopio
FI-70211 KUOPIO
FINLAND
Tel. +358 17 163 392
E-mail: molnar@uku.fi

Supervisors:
Professor Carsten Carlberg, Ph.D.
Department of Biochemistry
University of Kuopio

Paavo Honkakoski, Ph.D.
Department of Pharmacology
University of Kuopio

Professor Pekka Mäenpää, M.D.
Department of Biochemistry
University of Kuopio

Reviewers:
Assistant Professor Sander Kersten, Ph.D.
Nutrition, Metabolism and Genomics Group
Division of Human Nutrition Wageningen University
Wageningen, The Netherlands

Tommi Nyrönen, Ph.D.
Center for Scientific Computing
Espoo, Finland

Opponent:
Professor Kalervo Hiltunen, M.D.
Department of Biochemistry
University of Oulu

ISBN 951-27-0351-3
ISBN 951-27-0445-5 (PDF)
ISSN 1235-0486

Kopijyvä
Kuopio 2006
Finland

Molnár, Ferdinand. Structural analysis of the ligand-binding domains of human and mouse CAR, human VDR and human PPARs. Kuopio University Publications C. Natural and Environmental Sciences 193. 2006. 115 p.
ISBN 951-27-0351-3
ISBN 951-27-0446-3 (PDF)
ISSN 1235-0486

Abstract

Nuclear receptors (NRs) form a large family of transcription factors (48 human members) and have critical roles in nearly all aspects of vertebrate development and adult physiology by transducing the effects of small, lipophilic compounds into transcriptional response. The ligand-binding domains (LBDs) of most NRs consist of 11 to 13 α-helices that form a characteristic, 3-layer anti-parallel α-helical sandwich. Adopted orphan NRs such as constitutive androstane receptor (CAR), peroxisome proliferator-activated receptors (PPARs) and the classical endocrine receptor for vitamin D (VDR) show distinct functional, biochemical and physiological properties originating from their protein structures.

The main objective of the present study was to gain more insight into the structure-function relationship of PPARs, CAR and VDR using molecular dynamics simulations and structural analysis as tools. The results confirmed that although these receptors show high amino acid and spatial conservation in their LBDs they display major differences in the ligand recognition, in the affinity for coactivators and corepressor and in the LBD dynamics, which lead to conformational changes resulting in activation or inactivation of the receptor. All of the above mentioned processes are tightly connected with the dynamics of the most C-terminal helix of the LBD, called helix 12.

CAR and PPARs are of additional interest since they display exceptionally high constitutive activity, which originates in the ligand-independent CoA interaction. The data of the presented studies show that the molecular mechanism of this function is an intra- and extramolecular stabilization of the helix 12 via residues in helices 3, 4-5 and 11. In the case of PPARs there are at least four groups of amino acids to stabilize the helix 12. Some of the interactions are evolutionary conserved between both receptors. These findings suggest that the modulation of activity of these receptors is possible not only by increasing their activity using receptor specific agonists but also by lowering it via inverse agonists.

In conclusion, the studies presented in this doctoral thesis increased our knowledge on the structure-function relationship of NRs and provided detailed perception for understanding the molecular basis of ligand-recognition, cofactor interaction of the NRs and dynamic properties of activation and inactivation of these receptors.

Universal Decimal Classification: 577.112, 577.122, 577.214
National Library of Medicine Classification: QU 475, QU 34, QU 55

Medical Subject Headings: transcription factors; nuclear proteins; receptors, cytoplasmic and nuclear; peroxisome proliferator-activated receptors; receptors, calcitriol; ligands; binding sites; molecular structure; molecular conformation; computer simulation; structure-activity relationship

Édesanyámnak és édesapámnak

Acknowledgements

I would like to express my thanks to all people who supported me professionally or spiritually during the last years, helped me to achieve this milestone in my life and create this thesis.

This research was supported by funding from the Academy of Finland and National Technology Agency of Finland (TEKES).

I acknowledge the University of Kuopio and the Department of Biochemistry for the friendly and creative environment where it is a pleasure to work and study.

I am grateful to my principal supervisor Prof. Carsten Carlberg for his help and advice during these years. I am thankful for his excellent professional guidance, expedient discussions, and for providing an excellent working surrounding to accomplish my doctoral studies.

I acknowledge my second and third supervisor Dr. Paavo Honkakoski and Prof. Pekka Mäenpää who have greatly contributed towards shaping this thesis.

I thank Assistant Professor Sander Kersten and Dr. Tommi Nyrönen, the official reviewers of this thesis, for their critical and constructive comments.

Special thank goes to Tom for his suggestions and also language revision to improve the quality of this thesis.

I would like to express my appreciation to Drs. Moras, Wilson and Xu for "structural inspirations".

I would like to thank Taru, Liisa, Marjatta and Maija at the Department of Biochemistry for having been kind enough to advise and help me with administrative and technical issues during my doctoral studies.

I greatly appreciate all the former and present lab members Petra, Teemu, Marc, Manuel, Claire, Harri L., Harri M., Lasse, Christian, Sabine, Sami, Tom, Marjo, Anna,

Katri, Merja, Maija, Tatjana, Taru, Tiina and Mikko who created a very pleasant, friendly and productive environment.

I owe many thanks to my co-authors. Especially I wish to thank Mikael for great discussions and his interest in my work.

I would like to express my special thanks to my foreign family Nektaria, Boryana, Vlad, Quoc, Iain, Silvia, Jelena, Kostiq, Laura, Irina, Tatjana, Sabine, and others for all the mökki-weekends and parties we had together.

I would like to express my sincere thanks to my closest friends Manuel, Christian, Sami, Tom, Šárka, Jakub, Anička, Kaja and others who stood behind me from the first moment when I arrived to Finland and helped me to create my second home.

I wish to express my sincere gratitude to Martin and Mária who were my second family in Finland.

I wish to express my warmest thanks to András, Katalin, Olívia, Szabolcs and Csilla who were during these years my Hungarian family in Finland.

Last but not least I would like to dedicate this thesis to my family, my mom, dad and Ursi for their endless love and patience, understanding, multifarious support and for allowing me to spend most of my time on this thesis.

Kuopio, February 2006

Ferdinand Molnár

Abbreviations

$1\alpha,25(OH)_2D_3$	$1\alpha,25$-dihydroxyvitamin D_3
AF-1	activation function 1
AF-2	activation function 2
Androstanol	5α-androstane-3α-ol and 5β-pregnane-3,20dione
ANF	atrial natriuretic factor
AR	androgen receptor
CAR	constitutive androstane receptor
CPTI	carnitine palmitoyl transferase I
CITCO	6-(4-chlorophenyl)imidazo[2,1-b][1,3]thiazole-5-carbaldehyde-O-3,4-dichlorobenzyl) oxime
CoA	coactivator
CoR	corepressor
CYP	cytochrome P450
DMSO	dimethylsulfoxide
DBD	DNA-binding domain
DOTAP	N-[1-(2,3-dioleoyloxy)propyl]-N,N,N-trimethylammonium methylsulfate
DMEM	Dulbecco's Modified Eagle Medium
DR	direct repeat
DTT	dithiothreitol
EDTA	ethylenediaminetetraacetic acid
EMSA	electrophoretic mobility shift assay
ER	estrogen receptor
ERR	estrogen-related receptor
Gemini	21-(3-OH-methyl-butyl)-$1\alpha,25(OH)_2D_3$
GR	glucocorticoid receptor
GST	glutathione S-transferase
GW409544	2-(1-methyl-3-oxo-3-phenyl-propylamino)-3- (4-(2-(5-methyl-2-phenyl-pxazol-4-yl)-ethoxy)-phenyl)-propionic acid
GW501516	2-Methyl-4-((4-methyl-2-(4-trifluoromethylphenyl)-1,3-thiazol-5-yl)-methylsulfanyl)phenoxy-acetic acid
GW6471	N-((2S)-2-(((1Z)-1-methyl-3-oxo-3-[4-(trifluoromethyl) phenyl]prop-1-enyl)amino)-3-(4-[2-(5-methyl-2-phenyl- 1,3-oxazol-4-yl)ethoxy]phenyl)propyl)propanamide
FXR	farnesoid X receptor
h	hour
HAT	hiistone acetyltransferase
HEK293	human epithelial kidney cell line
HaCaT	human immortalized keratinocytes
HEPES	4-(2-hydroxyethyl)-1-piperazineethanesulfonic acid
HNF-4	hepatocyte nuclear factor 4
L783483	[3-chloro-4-[3-[7-propyl-3-(trifluoromethylenzo[d]isoxazol-6-yloxy]propylsulfonyl]phenyl]-acetic acid
LBD	ligand-binding domain
LRH-1	liver receptor homolog 1

LXR	liver X receptor
MC1288	20-epi-1α,25$(OH)_2D_3$
MCF-7	human breast cancer cell line
MD	molecular dynamics
min	minute
MR	mineralocorticoid receptor
NCoR	NR corepressor
NF-1	nuclear factor-1
MG-63	human osteosarcoma cell line
NR	nuclear receptor
Nurr-1	Nur-related factor 1
PB	phenobarbital
PBREM	phenobarbital responsive enhancer module
PPAR	peroxisome proliferator-activated receptor
PR	progesterone receptor
PXR	pregnane X receptor
RAC3	receptor-associated coactivator 3
RAR	retinoic acid receptor
RE	response element
REK	rat epidermal keratinocytes
RID	receptor interaction domain
ROR	retinoid orphan receptor
Ro43-83582	21-(3-OH-methyl-butyl)-23-yne-26,27-F_6-1α,25$(OH)_2D_3$
Ros17/2.8	rat osteosarcoma cell line
Rosiglitazone	5-[4-[(*N*-methyl-*N*-(2-pyridyl)amino)ethoxy]benzyl]thiazolidine-2,4-dione
RXR	retinoid X receptor
RMSD	root-mean-square deviation
s	second
SDS	sodium dodecyl sulphate
SF-1	steroidogenic factor 1
SOMs	self-organizing maps
SRC-1	steroid receptor coactivator 1
SULT	sulfotransferase
TCPOBOP	1,4-bis[2-(3,5-dichloropyridyloxy)]benzene
TIF2	transcription intermediary factor 2
TR	thyroid receptor
Tris	Tris Hydroxymethylaminoethane
TSS	transcription start site
UGT1A1	UDP-glucuronosyltransferase 1 A1
VAST	vector alignment search tool
VDR	1α,25$(OH)_2D_3$ receptor
VDRE	VDR response element
WY14643	[4-chloro-6-(2,3-dimethylphenylamino)pyrimidin-2-ylsulfanyl] acetic acid

List of original publications

This dissertation is based on the following publications referred to in the text by their Roman numerals (**I-V**):

I. Frank C., Molnár F., Matilainen M., Lempiäinen H. and Carlberg C. Agonist-dependent and -independent transactivation of the human constitutive androstane receptor are modulated by specific amino acid pairs (2004) *Journal of Biological Chemistry* 279: 33558-33566

II. Peräkylä M.*, Molnár F*. and Carlberg C. Structural basis for the species-specific antagonism of 26,23-lactones on vitamin D signaling (2004) *Chemistry & Biology* 11: 1147-1156

III. Molnár F., Matilainen M., and Carlberg C. Structural determinants of the agonist-independent association of human peroxisome proliferator-activated receptors with coactivators (2005) *Journal of Biological Chemistry* 280: 26543-26556

IV. Lempiäinen H., Molnár F., Macias Gonzalez M., Peräkylä M. and Carlberg C. Antagonist- and inverse agonist-driven interactions of the vitamin D receptor and the constitutive androstane receptor with co-repressor protein. (2005) *Molecular Endocrinology* 19: 2258-2272

V. Molnár F., Peräkylä M. and Carlberg C. Vitamin D receptor agonists specifically modulate the volume of the ligand-binding pocket (2006) *Journal of Biological Chemistry, in press*

* equally contributed

Table of contents

Abstract **5**
Acknowledgements **9**
Abbreviations **11**
List of original publications **13**
1 Introduction **17**
2 Review of Literature **19**
2.1 The NR superfamily 19
2.1.1 Classification of the NRs 20
2.1.2 Three-dimensional and functional organization of the NRs 22
2.1.2.1 Activation function-1 domain 23
2.1.2.2 DNA-binding domain 23
2.1.2.3 Hinge region 23
2.1.2.4 Ligand-binding domain 24
2.1.2.5 Helix 12 (AF-2 domain) 25
2.1.2.6 Ligand-binding pocket 25
2.2 CAR 26
2.2.1 3D-protein structure of the human and mouse CAR LBDs 26
2.2.2 Physiological role of the CAR 29
2.3 PPARs 30
2.3.1 3D-protein structure of the PPAR LBDs 30
2.3.2 Physiological roles of the PPARs 33
2.4 VDR 34
2.4.1 3D-protein structure of the VDR LBD 34
2.4.2 The physiological role of the VDR 37
2.5 Cofactors 37
2.5.1 CoAs 37
2.5.1.1 The SRC family of NR CoAs 38
2.5.1.1.1 SRC-1 38
2.5.1.1.2 TIF-2 38
2.5.1.1.3 RAC3 38
2.5.1.2 Functional domains and the LXXLL motif of the SRC CoA family 40
2.5.2 CoRs 41
2.5.2.1 The role of CoRs in transcription repression 43
2.6 The activation and inactivation of NRs from a structural perspective 43
2.6.1 Active and inactive conformations of human PPARα 43
2.6.2 Active and inactive conformations of mouse CAR 45
2.6.3 NR ligand classification 45
2.6.4 NR ligand classification 47

3 Aims of the Study 49

4 Materials and Methods 51

4.1 NR ligands 51

4.2 DNA constructs 52

4.2.1 Mammalian expression constructs for full-length NRs and cofactors 52

4.2.2 GST-fusion protein overexpressing constructs 52

4.2.3 Reporter gene constructs 52

4.3 Mutagenesis 54

4.3.1 Site-directed mutagenesis 54

4.3.2 Generation of helix 12 deletion mutants 54

4.3.3 Helix 12 extension NR mutants 54

4.4 Manual sequencing 56

4.5 *In vitro* transcription and translation 57

4.5.1 One-step *in vitro* translation 57

4.5.2 Two-step *in vitro* translation 57

4.6 Bacterial overexpression and purification of GST-fusion proteins 58

4.7 Limited protease digestion assay (LPD) 59

4.7.1 LPD of the VDR 59

4.7.2 LPD of the PPARs and CAR 59

4.8 Gel shift and supershift assays (EMSA) 59

4.9 Cellular transfection and *luciferase* reporter gene assay 60

4.10 *In silico* methods 60

4.10.1 Structural analysis and visualizations of the protein structures 60

4.10.2 Ligand-binding pocket volume calculations 60

4.10.3 Clustering of the amino acids using self-organizing maps (SOMs) 61

4.10.4 Visualization of the clustered SOMs using Sammon's mapping 61

5 Results 63

5.1 Mechanism of the constitutive activity in human and mouse CAR and human PPARs (I and III) 63

5.1.1 Constitutive activity of NRs 63

5.1.2 Ligand-independent association of CAR with p160 CoAs 63

5.1.3 Impact of helix 12 on the CoA recruitment of human CAR and VDR 64

5.1.4 Stabilization of helix 12 in human CAR, mouse CAR and human VDR 65

5.1.5 Ligand-independent association of human PPARs with p160 CoAs 66

5.1.6 Structural basis of the constitutive activity of human PPARs 67

5.2 A structural basis for the species-specific antagonism of 26,23-lactones on vitamin D signaling (II) 68

5.2.1 Molecular determinants of species-specific antagonism 69

5.3 Antagonist- and inverse-agonist triggered conformational changes in the LBD of human VDR, human and mouse CAR (IV) 71

5.3.1 Ligand-dependent interactions of VDR and CAR with CoAs and CoRs 71

5.3.2 Molecular basis of the VDR and CAR association with CoR 73

5.4 Molecular basis of the agonists-induced selective modulation of the ligand-binding pocket volume in human VDR (V) 74

5.4.1 Selective modulation of the ligand-binding pocket's volume by VDR agonists 74

5.4.2 Dynamics of the selective amino acids in the ligand-binding pocket 75
5.4.3 Agonist-selective rearrangement of the hydrophobic residues in helices 6 and 7 and the loop between them 76

6 Discussion 79

6.1 Mechanism of the constitutive activity in human and mouse CAR and human PPARs (I and III) 79
6.1.1 Constitutive activity of NRs 79
6.1.2 Mechanism of the constitutive activity in human and mouse CAR 80
6.1.3 Structural basis of the constitutive activity of human PPARs 81
6.1.4 Molecular mechanism of ligand-independent stabilization of the helix 12 in human PPARs 82

6.2 A structural basis for the species-specific antagonism of 26,23-lactone analogs on vitamin D signaling (II) 83
6.2.1 Species-specific affinity of the ligands 83
6.2.2 Molecular mechanisms for the species-specific differential profiles of ligands 83

6.3 Antagonist- and inverse-agonist triggered conformational changes in the LBD of human VDR, human and mouse CAR (IV) 84
6.3.1 Unified classification of antagonists and inverse agonists 84
6.3.2 Why is it difficult to classify ligands? 85
6.3.3 The mechanism of ligand antagonism or inverse agonism 85
6.3.4 Similarities in the interactions of CoAs and CoRs with NRs 86
6.3.5 A model for the fixed helix 12 by a CoR RID 86

6.4 Molecular basis for the agonist-induced selective modulation of the ligand-binding pocket volume in the human VDR (V) 87
6.4.1 Molecular mechanism of MC1288-induced conformational changes 87
6.4.2 Molecular mechanism of Gemini- and Ro43-83582-induced conformational changes in the LBD 88
6.4.3 Selective modulation of the ligand-binding pocket volume 88
6.4.4 Ligand-binding pocket volume calculations 89
6.4.5 Energy transmission in the LBD of NRs 89

7 Summary and Conclusions 91

8 Future Aspects 95

References 97

Appendix: Original publications

"It is those who get lost, who find the new ways."
Nils Kjaer (1870-1924)
Norwegian writer

Chapter 1

Introduction

During evolution most biological systems have had a tendency to increase their complexity. This trend also applies for the molecular processes occurring in cells such as replication, transcription and translation. They demand a strict level of organization and regulation since they involve multifunctional complexes and huge protein machineries.

One of the mentioned processes, transcription, requires such multitasking regulatory complexes containing rather diverse selection of nucleic acids and proteins with highly specific but distinguished functions. These complexes contain, amongst others, transcription factors, coregulators, and proteins with specific enzymatic activities, which makes their exploration and investigation challenging.

Luckily, modern study approaches gave rise to the research fields that try to answer the questions concerning the detailed molecular understanding of these processes by looking at a limited number of components at one time. One of the fields, structural biology, includes tools such as structural analyses that are useful in answering these questions.

Structural analysis is an approach trying to connect three dimensional protein structures with the function of the proteins. Usually certain amino acids are responsible for distinct functions in a protein such as catalytic activity, ligand binding, DNA binding and dimerization. Looking on the one or the other function separately can create very simple model with biased views. For example, certain amino acids are directly involved in the catalytic activity of the protein and they are essential for it. However, if we try to look at these processes in parallel the picture gains in its complexity and the dynamic sequence of actions can be recognized. As a direct example of this kind of continuity of causes is the binding of the ligand in the ligand-binding pocket of a receptor that induces conformational changes altering protein interactions on the surface of the protein. Exploration of these continual dynamic changes is a very difficult task since there is limited number of methods,

which can be used to observe proteins in their native environment and consequently measure the dynamic changes of their functional properties.

Most of the available techniques allow the measurement of functionality of a protein at a certain time point, which makes the obtained data more characteristic for the static state of the molecule at the beginning of the experiment. At the intersection of these two technical approaches are the *in silico* methods where molecular dynamics (MD) simulations play a very important role. These allow for a more dynamic view of processes and are very important tools in the investigation of the series of actions such as the impact of conformational changes on protein-protein interactions.

This thesis extends the research on the molecular mechanism of the transcription regulation via nuclear receptors (NRs) using structural analysis and MD simulations.

Chapter 2

Review of Literature

The NR family has the largest number of members of any class of transcription factors. The completion of the Human Genome Project allowed the definition of the complete functional set of 48 NR genes [Robinson-Rechavi *et al.*, 2001]. In contrast, in the genome of *D. melanogaster* there have been identified 21 NRs [Adams *et al.*, 2000], whereas in the nematode *C. elegans* their number is more than 270 [Sluder *et al.*, 2001]. Below will be discussed the present knowledge of the molecular biology of this class of proteins as well as cofactors, which have been found to interact with them.

2.1 The NR superfamily

NRs are characteristic of multi-cellular organisms and in many cases their activity can be modulated via small lipophilic compounds (ligands). For example, non-polar compounds, such as steroid hormones, fatty acids, cholesterol derivates or xenobiotics, can act as ligands for NRs. In this respect they behave as ligand-gated transcriptional switches. In response to the presence of these ligands, NRs regulate the expression of target genes to affect processes such as mineral homeostasis, reproduction, development and metabolism [Chawla *et al.*, 2001]. Since many of the ligands for NRs are products or potential metabolites of NRs' target gene action they provide a direct link between signaling molecules controlling the processes and molecular responses. Like other transcription factors, NRs work in concert with other proteins to achieve their effect. These proteins fall into two broad classes, namely coactivators (CoA) and corepressors (CoR), which are defined by the way they activate or repress NR action. These proteins in conjunction regulate NRs to achieve primarily chromatin remodeling events which lead to activation or suppression of target gene expression [Glass *et al.*, 2000] (Fig. 2.1). As mentioned already above the fact that NRs can bind small molecules makes them suitable for "smart" drug design because their size makes them readily synthesizable. In addition, NRs regulate many

our genes, which are often clustered into functional groups related to a pathological processes and thereby targeting of NRs may change the course of a disease in many cases. These interventions may be beneficial for controlling physiological cascades associated with major diseases (e.g. cancer, osteoporosis and type 2 diabetes).

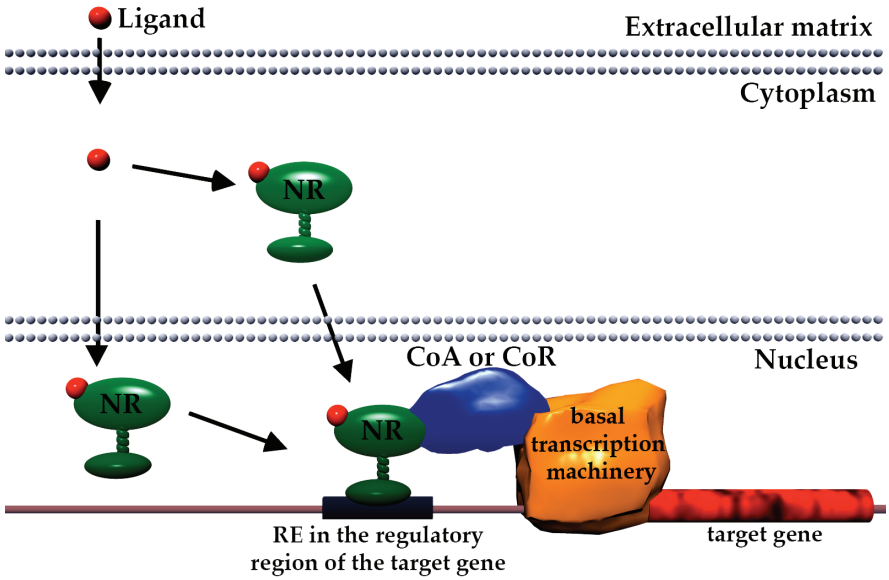

Fig. 2.1 The activation of NRs by ligands and the regulation of target genes. Small lipophilic compounds (Ligand, red) binds to the NR in the cytoplasm or the nucleus. The NR binds to the specific DNA sequence in the regulatory region of the target gene. Depending on the property of the ligand, NR interacts with CoA or CoR. In the case of activation, the basal transcription machinery is recruited and the target gene is up-regulated.

2.1.1 Classification of the NRs

NRs have been classified using evolutionary criteria, based on primary sequences of their genes and proteins or similarities in their functional profiles such as ligand affinity, ligand binding, or dimerization. Taking evolution into account, NRs can be divided into six related subfamilies, NR0-NR5 and 28 groups of receptors according to DNA sequence homology of DNA-binding domains (DBDs) and ligand-binding domains (LBDs) [The NR nomenclature committee, 1999].

The functional division of the superfamily based on affinities and properties of the ligands includes three subfamilies (Table 2.1). In the first group there are classical endocrine NRs, "receptors" that can bind high-affinity hormonal lipids in a concentration 1 nM or lower [Chawla *et al.*, 2001]. In this group, receptors for the hormones 3,5,3'-triiodothyroine (TRs, [Sap *et al.*, 1986; Weinberger *et al.*, 1986]), all-*trans* retinoic acid (RARs, [Petkovich *et al.*, 1987]), 1α,25$(OH)_2D_3$ (VDR, [Baker *et al.*,

1988]), 17β-estradiol (ERα, β), cortisol (GR), aldosterone (MR), progesterone (PR) and dihydrotestosterone (AR) are to be found.

Table 2.1 The human NR superfamily.

Subfamily	Name	Nomenclature	Ligand*
Receptors	AR	NR3C4	dihydrotestosterone
	ERα,β	NR3A1, NR3A2	17β-estradiol
	GR	NR3C1	cortisol
	MR	NR3C2	aldosterol
	PR	NR3C3	progesterone
	RARα, β, γ	NR1B1, NR1B2, NR1B3	all-trans retinoic acid
	TRα, β	NR1A1, NR1A2	3,5,3'-triiodothyronine
	VDR	NR1I1	$1\alpha,25(OH)_2D_3$
Sensors	CAR	NR1I3	androstanol, xenobiotics
	ERRα, β, γ	NR3B1, NR3B2, NR3B3	anti-estrogens
	FXR	NR1H4	bile acids
	HNF-4α, γ	NR2A1, NR2A2	fatty acids
	LRH-1	NR5A2	phospholipids
	LXRα, β	NR1H2, NR1H3	oxysterols
	PPARα, δ, γ	NR1C1, NR1C2, NR1C3	fatty acids and its derivatives
	PXR	NR1I2	pregnanedione, xenobiotics
	RORα, β, γ	NR1F1, NR1F2, NR1F3	fatty acids, cholesterol, retinoids
	RXRα, β, γ	NR2B1, NR2B2, NR2B3	retinoids, fatty acids
	SF-1	NR5A1	phospholipids
Orphans	COUPα, β, γ	NR2F1, NR2F2, NR2F3	unknown
	DAX	NR0B1	
	GCNF	NR6A1	
	NGFI-Bα, β, γ	NR4A1, NR4A2, NR4a3	
	PNR	NR2E3	
	RevErbAα, β	NR1D1, NR1D2	
	SHP	NR0B2	
	TLX	NR2E1	
	TR2α, β	NR2C1, NR2C2	

* synthetic or natural compounds co-crystallized with NRs, which have or may have physiological effects.

The second group covers "sensors" for xenobiotics and nutritional components such as fatty acids, lipids and cholesterol. These sensors are recognizing their ligand

mostly in micromolar range. In this group, we can find sensors for fatty acids (PPAR, [Desvergne *et al.*, 1999]), oxysterols (LXRs, [Repa *et al.*, 2000]), bile acids (FXR, [Mi *et al.*, 2003]) and xenobiotics (PXR and CAR, [Honkakoski *et al.*, 2003]). In addition, to this group belong the RXR isotypes, receptors for the natural ligand 9-*cis* retinoic acid, which are probably the most prominent adopted orphan NRs since many other NRs make heterodimers with them [Mangelsdorf *et al.*, 1990]. The heterodimerization is inevitable for the biological function of many of these receptors.

The third group of NRs is called "real orphans" because to date no high affinity ligand has been identified for them. It should be noted that many of the sensors when first cloned were described as orphans and when ligands were found for them, they became adopted orphans. This term is still widely used in the literature.

2.1.2 Three-dimensional and functional organization of the NRs

The functional and structural organization of NRs is highly conserved with most of them containing specific domains such as activation function–1 (AF-1), DBD, hinge region, LBD and activation function–2 (AF-2). However, it should be noted that the conservation of these domains varies throughout the NR family (Fig. 2.2). Specific NRs lack some of these domains, VDR lacks an AF-1, the orphan NRs SHP and DAX lack DBD and RevErb lacks an AF-2 domain.

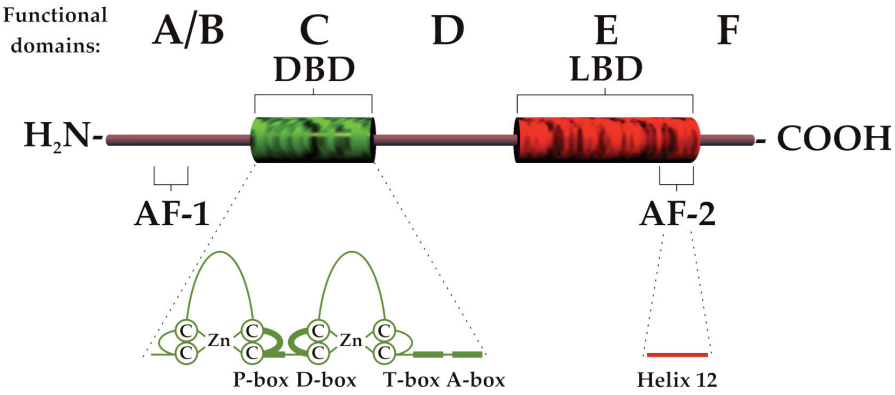

Fig. 2.2 Schematic overview of the functional domains of NRs. NRs consist of different domains that are connected with a distinct function of the protein. The least conserved region is the C-terminal region (E-F), which may vary in length and the AF-1 domain that can contains sites for CoA binding. Some receptors contain an additional F domain. The DNA-binding domain (DBD), which contains two zinc fingers, is the most conserved region and contains several functional domains (P-, D-, T- and A-box). The hinge region serves as a connector between DBD and the ligand-binding domain (LBD). It has very critical parts that serve for ligand recognition, heterodimerization and cofactor interaction. In addition, at the very end of the LBD the AF-2 (helix 12) is localized, which is crucial for ligand dependent conformational changes of the receptor

2.1.2.1 Activation function-1 domain

This domain is the part of the A/B region (Fig. 2.2), which is a modulatory region of variable size and sequence. The A/B domain is one of the most diverse parts of NRs, i.e. its sequence is not well conserved among the NRs. In many cases the function of this region is dependent on covalent modifications of its respective amino acid residues. There are several studies, which indicate that this domain in NRs can be phosphorylated by cyclin-dependent kinases and/or mitogen-activated protein kinases (MAPK) and this modification influences ligand-dependent and -independent transactivation function of the receptor [Kato *et al.*, 1995; Patrone *et al.*, 1996; Rochette-Egly *et al.*, 1997; Rochette-Egly *et al.*, 1992; Taneja *et al.*, 1997]. In PPARα the AF-1 domain is also modulated via MAPK phosphorylation, which results in enhancement of the transcriptional activity of the receptor [Juge-Aubry *et al.*, 1999]. In contrast to this, the phosphorylation by the same kinase on the PPARγ AF-1 results in the negative regulation of the receptor. Surprisingly, this posttranslational modification has a negative impact on the ligand-binding to the receptor, suggesting that the regulation of the transcriptional activity involves an intramolecular communication between the modulatory domains AF-1 and AF-2 (helix 12), which is located at the opposite end of the molecule [Shao *et al.*, 1998]. Furthermore, AF-1 can have a direct interaction with CoAs as it is the case for PGC-2 that interacts with the AF-1 of the PPARγ_2 NR [Castillo *et al.*, 1999].

2.1.2.2 DNA-binding domain

The DBD is the most conserved region in NRs, which confers their specific mechanism of action concerning the recognition of specific target sequence and the activation of nearby target gene. This domain contains amino acid residues, which are highly conserved among the members of the NR superfamily and are required for efficient DNA binding of the receptor. The DBD includes two "zinc-finger" motifs that consist of four conserved cysteine residues each, which bind and hold in place one zinc atom (Fig. 2.3) [Luisi *et al.*, 1991; Schwabe *et al.*, 1993; Shaffer *et al.*, 2002]. Besides the zinc-finger binding motifs that span usually 60-70 amino acids, there is a carboxy-terminal extension, which contains the so-called T- and A-boxes. Amino acids essential for the specific DNA recognition are located in the first zinc-finger in the region called P-box. NRs typically bind to the DNA sequences with the conserved hexanucleotide motif. In addition, the DBD is involved in the dimerization of NRs through the specific amino acids located in the region called D-box, which is in the second zinc-finger. The core of the DBD contains two α-helices, the first helix starting from the third cysteine residue of the first zinc-finger and the second one spans the carboxy terminus of the second zinc-finger (Fig. 2.3).

2.1.2.3 Hinge region

The hinge region, which is sometimes also called domain D (Fig. 2.2) with respect bridges the DBD and the LBD and allows the rotation of these two domains

selective to each other. In many cases it also contains a nuclear localization signal and also some residues that have been shown to be important for CoR interaction [Chen *et al.*, 1995; Hörlein *et al.*, 1995].

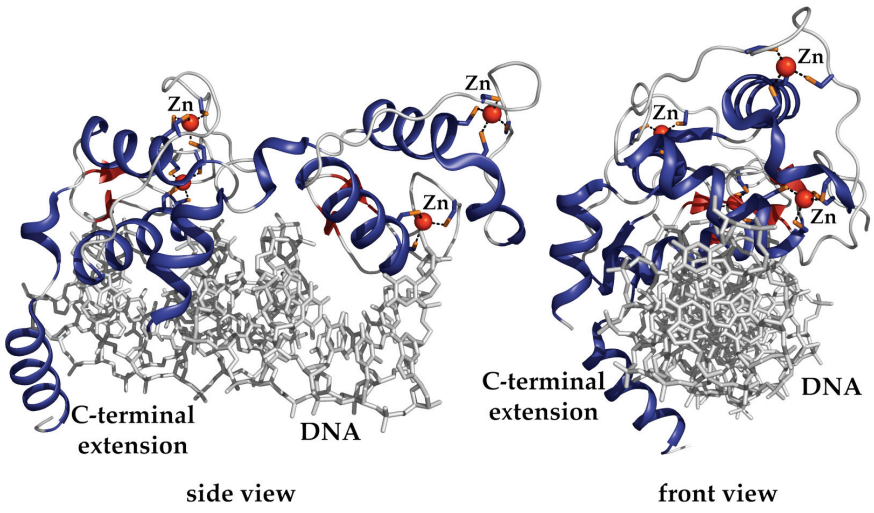

Fig. 2.3 Crystal structure of the human VDR DBD. The DBD consist of a highly conserved 66 amino acid stretch whose core is made up from two zinc fingers (red spheres) each contacted by four cysteine residues. The polypeptide chain around the zinc nuclei modules is folded into unified globular domains containing two α-helices (blue) and β-strands (red). The last adjacent helix is the C-terminal extension that may contain motifs for dimerization.

2.1.2.4 Ligand-binding domain

The LBD is a multifunctional domain involved primarily in the ligand recognition. It has also been shown to be responsible for dimerization with LBDs of other NRs and interactions with heat shock proteins as well as CoAs and other components of the basal transcriptional machinery. To date many crystal structures containing the LBDs of NRs have been solved that show rather similar canonical structures for different members of the NR superfamily. From the structural point of view (Fig. 2.4) the LBDs of most NRs are a characteristic 3-layer anti-parallel α-helical sandwich formed by 11 - 13 individual α-helices. The part of the LBD formed by helices 1, 8, 9, 10 and the upper part of helix 3 (Fig. 2.4) is structurally highly conserved among the members of the NR superfamily and shows less dynamic movements. Helices 4, 5, 6, 7, 11, 12 and the lower part of the helix 3 (Fig. 2.4) form a cavity of the ligand-binding pocket, which has the ability to adopt its volume according to the bound ligand. This part of the LBD displays the highest flexibility and dynamics [Molnár *et al.*, 2005; Nagy *et al.*, 2004; Nolte *et al.*, 1998]. For detailed description of the LBDs see Chapters 2.2.1, 2.3.1 and 2.4.1.

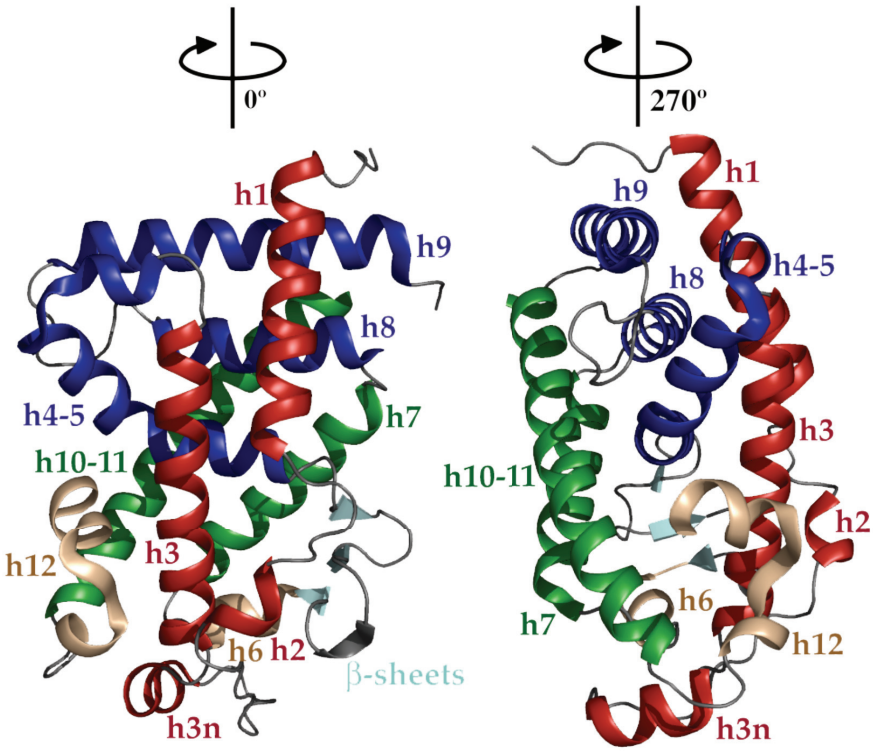

Fig. 2.4 3D-view of the structurally conserved NR LBD. The two views represent the same molecule turned 270°.The LBD of most NRs is a characteristic 3-layer anti-parallel α-helical sandwich formed by 11-13 α-helices. The three layers are depicted in color (red, blue and green). Helices h6 and h12 (light brown) make the lid of the LBD. The β-sheets are highlighted in light blue.

2.1.2.5 Helix 12 (AF-2 domain)

The helix 12 (Fig. 2.2 and 2.4) is considered to be the very last helix of the LBD, and its main function is to respond to ligand-triggered conformation change of the receptor allowing the docking of the CoA to LBD. In the whole receptor this part undergoes the biggest conformational changes and the direct effect of the ligand is also mediated through this domain [Li *et al.*, 2003].

2.1.2.6 Ligand-binding pocket

The ligand-binding pocket is the cavity inside the LBD of the NR, which contains amino acids essential for the recognition of the ligand. This pocket is mainly hydrophobic and is buried in the lower, more flexible, part of the LBD allowing the accommodation of its shape for the different non-polar ligands bound into the cavity of the ligand-binding pocket. Its lining is constructed from residues derived from the helices 3, 4, 6, 7, 11 and 12. Ligand-binding pockets vary in size among the receptors

from ≈ 0 Å^3 in the Nurr-1, which does not have a functional ligand-binding pocket, to ≈ 1400 Å^3 in the mammalian PPAR subtypes. However, it is very difficult to calculate the exact volume of the apo-receptor ligand-binding pocket, because the space of the pocket may considerably change within the same receptor depending on the volume of the ligand [Li *et al.*, 2003].

2.2 CAR

The human NR CAR (initially called MB67) was cloned in 1994 by using degenerated oligonucleotide probes against the conserved NR sequence motif in the DBD. Three years later the mouse orthologue was isolated [Baes *et al.*, 1994; Choi *et al.*, 1997]. An amino acid comparison of human CAR relative to human PXR, another orphan NR, results in an amino acid residue identity of 66 % and 45 % for the DBD and the LBD, respectively. In addition, like plenty of other NRs, CAR dimerizes with RXR. CAR is most abundantly expressed in the liver and intestine.

2.2.1 3D-protein structure of the human and mouse CAR LBDs

CAR was one of the most recent NRs to be crystallized and to date there are four different LBD crystal structures available (Table 2.1). Three of them represent either human or mouse CAR in an active conformation whilst the other one is mouse CAR in an inactive conformation. All crystal structures share the canonical 3-layer α-helical sandwich architecture typical for other NR LBDs. However, some of the helices that contribute to the LBD structure differ slightly in their composition. Both human and mouse CAR contain in their respective active conformation, 11 α-helices, two 3^{10} helices (helix 2 and helix 2′) and three short β-strands [Suino *et al.*, 2004; Xu *et al.*, 2004].

Table 2.1 The human and mouse CAR crystal structures.

PDB ID	Molecules	Ligand	Resolution from PDB header	Resolution from map calculation	Complete-ness of data	R value (free R) from PDB header	R value for map	Reference
1XVP	hCAR-RXRα	CITCO Penta-decanoic acid	2.60 Å	-*	86.3 %	0.180 (0.234)	-*	[Xu *et al.*, 2004]
1XV9	hCAR-RXRα	5β-pregnanedione C16-C18 FA	2.70 Å	-*	86.4 %	0.181 (0.239)	-*	[Xu *et al.*, 2004]
1XLS	mCAR-RXRα	TCPOBOP 9cRA	2.96 Å	19.99 – 1.97 Å	92.9 %	0.255 (0.303)	0.276	[Suino *et al.*, 2004]
1XNX	mCAR	Androstanol	2.90 Å	29.54 – 2.90 Å	100.0 %	0.229 (0.288)	0.241	[Shan *et al.*, 2004]

* the electron density map is not available

Interestingly, mouse CAR in the inactive conformation contains 12 α-helices with helix 2 being absent. Despite this, the rest of the molecule has an identical structural fingerprint when compared to the active CAR LBD. The inactive mouse CAR LBD shares the highest structural similarity with human PXR with root-mean-square deviation (rmsd) = 0.76 for 155 Cα atoms, sequence identity of 35.1 %, and VDR with rmsd = 0.97 for 155 Cα atoms, sequence identity of 30.8 % [Shan *et al.*, 2004]. Some additional interesting features occur in the CAR LBD, including the occurrence of the shortest known helix 12 for a NRs and the appearance of an additional helix called "X" that is located between helices 11 and 12 (Fig. 2.5). This latter structural feature is also present in other NRs, such as VDR [Rochel *et al.*, 2000], RORα [Kallen *et al.*, 2002] and RORβ [Stehlin *et al.*, 2001]. However, the character and number of amino acids linking the helices X and 12 are very critical. In case of CAR, this linker is one methionine residue, which influences the rigidity of this region and ultimately allows the fixation of the helix 12 in this NR. In other NRs the linker is comprised of two residues. In case of VDR, the leucine and threonine allow higher flexibility for this part of the LBD. This is in contrast to the occurrence of phenylalanine and proline residues in the ROR NR subtypes. The presence of these residues helps in the fixation of the helix 12 and thus contributes to the constitutive activity [Xu *et al.*, 2004].

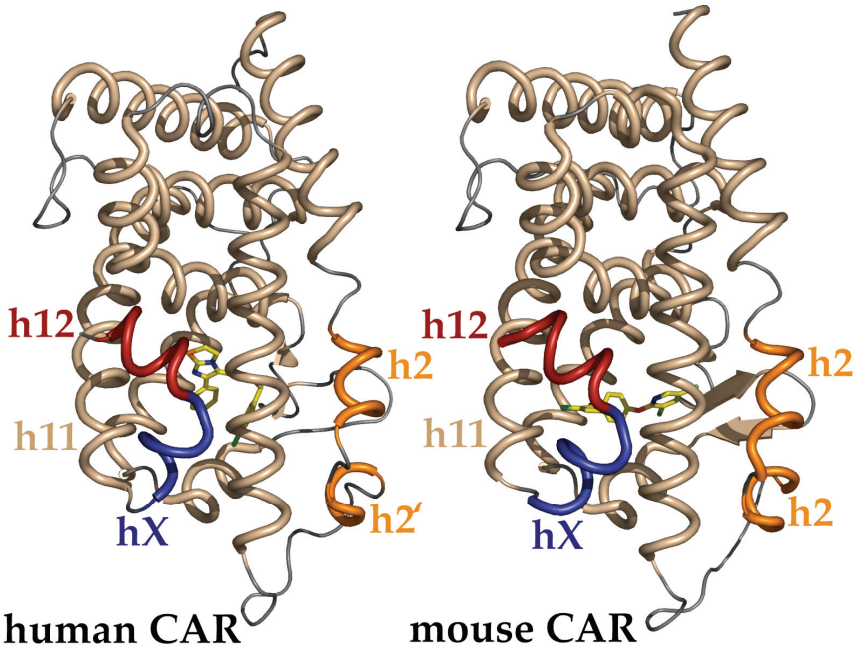

Fig. 2.5 The crystal structures of the human and mouse CAR LBDs. Both crystal structures show a high level of similarity. Helices h2 and h2′ (orange) are highlighted in orange. The additional helix hX (blue), located between helices h11 and h12, is depicted in color with helix h12 in dark red.

The short helix 12 in CAR allows for the free carboxyl group at the C-terminus to interact with the lysine in helix 4 (K195 in human and K205 in mouse CAR) and this interaction helps to stabilize helix 12. This lysine is conserved in many other NRs such as VDR and PPARs. However, in the latter it interacts with an aspartate residue located in helix 12 [Molnár *et al.*, 2005] and helps in the stabilization of PPARs' helix 12. In addition to this interaction, K205 (K195) together with S337 (S327) from helix 10 also interacts with other carbonyl groups in the C-terminus of the helix 12 [Suino *et al.*, 2004]. Furthermore, this same lysine appears to be critical for the interaction with CoRs [Lempiäinen *et al.*, 2005; Xu *et al.*, 2002]. Another special feature of CAR is the presence of the two short 3^{10} helices 2 and 2', which connect helices 1 and 3 (Fig. 2.5). Although these two helices show low thermal parameters (average b-factor = 33 $Å^2$) they contribute to the ligand-binding pocket since an evolutionary-conserved hydrophobic phenyalanine residue in helix 2' (F142 in mouse and F132 in human CAR) is part of the ligand-binding pocket. However, residues from helices 2 and 2' do not seem to be involved in direct interactions with the ligands but they contribute to the hydrophobic nature of the ligand-binding pocket. Finally, the topology suggests that this region is most likely the ligand entry point as it was postulated for PPARα [Gampe *et al.*, 2000; Nolte *et al.*, 1998; Shan *et al.*, 2004].

The CAR ligand-binding pocket is made up from the residues from helices 2, 3, 4, 5, 6, 7 and 10 and from β-sheets 3 and 4, and therefore resembles other NRs. However, the numbers of residues that frame the pocket are different in active and inactive mouse CAR, 31 and 27 residues, respectively [Shan *et al.*, 2004; Suino *et al.*, 2004]. As it is the case for many other NRs, most of the residues in the ligand-binding pocket of CAR have an apolar character. Two hydrophilic patches exist and they make it possible to form hydrogen bonds with the ligands. Interestingly, the sizes of the ligand-binding cavities of CARs are in between the classical endocrine NRs e.g ER and RAR and the adopted orphans such as PPARs and PXR. The volumes of the ligand-binding pockets are 525 $Å^3$ and 570 $Å^3$ for active and inactive mouse CAR, respectively. For human CAR it is 675 $Å^3$, which is more comparable to the 697 $Å^3$ of VDR's ligand-binding pocket bound to its natural ligand $1\alpha,25(OH)_2D_3$.

Although the chemical structures of the ligands bound to all four CAR LBDs are different, they share some similarities in binding to CAR. All of them are using the hydrophobic character of the cavities, and the hydrogen bonds formed between the polar residues and ligands serve to orient the ligand. In mouse CAR, none of the ligands make a direct hydrogen bond contact with the helix 12, but TCPOBOP forms a number of hydrophobic interactions with helix 12 (L353) and the linker helix (L346, T350). Since these interactions serve additionally for stabilization of the helix 12, they may be responsible for the superagonistic properties of this ligand. In human CAR neither of the ligands co-crystallized with the LBDs form direct contacts with helix 12. The closest residue to the atoms of the ligands is L343, which is positioned at a distance of 4.9 Å from the C21 of 5β-pregnadione and 3.9 Å from the thiazole

ring of CITCO. Between the ligand and helix 12 there is a barrier formed by residues of F161, N165, F234 and Y326 that excludes the possibility of a direct interaction.

2.2.2 Physiological role of the CAR

The role of CAR as a xenobiotic receptor was first suggested by Honkakoski *et al*. [Honkakoski *et al*., 1998b], who characterized the transcription factors that regulate the expression of the *CYP2B* P450 cytochrome oxidase enzyme producing gene family. Like the xenobiotic responsive enhancer module (XREM) of the *CYP3A* gene promoter, the *CYP2B* promoter contains clusters of simple NR REs in close proximity to each other. The phenobarbital responsive enhancer module (PBREM) of the mouse *CYP2B10* gene contains two direct repeat (DR) 4-types of response elements (REs), which have an arrangement of two hexanucleotide half-sites with a four-nucleotide spacer, and a nuclear factor (NF) 1-binding site at positions -2290 to -2237 relative to the transcription start site (TSS) [Honkakoski *et al.*, 1998b]. In human, a similar PBREM was found at position -1733 through -1683 relative to the TSS of the *CYP2B6* gene, which is the orthologue of the mouse *CYP2B10* gene [Sueyoshi *et al.*, 1999]. Mutation of one of these DR4-type REs decreased activity to one third of the wild type activity in transfected primary hepatocytes, while simultaneous mutation of both NR REs abolished PBREM activity [Honkakoski *et al.*, 1998a; Paquet *et al*., 2000]. Recently, Wang *et al*. further analyzed the *CYP2B6* regulatory region and were able to identify an additional phenobarbital (PB)-responsive element located 8.5 kB upstream of the TSS containing a DR4-type RE [Wang *et al*., 2003a]. Moreover, the generation of CAR knockout mice provided definitive proof for the role of CAR in the regulation of *CYP2B* expression *in vivo*, since these mice were unable to induce *CYP2B* expression upon exposure to the mouse CAR activator PB [Wei *et al*., 2000].

Sugatani *et al*. [Sugatani *et al*., 2001] identified another PBREM-like cluster of CAR REs (CAREs) in the regulatory region of the human *UGT1A1* gene. The *UGT1A1* PBREM contains three CAREs and all are essential for the responsiveness of the gene to CAR (as mediator of PB action). Surprisingly, there is only significant binding of CAR-RXR heterodimers to one of the REs. How the three REs act together to confer full enhancer activity was an interesting question at the start of the studies presented here.

Phase I genes regulated by CAR in various species include members of the *CYP1A* [Maglich *et al*., 2002], *CYP3A* [Maglich *et al*., 2002; Sueyoshi *et al*., 2001] and *CYP2C* [Chen *et al*., 2003; Ferguson *et al*., 2002; Gerbal-Chaloin *et al*., 2002] subfamilies. In addition to the phase II enzyme UGT1A1, CAR regulates, in mouse, the expression of gluthathione S-transferases (GSTs) [Maglich *et al*., 2002] and sulfotransferases (SULTs) [Maglich *et al*., 2003; Maglich *et al*., 2002]. Moreover, mouse CAR has been shown to regulate the expression of the transporters multi-drug resistance-associated protein (MRP) 1, MRP2 and MRP3 [Kast *et al*., 2002; Maglich *et al*., 2002].

2.3 PPARs

Although it was not known at the time, the first molecular sensor for fatty acids was discovered in 1990 and was termed peroxisome proliferator-activated receptor α (PPARα), since it was able to bind chemicals known to induce peroxisome organelle proliferation in rodents [Issemann *et al.*, 1990]. The organelles contribute to the oxidation of the fatty acids.

The following years uncovered two other related receptors, PPARγ and δ (also called β) [Dreyer *et al.*, 1992; Kliewer *et al.*, 1994].

2.3.1 3D-protein structure of the PPAR LBDs

To date (November 2005) there are 19 PPAR crystal structures available in the Protein Data Bank (Table 2.2), and this number is expected to increase. This high number, compared to CAR and human VDR crystal structures, reflects how significant these receptors are for the NR research community. A simple division of these structures can be made according to what protein molecules are in the basic unit of the crystals (e.g. monomer or heterodimer PPAR with RXR). Another way in which to classify these structures is according to ligand properties or whether the structure contains CoA peptide. It is an interesting fact that, currently there is only one structure available of a NR containing a CoR peptide. This crystal structure is PPARα co-crystalized with the SMRT CoR peptide. For a detailed description of this structure see Chapter 2.6.1. One of the first PPAR structures to be published was PPARγ [Nolte *et al.*, 1998]. The authors presented the apo-PPARγ LBD and a ternary complex of PPARγ-SRC1 with rosiglitazone (Fig. 2.6). These structures resembled well the classical architecture of the canonical NR LBD of 13 α-helices sandwiched in three layers and a small four-stranded β-sheet. The unique features of this LBD is the existence of the helix 2′ between the first β-sheet and helix 3. Most of the amino acids have well-defined electron-density maps except for those which were in the loop region between helices 2′ and 3 (Fig. 2.6), which appears to be the most thermally mobile loop. The spatial placement of the helix 2 suggests that it is a ligand entry point. The top part of the LBD, where helices 4, 5 and 8 are tightly packed between the helices 1, 3, 7 and 10, shows that there is a very rigid composition of the tertiary structure [Molnár *et al.*, 2005; Nagy *et al.*, 2004; Nolte *et al.*, 1998]. This arrangement of the helices defines well the large ligand-binding pocket.

Table 2.2 Human PPAR crystal structures.

PDB ID	Molecules	Ligand	Resolution from PDB header	Resolution from map calculation	Completeness of data	R value (free R) from PDB header	R value for map	Reference
1I7G	PPARα	Az 242	2.20 Å	-*	99.3 %	0.237 (0.271)	-*	[Cronet *et al.*, 2001]
1K7L	PPARα-SRC1	GW409544	2.50 Å	-*	98.3 %	0.247 (0.284)	-*	[Xu *et al.*, 2001]
1KKQ	PPARα-SMRT	GW6471	3.00 Å	-*	98.8 %	0.258 (0.290)	-*	[Xu *et al.*, 2002]
1GWX	PPARδ	2-Methyl-propionic acid	2.50 Å	13.18 – 2.50 Å	73.1 %	0.246 (0.303)	0.269	[Xu *et al.*, 1999]
2GWX	PPARδ	No ligand	2.30 Å	8.00 - 2.00 Å	72.0 %	0.246 (0.288)	0.263	[Xu *et al.*, 1999]
3GWX	PPARδ	Eicosa-pentanoic acid	2.40 Å	19.50 - 2.20 Å	60.0 %	0.242 (0.301)	0.272	[Xu *et al.*, 1999]
1Y0S	PPARδ	GW2331	2.65 Å	19.76 - 2.64 Å	94.5 %	0.210 (0.261)	0.226	[Takada *et al.*, 2000]
1PRG	PPARγ	No ligand	2.20 Å	50.99 - 2.00 Å	76.1 %	0.246 (0.318)	0.271	[Nolte *et al.*, 1998]
2PRG	PPARγ-SRC1	Rosiglitazone	2.30 Å	-*	89.9 %	0.207 (0.264)	-*	[Nolte *et al.*, 1998]
3PRG	PPARγ	No ligand	2.90 Å	19.73 - 2.91 Å	95.7 %	0.209 (0.271)	0.226	[Uppenberg *et al.*, 1998]
4PRG	PPARγ	GW0072	2.90 Å	-*	78.6 %	0.240 (0.283)	-*	[Oberfield *et al.*, 1999]
1I7I	PPARγ	Az 242	2.35 Å	-*	91.3 %	0.238 (0.284)	-*	[Cronet *et al.*, 2001]
1KNU	PPARγ	Alkyloxy-phenylpro-pionic Acid	2.50 Å	39.89 - 2.50 Å	97.4 %	0.224 (0.264)	0.249	[Sauerberg *et al.*, 2002]
1NYX	PPARγ	Ragaglitazar	2.65 Å	-*	80.0 %	0.237 (0.306)	-*	[Ebdrup *et al.*, 2003]
1WM0	PPARγ-TIF2	2-Benzoyl-amino-benzoic acid	2.90 Å	14.83 - 2.81 Å	87.7 %	0.195 (0.295)	0.212	[Ostberg *et al.*, 2004]
1K74	PPARγ-RXRα-SRC1	GW406544 9cisRA	2.30 Å	-*	N/A	0.238 (0.279)	-*	[Xu *et al.*, 2001]
1FM6	PPARγ-RXRα-SRC1	Rosiglitazone 9cisRA	2.10 Å	44.00 – 2.10 Å	87.8 %	0.250 (0.292)	0.265	[Gampe *et al.*, 2000]
1FM9	PPARγ-RXRα-SRC1	GI262570 9cisRA	2.10 Å	19.69 - 2.10 Å	91.9 %	0.239 0.268)	0.258	[Gampe *et al.*, 2000]
1RDT	PPARγ-RXRα-CoA peptide	GI262570 2-propanoic acid	2.40 Å	-*	97.1 %	0.221 (0.259)	-*	[Haffner *et al.*, 2004]

* the electron density map is not available or cannot be calculated

Both the apo- and the holo-PPARγ structures contain homodimers that probably mimic the herodimerization with RXR, since to date there is no evidence for a biological function of PPAR homodimers. It remains interesting that the dimerization interface of PPARγ resembles that of ERα and RXRα, which are both capable of homodimerization. The protein sequence homology between PPAR and RXR is 27 % in this region. However, several amino acids that form the strongest interaction in

RXR homodimers are conserved in PPAR (F432, A433, L436, E418, E407 and K438 of human PPARγ$_1$). The ligand-binding pocket of apo-PPARγ is a large T-shape pocket, which is bordered by helices 3, 6, 12 and the β-sheets. The total volume of the apo-PPARγ pocket is ~1300 Å^3. In the holo-PPARγ, rosiglitazone occupies only 40 % of the ligand-binding pocket. This ligand makes several specific interactions with amino acid in helices 3, 4, 10 and 12. The carbonyl group of rosiglitazone forms hydrogen bonds with both H323 and H449. Unlike ligands for CAR, in PPARγ the ligand has a direct contact with helix 12 that helps to stabilize helix 12.

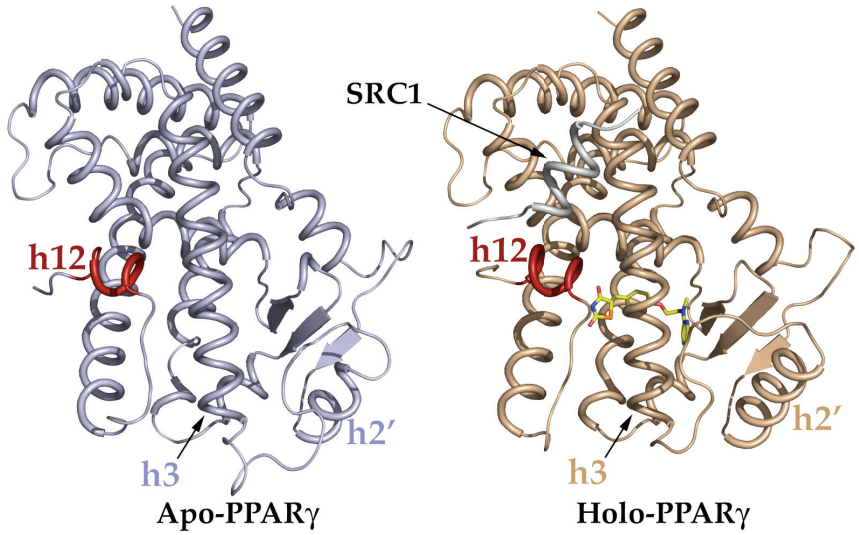

Fig. 2.6 The crystal structure of human apo- and holo-PPARγ LBDs. The helices of the LBDs are depicted in slate blue and wheat color for apo-PPARγ and holo-PPARγ, respectively. The helix 12 in both LBDs is highlighted in red color. The holo-PPARγ structure contains the SRC1 peptide (white) and rosiglitazone (yellow). The most thermally labile part of the structure is the loop between helices h2′ and h3.

The origin of this very specific contact is the second last tyrosine in the helix 12 that is conserved in all human PPARs. Except these polar interactions there are many apolar interactions with the benzene rings and the sulphur atom of the TZD ring, since the pocket has a hydrophobic character, as is it the case also for other NRs. The position of the helix 12 in the apo-PPARγ homodimer interestingly adopts in one molecule an active and in the other one an inactive conformation suggesting that in the apo-PPARγ the helix 12 can assume both conformations and the ligand then acts to lock-down the receptor into the active conformation [Nolte *et al.*, 1998]. Although this scenario is highly possible, detailed analysis of the crystal structure suggests that the helix 12 of the inactive PPARγ molecule contacts the helix 12 of the active neighboring symmetry-related molecule. Thus it appears that the inactive helix 12 mimics the interaction with a CoA peptide. In the process of ligand-dependent activation the interaction of the LBD with CoAs is required and the ternary structure

of the crystalized complex suggests that each member of the receptor in the dimer interacts with a single interaction motif from the CoA.

2.3.2 Physiological roles of the PPARs

All three subtypes have distinct tissue distribution and selective function in the regulation of metabolism in the organism. In the cell they act by regulating networks of target genes.

PPARα can be found primarily in the liver and in smaller amounts in heart and skeletal muscle tissue, where it has a critical role in controlling fatty acid oxidation [Reddy *et al.*, 2001]. Under conditions of prolonged fasting or during night, fatty acids are released from adipose tissue and transported to the liver where PPARα becomes highly up-regulated [Kersten *et al.*, 1999]. The activation of PPARα by fatty acids promotes hepatic fatty acid oxidation to generate ketone bodies, providing an energy source for peripheral tissues. This regulation is very important and is supported by evidence derived from the PPARα-null mouse, which is unable to meet energy requirements during fasting [Kersten *et al.*, 1999]. The PPARα-induced fatty acid oxidation improves plasma lipid profiles and in many mouse models PPARα agonists have an effect on plasma triglycerides, reduce adiposity and improve hepatic and muscle steatosis leading to improved insulin sensitivity [Chou *et al.*, 2002; Guerre-Millo *et al.*, 2000; Kim *et al.*, 2003]. This is reflected by the fact that, in clinical practice, PPARα-selective agonists are widely used to treat hypertriglyceridemia. However, the beneficial effect on insulin sensitivity has not been rigorously examined.

PPARδ in the beginning received less attention than the other PPARs due to its ubiquitous expression profile in addition to lack of selective ligands. However, recent development of specific PPARδ agonists has made it possible to study more extensively this subtype, and this receptor has turned out to be a prominent regulator of fatty acid catabolism and energy homeostasis [Barak *et al.*, 2002; Peters *et al.*, 2000]. GW501516, a PPARδ selective agonist, was shown to lower plasma triglyceride levels in obese monkeys while raising HDL levels suggesting a beneficial effect in hyperlipidemic patients [Oliver *et al.*, 2001]. Ectopic expression of an activated PPARδ in adipose tissue produced lean mice that are resistant to obesity and hyperlipidemia [Wang *et al.*, 2003b]. The mechanism of this protective effect appears to be due to the up-regulation of genes involved in fatty acid catabolism and adaptive thermogenesis. PPARδ deficient mice fed with high-fat diet show reduced energy uncoupling and are susceptible to obesity [Wang *et al.*, 2003b]. All these data suggest a role for PPARδ as a fat-burning opposite to the fat-storing PPARγ [Wang *et al.*, 2003b]. However, its potential therapeutic value in obesity and diabetes has to be further explored.

PPARγ is the most studied PPAR isoform and large amounts of evidence show that it is a master regulator of adipocyte formation and their ability to function

normally in the adult body [Rosen *et al.*, 2000]. Its expression is induced during the differentiation of fat cells, which can be mimicked via ectopic expression of this receptor in nonadipogenic cells. These cells consequently differentiate to mature adipocytes [Tontonoz *et al.*, 1994]. Furthermore, PPARγ null mice fail to develop adipose tissue [Barak *et al.*, 1999; Kubota *et al.*, 1999; Rosen *et al.*, 1999]. Although adipose tissue only represents about 10 % of the insulin-stimulated glucose disposal, it has a key role in directing whole body glucose homeostasis. The hints for this function come from the fact that TZDs, PPARγ selective agonists, act as insulin-sensitizing drugs [Forman *et al.*, 1995; Lehmann *et al.*, 1995]. At the molecular level, two plausible mechanisms have been suggested to explain this process. Firstly, activation of PPARγ in adipocytes improves their ability to store lipids, thereby reducing lipotoxicity in muscle and liver tissue. The activation of this metabolic pathway involves repartitioning of lipids in the body by increasing the content of triglycerides in adipose tissue and lowering free fatty acids and triglycerides in plasma, liver and muscle, and consequently improving insulin sensitivity [Guan *et al.*, 2002; Yamauchi *et al.*, 2001]. Secondly, PPARγ-agonists affect the release of adipokines such as leptin, resistin and adiponectin, which have potent metabolic effects on other tissues. For example, PPARγ specific drugs inhibit the expression of tumor necrosis factor α and resistin which both promote insulin resistance [Guan *et al.*, 2002; Peraldi *et al.*, 1997; Rajala *et al.*, 2003; Steppan *et al.*, 2001]. Tissue-specific knockout studies strengthen the conclusions that the adipose tissue is the primary target of TZDs and suggest a critical biological role for PPARγ in both muscle and liver. These studies also provide direct evidence for a molecular link between glucose homeostasis and lipid metabolism [Evans *et al.*, 2004].

2.4 VDR

The first evidence for the existence of a vitamin D binding protein or receptor was provided by Haussler and Norman in 1969 [Haussler *et al.*, 1969]. However, for the isolation of the full coding sequence of the human and rat receptor, one had to wait nearly two decades until 1988 [Baker *et al.*, 1988; Burmester *et al.*, 1988a; Burmester *et al.*, 1988b]. VDR was first discovered in extracts from chicken intestine, because this animal was used as a model system for examining the role of vitamin D in calcium homeostasis [Pike *et al.*, 1980]. Later on, the actions of vitamin D have been extended beyond those identified in the intestine. The target tissues of vitamin D include the kidney, bone, parathyroid gland as well as many others, which reflects the fact that VDR is a widely expressed NR.

2.4.1 3D-protein structure of the VDR LBD

To date there has been six human VDR crystal structures (Table 2.3) made available in the Protein Data Bank (PDB).

Table 2.3 The human VDR crystal structures.

PDB ID	Ligand	Resolution from PDB header	Resolution from map calculation	Complete-ness of data	R value (free R) from PDB header	R value for map	Reference
1DB1	1α,25(OH)$_2$D$_3$	1.80 Å	19.94 – 1.80 Å	95.6 %	0.191 (0.214)	0.202	[Rochel *et al.*, 2000]
1IE8	KH1060	1.52 Å	18.53 – 1.37 Å	90.3 %	0.212 (0.230)	0.223	[Tocchini-Valentini *et al.*, 2001]
1IE9	MC1288	1.40 Å	14.88 – 1.40 Å	73.2 %	0.214 (0.248)	0.224	[Tocchini-Valentini *et al.*, 2001]
1S0Z	EB1089	2.50 Å	14.95 – 2.50 Å	97.2 %	0.170 (0.204)	0.187	[Tocchini-Valentini *et al.*, 2004]
1S19	MC903	2.10 Å	19.90 – 2.00 Å	93.9 %	0.179 (0.214)	0.194	[Tocchini-Valentini *et al.*, 2004]
1TXI	TX522	1.90 Å	19.83 – 1.90 Å	96.0 %	0.191 (0.218)	0.196	[Eelen *et al.*, 2005]

The first one was solved with the natural ligand, 1α,25(OH)$_2$D$_3$ [Rochel *et al.*, 2000]. The VDR molecule used for crystallization has a deletion of a hinge region insertion domain, which acted to stabilize the LBD and allowed the formation of crystals. The complex was solved at resolution 1.8 Å by a combination of molecular replacement using a homology model based on the RARγ [Klaholz *et al.*, 1998; Renaud *et al.*, 1995] and isomorphous replacement with a mercurial derivative. The structure has the general topology of NR LBDs with the canonical 13 α-helices sandwiched in three layers and a three-stranded β-sheet (Fig. 2.7). Helices 1 and 3 are connected via two small helices 2 and 3n.

The missing insertion domain is rather distant from the ligand-binding pocket and therefore most likely it does not affect the ligand binding. On the other hand the insertion domain may play a role in cofactor binding. However, this hypothesis has not been investigated in detail. The crystal structure has the highest homology to holo-human RARγ LBD [Klaholz *et al.*, 1998; Renaud *et al.*, 1995]. The clearest difference between LBDs of VDR and RARγ corresponds to the connection between helices 1 and 3, which in RARγ surrounds the β-sheet. Contrary to this, in VDR the tip of the β-sheet is shifted outward and thus allowing an enlargement of the ligand-binding pocket. The position of this β-sheet is very similar to that found in ERα [Brzozowski *et al.*, 1997]. All the individual strands of β-sheet have residues which contact the ligand 1α,25(OH)$_2$D$_3$. In the β1-sheet, W286, a very specific residue in VDR, helps to position the ligand in the ligand-binding pocket. In addition, the residues from the β-sheets help to stabilize the connecting loop formed between helices 2 and 3n.

Another interesting property leading to the enlargement of the ligand-binding pocket is the shifted loop between helices 6 and 7 towards the surface of LBD. The comparison among the various NRs showed that this loop is highly flexible. The crucial helix 12 is in the active conformation and makes two direct van der Waals contacts with the methyl group of the ligand via two residues V418 and F422. The position of the helix 12 is stabilized by several hydrophobic interactions (T415, L417, V418, L419, V421, F422) with the residues from helices 3 (D232, V234, S235, I238,

Q239), 5 (A267, I268) and 11 (H397, Y401). In addition, the fixation of helix 12 involves two pairs of polar residues, the conserved salt bridge between K264 (helix 4) and E420 (helix 12) and a hydrogen bond between S235 (helix 3) and T415 (helix 12). Some of the above mentioned residues (V234, I268, H397 and Y401) directly interact with the ligand and therefore they contribute to the ligand-induced switch of the helix 12. The volume of the ligand-binding pocket of the receptor is 697 $Å^3$ and 1α,25$(OH)_2D_3$ occupies only 56 % of the pocket. In the space where the A-ring of the ligand is situated, there is an enlargement of the pocket due to two water molecules [Rochel *et al.*, 2000]. This adaptation of the pocket can explain the activity of the 2α-methyl derivative of 1α,25$(OH)_2D_3$, which shows 4-fold higher affinity than the natural ligand [Fujishima *et al.*, 1998].

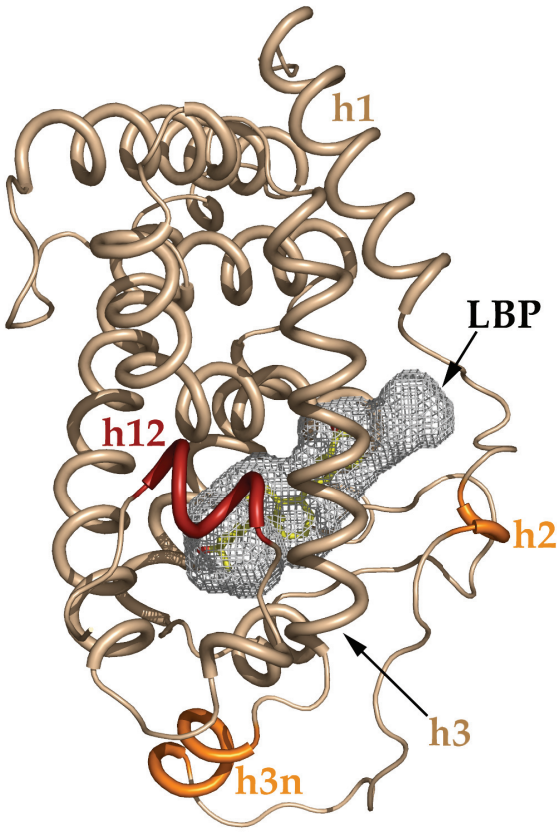

Fig. 2.7 The crystal structure of the human VDR LBD. Helices are depicted in wheat color with helix 12 is highlighted in red. The deleted insertion domain is between helices h3n and h2 (orange). The ligand-binding pocket (LBP) is displayed in mesh representation (grey). In the pocket the natural ligand 1α,25$(OH)_2D_3$ is bound and is highlighted in yellow color

In addition, the empty space around the aliphatic chain in the pocket would suggest that analogs with differing chain lengths could fit. Some vitamin D derivatives [Bouillon *et al.*, 1995] have been shown to have different effects on transcriptional regulation and CoA recruitment [Rachez *et al.*, 1998; Takeyama *et al.*, 1999]. To understand their specificity, preliminary ligand docking was made [Rochel *et al.*, 2000], which showed that synthetic ligands with a rigid aliphalic chain at position C17 (MC903, EB1089), can be accommodated in the ligand-binding pocket with only minor changes in geometry with the respect to the position of $1\alpha,25(OH)_2D_3$. In contrast, the 20-epi analogs' (MC1288, KH1060) C21-methyl group points to the same part of the pocket as the natural ligand's one while the rest of the chain is lining the opposite side of the pocket. Ligands with longer aliphatic chain adopt more compact conformation and form additional van der Waals contacts with the ligand-binding pocket, which may further stabilize the LBD.

2.4.2 The physiological role of the VDR

The physiological role of vitamin D metabolites and its receptor include a variety of processes and perhaps one of the most interesting is its biological effect on regulation of proliferation and differentiation [Feldman *et al.*, 1980]. These effects are rather different from the effects of other steroid hormones. The observed antiproliferative effects are considered to have a potential therapeutic role in the treatment of various cancers as well as in the treatment of human psoriasis and hyperproliferative disorders of the skin [Nagpal *et al.*, 2001].

In mammals, the most responsive primary VDR target gene is the *24-hydroxylase* (*CYP24*). The product of this gene is an enzyme which forms a negative feedback loop mechanism in the vitamin D signaling due to its primary role in inactivation of the natural ligand for VDR, $1\alpha,25(OH)_2D_3$.

VDR is known to bind as a heterodimer with RXR to DR3-type of elements. These elements can be found in the *CYP24* promoter and this is the reason for the strong responsiveness of this gene. The two DR3-type elements are located in the proximal part of the promoter and are separated by a distance of less than 100 bp. These RE clusters are evolutionary conserved between men and rodents [Kerry *et al.*, 1996; Zierold *et al.*, 1995].

2.5 Cofactors

2.5.1 CoAs

CoAs represent a diverse group of proteins that have the ability to enhance NR-mediated transcription mainly via direct interaction with the LBD of the receptor in its active conformation. Most CoAs contain one or more NR interaction boxes, bearing a short consensus peptide interaction motif LXXLL, where L is leucine and X

is any amino acid [Heery *et al.*, 1997]. This motif directly interacts with the CoA binding groove on the surface of the LBD and its active part is the helix 12. CoA interaction can also occur in the N-terminal part of the receptor primarily in the AF-1 domain [Wärnmark *et al.*, 2003]. CoAs do not show such common structural themes like NRs, they are highly diverse in both structure and function (Table 2.4). Some can serve as adapters between NRs or other transcriptional factors and the basal transcriptional machinery (Fig. 2.1). Many CoAs have shared characteristic enzymatic activities that can enhance the transcriptional activity, e.g. the SRC family, whose members have histone acetyltransferase (HAT) activity that targets histones or other proteins at NR-regulated gene promoters for acetylation [McKenna *et al.*, 1999].

2.5.1.1 The SRC family of NR CoAs

This family of CoAs has been the focus of intensive study in recent years. There are three protein members in this family each derived from a separate gene.

2.5.1.1.1 SRC-1

The first member of this family, SRC-1, was cloned using PR-LBD as a bait in yeast-two-hybrid experiments [Oñate *et al.*, 1995]. Although SRC-1 interacts with the LBD of NRs in a ligand-triggered manner there have been reports that it can enhance the activity of ER and AR through the AF-1 domain of these NRs [Alen *et al.*, 1999; Bevan *et al.*, 1999; Ma *et al.*, 1999; Webb *et al.*, 1998]. In addition, Takeshita *et al.* [Takeshita *et al.*, 1996] and Ikeda *et al.* [Ikeda *et al.*, 1999] reported the interaction of SRC-1 with general transcription factors such as TBP and TFIIB. However, the functional consequences of these interactions remain uncovered. Furthermore, SRC-1 can interact and enhance the activity of other transcription factors such as NF-κB, SMAD3 and AP-1, which are responsible for multiple cellular processes [Lee *et al.*, 1998; Na *et al.*, 1998; Yanagisawa *et al.*, 1999].

2.5.1.1.2 TIF-2

Human TIF2 was isolated by Voegel *et al* [Voegel *et al.*, 1996] as an ER- and RAR-interacting factor (GRIP1) and its mouse orthologue GRIP-1 by Hong *et al* [Hong *et al.*, 1996] as a GR-interacting protein. The two proteins share 94 % amino acid identity. Both associate ligand-dependently with classical NRs such as RAR, ER and PR *in vivo*. GRIP has been also shown to enhance NR receptor activity through the AF-1 domain in addition to that of the helix 12 [Ma *et al.*, 1999].

2.5.1.1.3 RAC3

The third member of the family was discovered simultaneously by several groups as a RAR-interacting (RAC3), a CBP-interacting (p/CIP), a hRARβ-stimulatory protein (ACTR), a gene amplified in breast cancer (AIB-1) and a TR-interacting protein (TRAM-1) [Anzick *et al.*, 1997; Chen *et al.*, 1997; Li *et al.*, 1997; Takeshita *et al.*, 1996; Torchia *et al.*, 1997]. RAC3/ACTR/AIB-1/TRAM represent the

human protein whereas p/CIP is the mouse orthologue. In addition to the interactions and coactivation of many NRs, p/CIP has been shown to enhance the activity of interferon-α and cAMP regulatory element binding protein (CREB), suggesting the involvement of this CoA in multiple signaling pathways [Torchia *et al.*, 1997]. Furthermore, RAC3/TRAM-1 expression can be upregulated by hormone treatment, which is another possible mechanism, how CoAs can potentiate hormone action [Li *et al.*, 1998; Misiti *et al.*, 1998].

Table 2.4 The diversity of coactivators.

Function	Coactivator	
	Abbreviation	**Name**
Histone acetyltransferases	SRC-1	Steroid receptor coactivator-1
	TIF2	Transcription intermediary factor 2
	RAC3	Receptor-associated coactivator 3
	p300	300-kD protein
	CBP	cAMP-response-element-binding (CREB)-binding protein
Histone methyltransferases	CARM1	Coactivator-associated arginine methyltransferase 1
	PRMT1	Protein arginine methyltransferase 1
Receptors or general transcription-factor-bridging factor	TRAP220	Thyroid-hormone-receptor-associated protein of 220 kDa
Chromatin remodeling	Brg1	Brahma-related gene 1
Ubiquitin proteasome pathway	RPF1	Receptor potentiating factor 1
	E6-AP	E6-associated protein
	UbcH7	Ubiquitin conjugating enzyme 7
	TRIP1-mSUG1	Suppressor of Gal4-thyroid hormone interacting protein 1
	MIP224	MB67-interacting protein 224
	TBP-1	TATA-binding protein-1
Splicing control	PGC-1	PPARγ coactivator-1
	CoAA	Coactivator activator
	p72	72-kDa protein
	TRBP/AIB3	Thyroid-hormone-receptor-binding-protein/amplified in breast cancer 3
	CAPER	Coactivator of activating protein-1 (AP-1) and estrogen receptors
	P54nrb	Nuclear RNA-binding protein p54
	p102	U5 small nuclear ribonucleoprotein particle-binding protein
Signal-integrating coactivators	SRC-1	Steroid receptor coactivator-1
	TIF2	Transcription intermediary factor 2
	RAC3	Receptor-associated coactivator 3
	PGC-1	PPARγ coactivator-1
	TORC2	Transducer of regulated CREB activity 2

2.5.1.2 Functional domains and the LXXLL motif of the SRC CoA family

The SRC family shares a common domain structure (Fig. 2.8), the most conserved N-terminal basic loop-helix-loop (bHLH)-PAS domain, which functions in many proteins especially in transcription factors as a DNA-binding or heterodimerization domain. The PAS motif is also found in several transcription factors such as Period (Per), Aryl hydrocarbon receptor (AhR) and single-minded (Sim). Although similar to the bHLH domain, the PAS domain (Fig. 2.8) plays also an important role in protein-protein interaction and dimerization. The function of these domains in SRC CoAs remain unknown, though it probably mediates intra- or intermolecular interactions. The bHLH-PAS domain is followed by a centrally located receptor interaction domain (RID) and C-terminal transcriptional activation domain (AD). The RID mediates ligand-dependent, direct interacions with NRs [Li *et al.*, 1998; Oñate *et al.*, 1995; Voegel *et al.*, 1996]. The detailed protein sequence analysis of this domain identified a conserved LXXLL motif. This motif is also often called the NR box [Heery *et al.*, 1997].

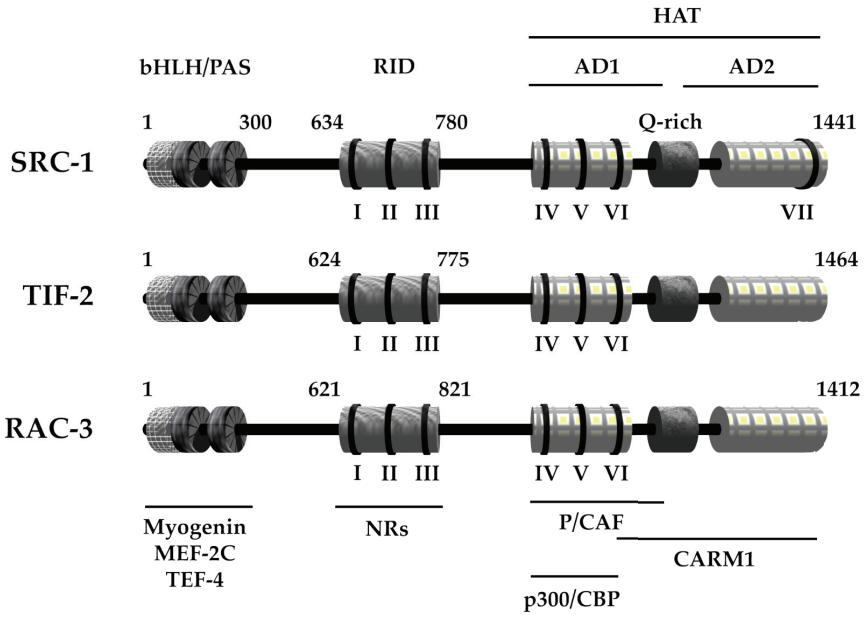

Fig. 2.8 A representation of the functional domains found in the p160 family of CoAs. The functional domains of the three p160 CoA family members (SRC-1, TIF-2 and RAC-3) are visualized in cylindrical representation. The basic helix-loop-helix (bHLH) and the PAS heterodimerization domains are located within the first 300 amino acid residues on the N-terminus. It allows the CoAs to interact with proteins such as myogenin, MEF-2C and TEF-4. The NR RID is placed in the middle part of the proteins. Other domains (AD1 and AD2) also contain protein interaction motifs. SRC1 contains an additional interaction motif in the AD2 domain. The LXXLL motifs are numbered with Roman numerals (I-VII). The activation domains (AD1 and AD2) serve for interaction also with HATs. The other possible protein-protein interactions (P/CAF, CARM1 and p300/CBP) are shown with black lines.

The SRC family of CoAs has three LXXLL motifs, with additional, non-conserved NR boxes present at different locations outside the RID (Fig. 2.8). Peptide competition assays and site-directed mutagenesis experiments provided a solid evidence for the requirement of LXXLL motifs in interaction with the LBDs of NRs [Ding *et al.*, 1998; Heery *et al.*, 1997; Torchia *et al.*, 1997]. In addition, protein structure prediction and crystallographic analysis have shown that LXXLL motifs form amphipathic α-helices with the hydrophobic leucines on one side of the helix. This α-helix is then able to interact efficiently with helix 12 of the NR's LBD. In addition, the interacting surface of NR includes helices 3, 4 and 5, which actively participate in creation of a LXXLL compatible hydrophobic groove where the CoA interaction motif can fit [Darimont *et al.*, 1998; Feng *et al.*, 1998; Nolte *et al.*, 1998; Shiau *et al.*, 1998; Torchia *et al.*, 1997]. One of the most interesting aspects of NR box function is that different NRs prefer different NR boxes of RID for interaction with CoAs [Darimont *et al.*, 1998; Ding *et al.*, 1998; Leers *et al.*, 1998; McInerney *et al.*, 1998].

2.5.2 CoRs

In general, CoRs are proteins, which can mediate gene silencing through interaction with transcription factors that bind to DNA. Several NRs, including RAR, TR and VDR, appear to bind to their target genes in the absence of ligand and actively repress transcription. In majority of the cases the interaction partner for these receptors is NCoR or its homolog SMRT, which were the first identified CoRs for NRs [Chen *et al.*, 1995; Hörlein *et al.*, 1995]. They are the best-characterized CoRs and they also share high functional and structural similarities (Fig. 2.9). Since then, several other CoRs for NRs that differ clearly from NCoR and SMRT have been isolated. These include Alien [Dressel *et al.*, 1999], SUN-CoR [Zamir *et al.*, 1997], Rip140 [Cavailles *et al.*, 1995], Hairless [Potter *et al.*, 2001] and SMRTER [Tsai *et al.*, 1999] (Table 2.5).

Table 2.5 The NR corepressors.

Corepressor		
Name	**Abbreviation**	**Function**
NR corepressor 1	NCoR	Development Differentiation
Silencing mediator for retinoid and thyroid hormone receptors	SMRT	Development Differentiation
Thyroid hormone receptor interactor 15	Alien (TRIP15)	Development Differentiation
Small unique NR corepressor	SUN-CoR	Development Differentiation
Homolog of mouse hairless	Hairless	Hair development

SMRT, NCoR and other CoRs harbor several domains that are critical for their function (Fig. 2.9). There are at least three repressor domains (RDs), which mediate

the repression function of the CoRs, since they are critical for contacting the proteins with additional properties important for the silencing of the target genes. One of these properties is histone deacetylation, which acts to reverse the effects of CoAs

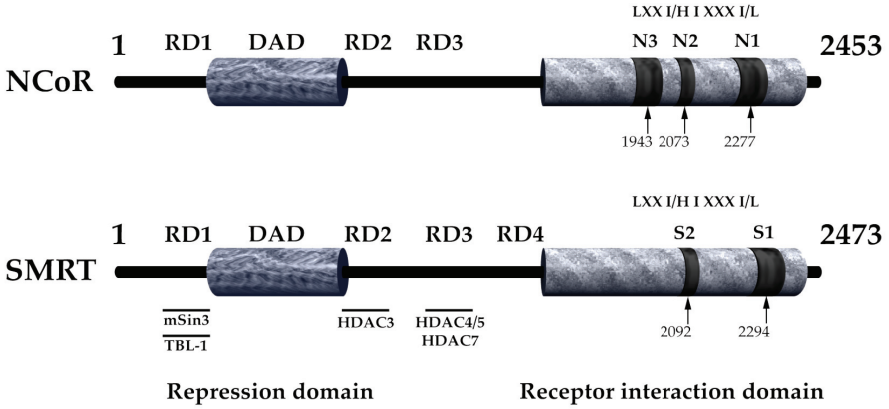

Fig. 2.9 Functional domains in the CoRs NCoR and SMRT. The primary structure of NCoR and SMRT is sketched from N- to C-terminus. The functional domains are visualized in cylindrical representation. The location of the repression domains (RD1 to RD4) and deacetylase-activating domain (DAD) are indicated within each CoR. These domains allow the CoRs to interact with histone deacetylases (HDAC3, HDAC4/5 and HDAC7) and they are crucial for their function. The CoRNR box/NR interaction sites (N1, N2, and N3 in NCoR verses S1 and S2 in SMRT) that contain the LXX(I/H)IXXX(I/L) motifs are indicated within each corepressor schematically in dark cylinders. Transducin beta-like protein 1 (TBL1), which is part of the repression complex, interacts with the RD1 domain. *In vivo*, TBL1 is bridged to HDAC3 through SMRT and can potentiate repression by NRs such as TR. With the same domain, SIN3 is able to interact and thus serves as a scaffold on which the corepressor complex assembles, since it contains multiple protein-protein interaction domains.

like the SRC family members. The C-terminal domain of SMRT and NCoR contains two or three receptor interacting domains (RIDs) crucial for their interaction with NRs (Fig. 2.9). The primary structure of the CoR RID resembles that of the LXXLL motif of CoAs. However, it has an extended α-helical motif with the consensus sequence LXXI/HI XXXI/L (L = leucine, I = isoleucine, H = histidine, X = any amino acid) [Perissi *et al.*, 1999].

NCoR and SMRT are mainly localized in the nucleus. Recent findings, however, suggest that changes in signaling at the cell surface can activate second messenger systems leading to posttranslational modification, such as phosphorylation of these proteins that can induce nuclear-cytoplasmic shuttling of the CoRs. In the case of SMRT, MAPK-directed phosphorylation has been implicated [Hong *et al.*, 2001]. For NCoR the phosphorylation of an associated protein, TAB2, by IKK kinase has been reported to induce nuclear exit [Baek *et al.*, 2002].

2.5.2.1 The role of CoRs in transcription repression

NCoR and SMRT have distinctly different properties when they are bound to NRs in solution, on DNA, and on target gene promoters in living cells [Hu *et al.*, 2001; Ishizuka *et al.*, 2003; Makowski *et al.*, 2003; Webb *et al.*, 2000; Zamir *et al.*, 1997]. They also function as CoRs for other transcription factors [Xu *et al.*, 1998]. The apparent evidence of non-redundant functions and the irreplaceable role of NCoR and SMRT comes from the knockout mouse model of NCoR, which is embryonic lethal [Jepsen *et al.*, 2000], indicating that SMRT cannot compensate for the lack of NCoR. The physiological importance of CoRs has been demonstrated by analyzing the association between CoR dysfunctions and disease states in mice and humans. For example, in the syndrome resistance to thyroid-hormone (RTH) mutated TRβ fails to release CoRs in response to physiological concentrations of the hormone. Therefore, dysfunctional gene activation through TRβ is causing an abnormal physiological state [Tagami *et al.*, 1997; Yoh *et al.*, 1997]. NR CoRs have also been implicated in the mechanisms of human diseases, including acute promyelocytic leukemia due to RAR translocations [Grignani *et al.*, 1998; Guidez *et al.*, 1998; He *et al.*, 1998], acute myeloid leukemia due to the AML1-ETO translocation [Gelmetti *et al.*, 1998; Lutterbach *et al.*, 1998; Wang *et al.*, 1998], and insulin resistance due to mutations in PPARγ [Gurnell *et al.*, 2000]. Furthermore, NCoR and/or SMRT have been connected with cancer. In studies where chimeric NCoR-ER proteins were created it has been shown that they lack transcriptional activity and inhibit ER-mediated transcription in T47D and MDA-MB-231 breast cancer cells. The chimeric proteins also repressed the growth of T47D cells when delivered to the cells by a retroviral vector. In addition, it has been shown that decreased levels of NCoR correlate with the acquisition of tamoxifen resistance in a mouse model system for human breast cancer [Lavinsky *et al.*, 1998].

2.6 The activation and inactivation of NRs from a structural perspective

2.6.1 Active and inactive conformations of human PPARα

The superimposition of the agonist- and antagonist- bound PPARα structure shows that the CoR binding site partially overlaps with the CoA binding site [Xu *et al.*, 2002] (Fig. 2.10). Compared to the CoA motif LXXLL, the CoR motif LXXI/HIXXXI/L has one additional α-helical turn. This additional turn binds to the same region on the surface of the NR-LBD that is occupied by helix 12 in the agonistic conformation of the LBD. Therefore, the repositioning of the helix 12 is necessary to allow the binding of the larger CoR motif and to prevent the folding back of the helix 12 to its active conformation.

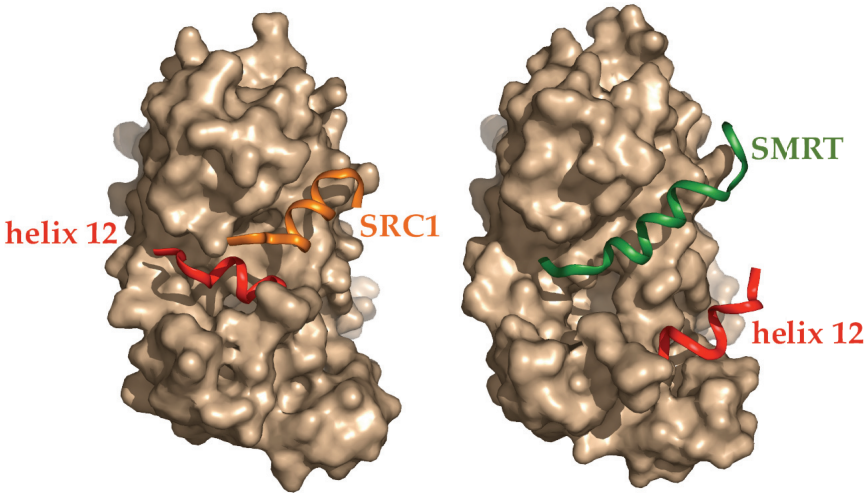

Fig. 2.10 Crystal structures of human PPARα LBDs co-crystalized with SRC1 and SMRT peptides. The crystal structures of PPARα in active (1KL7) and inactive (1KKQ) conformations are shown. The surface of the LBD is displayed in green color. The active conformation shows the helix 12 (red) as it is fixed to the body LBD and CoA peptide from SRC1 (orange color) can bind. Inactivation involves the repositioning of helix 12 (red color) creating a hydrophobic groove where the CoR SMRT (green color) can bind. The two crystal structures show that the binding surfaces for CoA and CoR overlap.

In the crystal structure of PPARα LBD bound with antagonist, GW6471, adopts a U-shaped conformation and wraps around C276 of helix 3. The amide head group modification of GW6471 prevents the establishment of the hydrogen bond with Y464, the conserved tyrosine contact point in helix 12 of all PPAR isoforms. Moreover, this ligand extends to the space, which is normally occupied by Y464 and thereby abrogates the stable position of the helix 12 in the agonist-bound conformation [Xu *et al.*, 2002]. However, unlike in the case of ER bound to antagonist, the helix 12 does not occupy the CoA binding groove, but it is loosely packed against helix 3. Although there is an overlap between the binding spaces of CoAs and CoRs there are some differences in the binding interfaces. First, the SMRT LXXXIXXXL motif overlays 736 $Å^2$ of Connolly surface of PPARα whilst the SRC-1 buries only 478 $Å^2$ suggesting the preferable binding of CoRs' interaction motif in the presence of antagonist over the smaller CoA motif. Second, CoR is anchored to PPARα LBD by three hydrogen bonds between the C-terminal carbonyl and the conserved K292 from helix 3, which also interacts with the CoA. Finally, the three-turn α-helical RID of CoR deviates from the regular α-helix, which helps the motif to make hydrophobic interactions with the receptor.

The GW409544 agonist-bound human PPARα structure shares the classical properties of the NR LBDs with its helical sandwich and a four-stranded β-sheet [Xu *et al.*, 2001]. GW409544 adopts a U-shape conformation and its acidic head group

forms hydrogen bonds with Y314 (helix 5) and Y464 (helix 12). This bridg e stabilizes the C-terminus of the LBD in the active conformation allowing the formation of the charge clamp between E462 and K292, directing the LXXLL motif of the CoA to the hydrophobic cleft on the surface of the receptor. The amide group from the tyrosine nitrogen of GW409544 is buried in the part of the pocket created by helices 3, 6 and 10. The rest of the ligand wraps around helix 3 and the phenyloxazol tail faces the helices 2′, 3 and the β–sheet [Xu *et al.*, 2001].

From both structures it is obvious that the balance between CoA and CoR binding is tightly modulated by the position of helix 12. Helix 12 senses the presence of different ligands and recruits CoAs or CoRs that either activate or repress transcription.

2.6.2 Active and inactive conformations of mouse CAR

Unlike the PPARα antagonist GW6471, androstanol does not contain any side chain or other modification on its steroid backbone and thereupon it cannot extrude helix 12 from its active conformation by creating a steric tension.

The molecular mechanism of the conformation change when androstanol is in the pocket of LBD depends on the presence of the specific "kink" between helices 10 and 11 (Fig 2.11). Intriguingly, the conformation of the helices 10 and 11 in the androstanol-bound mouse CAR resembles the inactive apo conformations of classical NRs. Although this arrangement of helices 10 and 11 is present in the inactive mouse CAR crystal structure, it is missing from the TCPOBOP agonist-bound mouse CAR structure. The important existence of this kink is based on the hydrogen bond between E339 and the backbone amide of Q245 that holds the kink in its position (Fig 2.11). This interaction is considered to be important because it is conserved in many NRs such as ERα, LXRα, ERRγ, RARα, PR, VDR, and TR. This kink has an important role in fixing helices 10 and 11 to the loop between helices 6 and 7. This fixation plays an important role in fortification of certain parts of ligand-binding pocket. In the TCPOBOP-bound mouse CAR structure, E339 can potentially interact with the ligand. However, no such interaction can be seen for androstanol [Shan *et al.*, 2004]. The dynamic properties of activation and inactivation of CAR are largely different from PPARα LBD dynamics. Since the inactive mouse CAR was not crystallized in the presence of CoR peptide, it is not possible, at this point, to make any comparisons between the binding modes of CoA and CoR.

2.6.3 NR ligand classification

NR ligands can be classified into two main groups according to what conformation of the LBD they are inducing and stabilizing. In the first group there are agonists, which stabilize the receptor in an active conformation and thus promote

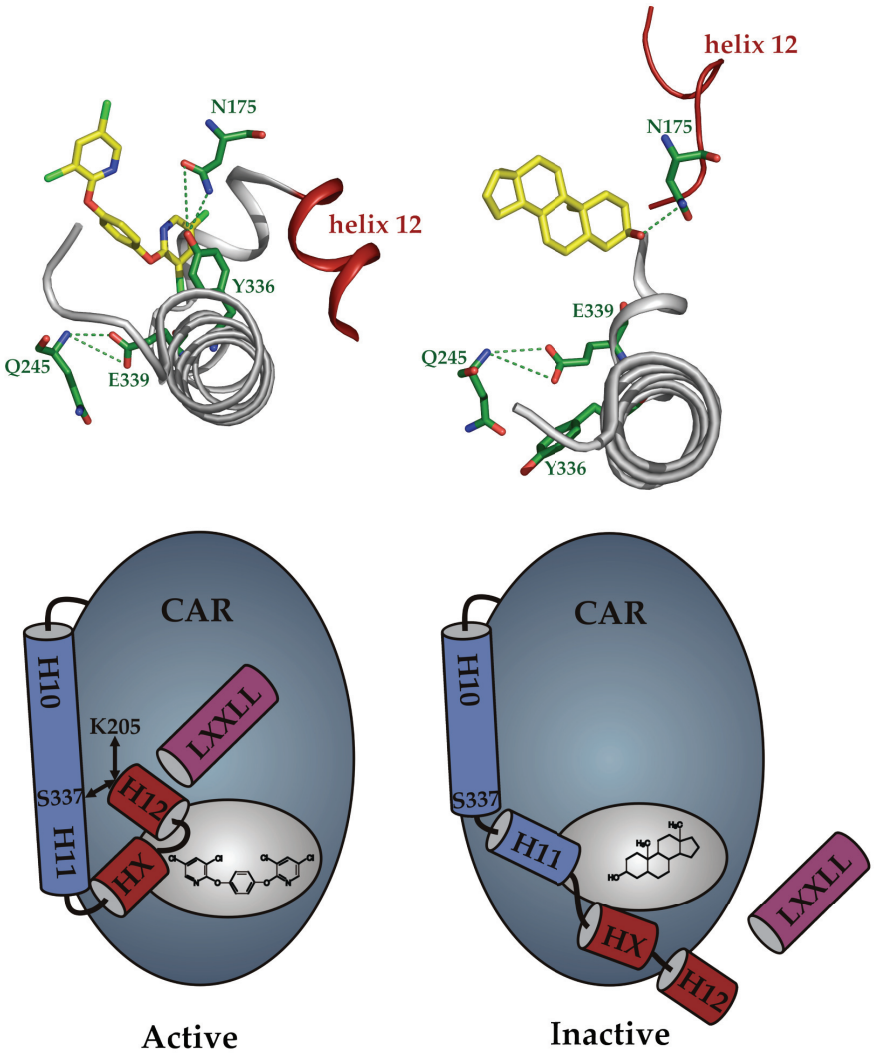

Fig. 2.11 Crystal structures and schematic representations of mouse CAR LBDs in the active and inactive conformations. Crystal structures of superagonist TCPOBOP (yellow, left) and inverse agonist androstanol (yellow, right) bound protein structures are shown (upper part). The hydrogen bond interaction between Q245 (helices H6-H7) E339 (helices H10-H11) represents the "kink" that is responsible for the molecular mechanism of inactivation via androstanol. The two additional residues Y336 and N175 displayed in the figure are responsible for ligand recognition. The helix H12 is highlighted in red color. The lower figures represent the two conformations in schematic views. In the active conformation the helices H10-H11 form a compact unit (left side) that is upon the binding of andostanol divided to two helices H10 and H11. This conformational change creates tension, which is released via a repositioning of the helix H12. Since CoAs are unable to bind to the LBD they dissociated allowing the CoR to bind instead of it.

the association of the LBD with CoAs. A typical example of this group is the natural ligand of VDR, $1\alpha,25(OH)_2D_3$, or TCPOBOP in the case of mouse CAR. In addition, these ligands disable the interaction of the receptor with CoRs. The second group

represents the inverse agonists and antagonists that support the interaction of the receptor with CoRs and thereby stabilize the receptor in an inactive conformation. ZK168281, a VDR antagonist, and a mouse CAR inverse agonist, androstanol, belong to this group. In the presence of these ligands, CoAs are unable to bind to the receptor [Lempiäinen *et al.*, 2005; Peräkylä *et al.*, 2004].

2.6.4 NR ligand classification

NR ligands can be classified into two main groups according to what conformation of the LBD they are inducing and stabilizing. In the first group there are agonists, which stabilize the receptor in an active conformation and thus promote the association of the LBD with CoAs. A typical example of this group is the natural ligand of VDR, $1\alpha,25(OH)_2D_3$, or TCPOBOP in the case of mouse CAR. In addition, these ligands disable the interaction of the receptor with CoRs. The second group represents the inverse agonists and antagonists that support the interaction of the receptor with CoRs and thereby stabilize the receptor in an inactive conformation. ZK168281, a VDR antagonist, and a mouse CAR inverse agonist, androstanol, belong to this group. In the presence of these ligands, CoAs are unable to bind to the receptor [Lempiäinen *et al.*, 2005; Peräkylä *et al.*, 2004].

From the physiological point of view NR agonists are compounds that bind to a receptor, activate them and trigger a response in the cell. Antagonists also bind to a receptor, but they fail to activate it and actually block the activation by agonists competing for the binding site in the ligand-binding pocket. Interestingly, the overall effect when an antagonist is administered together with an agonist is less than the sum of their individual effects. The terms agonist and antagonist are often inappropriate for the description of NR ligands, since many of them may function as agonists in certain tissues but as antagonists in others [Weatherman *et al.*, 1999].

Chapter 3

Aims of the Study

Some major areas of uncertainty concerning the structure-function relationship of PPARs, CAR and VDR LBDs were not investigated in detail. In addition, the molecular mechanisms of some structural features in the LBDs of these receptors were unknown.

Therefore the specific aims of the study were:

1. To investigate the mechanism of the constitutive activity in human and mouse CAR.
2. To study specific ligand selective conformational changes in human and rat VDR to explain species-specific ligand effects.
3. To investigate the mechanism of ligand independent CoA interaction of human PPARs leading to recognition of their constitutive activity.
4. To study the antagonist- and inverse agonist-triggered conformational changes in the LBDs of human VDR, human and mouse CAR.
5. To investigate the mechanism of superagonism of the ligands with high affinity for human VDR.

Chapter 4

Materials and Methods

The detailed description of material and methods can be found in the original articles referred to by their Roman numerals (**I-V**).

4.1 NR ligands

Table 4.1 NR ligands used in the studies.

Compound	NR	Functional property	Source	Used in
1α,25(OH)$_2$D$_3$	VDR	agonist	Dr. L. Binderup, LEO Pharma, Ballerup, Denmark	**I-V**
Androstanol	mCAR	inverse agonist	Steraloids, Newport, RI, USA	**IV**
CITCO	hCAR	agonist	Biomol, Copenhagen, Denmark	**I, III, IV**
Clotrimazole	hCAR	inverse agonist	Sigma-Aldrich, St. Louis, MO, USA	**IV**
Gemini	VDR	agonist	Dr. M. Uskokovic, BioXell Inc., Nutley, NJ, USA	**V**
Ro43-83582	VDR	agonist	Dr. M. Uskokovic, BioXell Inc., Nutley, NJ, USA	**V**
L783483	PPARδ	agonist	Dr. M.W. Madsen, Leo Pharma, Ballerup, Denmark	**III**
MC1288	VDR	agonist	Dr. L. Binderup, LEO Pharma, Ballerup, Denmark	**V**
Rosiglitazone	PPARγ	agonist	Dr. M.W. Madsen, Leo Pharma, Ballerup, Denmark	**III**
TCPOBOP	mCAR	agonist	Dr. P. Honkakoski, University of Kuopio, Finland	**I, IV**
TEI-9647	VDR	antagonist	Dr. S. Ishizuka, Teijin Institute for Biomedical Research, Tokyo, Japan	**II**
WY14643	PPARα	agonist	Dr. P. Honkakoski, University of Kuopio, Finland	**IV**
ZK168281	VDR	antagonist	Dr. A. Steinmeyer, Schering AG, Berlin, Germany	**II, IV**

Long term stocks of 1α,25(OH)$_2$D$_3$, Gemini, Ro43-83582, MC1288, TEI-9647 and ZK168281 were dissolved in 2-propanol; whereas the other compounds were dissolved in DMSO. Further dilutions were made in DMSO (for *in vitro* assays) or in ethanol (for cell culture assays).

4.2 DNA constructs

4.2.1 Mammalian expression constructs for full-length NRs and cofactors

T7 RNA polymerase-driven mammalian expression vectors were used for mutagenesis, *in vitro* transcription/translation of the respective cDNAs and the over-expression of the respective proteins in mammalian cells. The full-length cDNAs for human CAR [Baes *et al.*, 1994], human VDR [Carlberg *et al.*, 1993], human RXRα [Mangelsdorf *et al.*, 1990], human PPARα [Sher *et al.*, 1993], PPARδ [Schmidt *et al.*, 1992] and PPARγ_2 [Tontonoz *et al.*, 1994] were previously sub-cloned into the T7/SV40 promoter-driven pSG5 (Stratagene) or pcDNA3.1 (Invitrogen) mammalian expression vectors (Table 4.2). The full-length cDNA for mouse CAR [Choi *et al.*, 1997] was already sub-cloned into the T7/CMV promoter-driven pCMX [Umesono *et al.*, 1991] expression vector (Table 4.2). The full cDNA of NCoR [Hörlein *et al.*, 1995] was previously sub-cloned to the pCMX [Umesono *et al.*, 1991] eukaryotic expression vector.

4.2.2 GST-fusion protein overexpressing constructs

The NR interaction domain of mouse SRC-1 (amino acids 596 to 790), human TIF2 [Voegel *et al.*, 1996] (amino acids 646 to 926), human RAC3 (amino acids 673 to 1106) and mouse NCoR [Hörlein *et al.*, 1995] (amino acids 1679 to 2453), were previously subcloned into the GST fusion vector pGEX-KGK or pGEX-AHK (Amersham Biosciences). The GST fusion protein constructs were used for supershift assays (Table 4.2).

4.2.3 Reporter gene constructs

The core sequences of the REs are indicated in the original articles (**I**, Fig. 1A, **IV**, Fig. 2A). The REs were each cloned immediately upstream of the *thymidine kinase* (*tk*) promoter driving the firefly *luciferase* gene (LUC) in a derivate of the pGL3 *Luciferase* Reporter Vector (Promega) (Fig. 4.1). The *Xba*I-restriction site at nucleotide position 1742 was removed from the original vector by mutagenesis. All constructs were verified by sequencing (for details, see Section Manual sequencing 4.4).

Table 4.2 List of NR and cofactor constructs used in the studies.

Construct	Expression vector	NR cDNA	Cloning site	Used in
pSG5-hCAR	pSG5	hCAR	*Bam*HI	**I, III, IV**
pSG5-hVDR	pSG5	hVDR	*Bam*HI/*Hind*III	**I- V**
pSG5-hRXRα	pSG5	hRXRα	*Eco*RI/*Bgl*II	**I-IV**
pSG5-hPPARα	pSG5	hPPARα	*Eco*RI, *Xba*I	**III**
pcDNA3.1-hPPARδ	pcDNA3.1	hPPARδ	*Kpn*I, *Bam*HI	**III**
pSG5-hPPARγ$_2$	pSG5	hPPARγ$_2$	*Kpn*I, *Xba*I	**III**
pCMX-mCAR	pCMX	mCAR	*Bam*HI	**I, IV**
pCMX-mNCoR$^{1\text{-}2453}$	pCMX	NCoR$^{1\text{-}7359}$	*Not*I, *Sal*I	**III, IV**
pGEX-mSRC-1$^{596\text{-}790}$	pGEX-KGK	mSRC-1$^{1786\text{-}2368}$	*Bam*HI/*Hind*III	**I, III**
pGEX-hTIF2$^{646\text{-}926}$	pGEX-KGK	hTIF2$^{1938\text{-}2778}$	*Bam*HI/*Hind*III	**I-V**
pGEX-hRAC3$^{673\text{-}1106}$	pGEX-KGK	hRAC3$^{2017\text{-}3316}$	*Bam*HI/*Hind*III	**I, III**
pGEX-mNCoR$^{1679\text{-}2453}$	pGEX-AHK	mNCoR$^{5073\text{-}7359}$	*Noc*I/*Not*I	**IV**

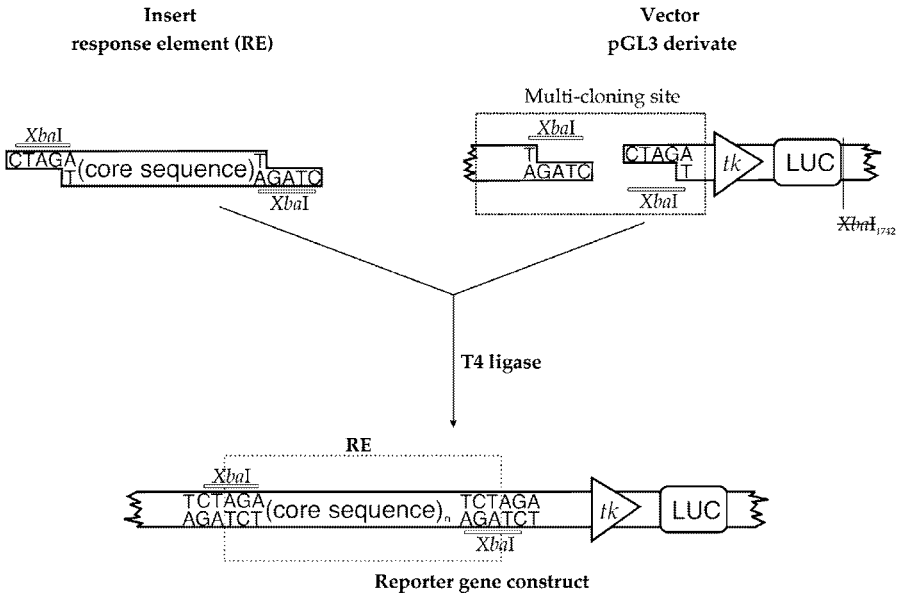

Fig. 4.1 Cloning strategy for the reporter constructs. Double-stranded annealed oligonucleotides containing the core sequence of the RE and the target vector pGL3 were digested with *Xba*I. The insert and vector were ligated together with T4-ligase and the construct was verified by manual sequencing.

4.3 Mutagenesis

4.3.1 Site-directed mutagenesis

The protein expression constructs pSG5-hCAR, pCMX-mCAR, pSG5-hVDR and pSG5-PPARγ_2 were used as a template for site-directed mutagenesis using the QuickChange™ Site-Directed Mutagenesis Kit (Stratagene). The mutants were created by changing the chosen amino acid residues separately into the mutated ones, as described by the manufacturer. In general, we used the widely accepted Ala scan, but in case of some particular amino acids such as Y501 for PPARγ the mutant Y501F was created in order to test the role of the phenylalanine's hydroxyl moiety. I other cases the aim was either to increase the hydrophobicity of a certain region (VDR_{Y401I}), charge inversion in both NR (VDR_{K264E}) and CoR ($NCoR_{E2278K}$) to test the functionality of the ionic interaction or introducing rodent-specific amino acids into the human receptor (VDR_{C410N}). All oligonucleotides for mutagenesis were purchased from MWG Biotech AG. The cDNAs of the clones were purified with Qiagen Plasmid Kit (Qiagen) and each point mutation was confirmed by sequencing (for details, see Section Manual sequencing 4.4).

4.3.2 Generation of helix 12 deletion mutants

The helix 12 deletion mutants of human VDR, human CAR and human PPARγ_2 were created using the site-directed mutagenesis protocol (see Section Side-directed mutagenesis 4.3.1) by introducing a stop codon at amino acid position 413, 342 and 492, respectively (Table 5.3). All three mutants were confirmed by sequencing (see Section Manual sequencing 4.4).

4.3.3 Helix 12 extension NR mutants

The site-directed mutagenesis protocol (see Section Side-directed mutagenesis 4.3.1) was used for the preparation of the helix 12-extension mutants of human and mouse CAR. The original stop codon and the following six nucleotides were mutated to three triplets that each translate into alanine. A new stop codon was introduced after this sequence (Table 4.3). Both helix 12 extension mutants were confirmed by sequencing (see Section Manual sequencing 4.4).

Table 4.3 Mutated NRs and CoR used in the studies.

Mutation	Template vector	Amino acid residue change	Position	Used in
$pSG5\text{-}hCAR_{K177A}$	pSG5-hCAR	Lys to Ala	177	**I, IV**
$pSG5\text{-}hCAR_{K195A}$		Lys to Ala	195	**I, IV**
$pSG5\text{-}hCAR_{K195E}$		Lys to Glu	195	**IV**

pSG5-hCAR$_{I322A}$		Ile to Ala	322	**I**
pSG5-hCAR$_{Y326A}$		Tyr to Ala	326	**I, IV**
pSG5-hCAR$_{I330A}$		Ile to Ala	330	**I**
pSG5-hCAR$_{\Delta H12}$		helix 12 deletion	342	**I**
pSG5-hCAR$_{L343A}$		Leu to Ala	343	**I, IV**
pSG5-hCAR$_{E345A}$		Glu to Ala	345	**I**
pSG5-hCAR$_{C347A}$		Cys to Ala	347	**I, IV**
pSG5-hCAR$_{H12+3AA}$		helix 12 extension		**I, IV**
pCMX-mCAR$_{K187A}$	pCMX-mCAR	Lys to Ala	187	**IV**
pCMX-mCAR$_{K205A}$		Lys to Ala	205	**I, IV**
pCMX-mCAR$_{K205E}$		Lys to Glu	205	**IV**
pCMX-mCAR$_{L332A}$		Leu to Ala	332	**I**
pCMX-mCAR$_{Y336A}$		Tyr to Ala	336	**IV**
pCMX-mCAR$_{I340A}$		Ile to Ala	340	**I**
pCMX-mCAR$_{L353A}$		Leu to Ala	353	**I, IV**
pCMX-mCAR$_{C357A}$		Cys to Ala	357	**IV**
pCMX-mCAR$_{H12+3AA}$		helix 12 extension		**I, IV**
pSG5-hVDR$_{F150A}$	pSG5-hVDR	Phe to Ala	150	**V**
pSG5-hVDR$_{K246A}$		Lys to Ala	246	**I, IV**
pSG5-hVDR$_{K264A}$		Lys to Ala	264	**IV**
pSG5-hVDR$_{K264E}$		Lys to Glu	264	**IV**
pSG5-hVDR$_{Y295A}$		Tyr to Ala	295	**V**
pSG5-hVDR$_{A303V}$		Ala to Val	303	**V**
pSG5-hVDR$_{L309A}$		Leu to Ala	309	**V**
pSG5-hVDR$_{L309F}$		Leu to Phe	309	**V**
pSG5-hVDR$_{H397A}$		His to Ala	397	**I, IV, V**
pSG5-hVDR$_{Y401A}$		Tyr to Ala	401	**I**
pSG5-hVDR$_{Y401I}$		Tyr to Ile	401	**I**
pSG5-hVDR$_{C403S}$		Cys to Ser	403	**II**
pSG5-hVDR$_{C410N}$		Cys to Asn	410	**II**
pSG5-hVDR$_{C403S/C410N}$		Cys to Ser Cys to Asn	403 410	**II**
pSG5-hVDR$_{\Delta H12}$		helix 12 deletion	413	**I**
pSG5-hVDR$_{V418A}$		Val to Ala	418	**I, IV**
pSG5-hVDR$_{V418L}$		Val to Leu	418	**I**
pSG5-hVDR$_{E420A}$		Glu to Ala	420	**I**
pSG5-hVDR$_{F422A}$		Phe to Ala	422	**I, V**
pSG5-hVDR$_{N424*}$		truncation	424	**IV**
pSG5-hVDR$_{S427A}$		Ser to Ala	427	**IV**
pSG5-hVDR$_{Y401I/V418L}$		Tyr to Ile Val to Lau	401 418	**I**
pSG5-PPAR$\gamma_{2\ K329A}$	pSG5-PPARγ_2	Lys to Ala	329	**III**
pSG5-PPAR$\gamma_{2\ K347A}$		Lys to Ala	347	**III**
pSG5-PPAR$\gamma_{2\ H351A}$		His to Ala	351	**III**
pSG5-PPAR$\gamma_{2\ E352A}$		Glu to Ala	352	**III**

pSG5-PPARγ$_{2\ Y355A}$		Tyr to Ala	355	**III**
pSG5-PPARγ$_{2\ D424A}$		Asp to Ala	424	**III**
pSG5-PPARγ$_{2\ R425A}$		Arg to Ala	425	**III**
pSG5-PPARγ$_{2\ R471A}$		Arg to Ala	471	**III**
pSG5-PPARγ$_{2\ H477A}$		His to Ala	477	**III**
pSG5-PPARγ$_{2\ E499A}$		Glu to Ala	499	**III**
pSG5-PPARγ$_{2\ Y501A}$		Tyr to Ala	501	**III**
pSG5-PPARγ$_{2\ D503A}$		Asp to Ala	503	**III**
pSG5-PPARγ$_{2\ \Delta H12}$		helix 12 deletion	492	**III**
pSG5-PPARγ$_{2\ Y505A}$		Tyr to Ala	505	**III**
pSG5-PPARγ$_{2\ Y505F}$		Tyr to Phe	505	**III**
pGEX-NCoR$_{E2278K}$	pGEX-NCoR	Glu to Lys	2278	**IV**
pGEX-NCoR$_{K2283E}$		Lys to Glu	2283	**IV**

4.4 Manual sequencing

To confirm the desired mutants generated via site-directed mutagenesis (see Section 4.3) and also the cloned reporter gene constructs (see Section 4.2.4), manual sequencing was performed using a modified version of the dideoxy method [Sanger *et al.*, 1977]. For this purpose 20 µl of template DNA (2-3 µg) was denatured by incubation with 1 µl of 10 M NaOH for 15 min at room temperature. Denatured plasmids were precipitated using 4 µl of 7.5 M NH_4Ac and 40 µl of 96 % ethanol. The samples were centrifuged for 15 min at 20000 x g and the pellets were subsequently washed with 100 µl of 70 % ethanol and centrifuged for further 7 min at 20000 x g. Afterwards the plasmid templates were dried and dissolved in 10 µl 1x MultiCore buffer (25 mM Tris, pH 7.8; 10 mM MgAc; 1 mM DTT; 100 mM KAc) including 200 ng of the respective sequencing primer. Annealing was performed by first incubating for 5 min at 75 °C and then the samples were cooled down to room temperature (annealing-mixture). To the annealing mixture was then added 2.5 µl of sequencing reaction mixture (2 µM dATP; 2 µM dGTP; 2 µM dTTP; 20 mM DTT; 1 µl T7 polymerase buffer and 2.5 U T7 DNA polymerase (Amersham); 0.3 µl [α-^{32}P]-dCTP (Hartmann Analytic)) and the samples were incubated for further 10 min at room temperature. The mixture was divided into four equal parts and 2.5 µl of the respective ddNTP-mix (50 mM NaCl; 80 µM each dNTP; 8 µM one ddNTP) was added to each of them. The reactions were incubated for 15 min at room temperature. To terminate the reaction, 4 µl of stop solution (95 % formamide; 20 mM ethylenediaminetetraacetic acid (EDTA); 0.05 % bromphenolblue; 0.05 % xylene cyanol) was added and DNA was denatured for 3 min at 95 °C before the samples were loaded into the gel. DNA fragments were resolved by electrophoresis through a 8 % denaturating polyacrylamide gel (7 M urea) in 1 x TBE buffer (90 mM Tris, pH 8.3; 90 mM boric acid; 2 mM EDTA). Gel images were captured on a Fuji FLA3000 reader using Image Gauge Software (Fuji).

4.5 *In vitro* transcription and translation

4.5.1 One-step *in vitro* translation

In vitro-translated wild type or mutated NR proteins were generated by a coupled *in vitro* transcription/translation [Craig *et al.*, 1992] using rabbit reticulocyte lysate as recommended by the supplier (Promega). The reaction volume of 50 µl contained the following components:

25 µl	rabbit reticulocyte lysate, nuclease treated (Promega)
10 µl	rNTPs (5 mM)
6 µl	$MgCl_2$ (25 mM)
1 µl	amino acid mix (1 mM each, Promega)
1 µl	RNasin (40 U/µl, Fermentas)
1 µl	T7 RNA-polymerase (20 U/µl, Fermentas)
5 µl	circular DNA template (400 ng/µl)

The reaction mixture was incubated for 90 min on 30 °C. Protein batches were quantified by test-translation in the presence of [^{35}S]-methionine. The specific concentration of the receptor proteins was adjusted to approximately 4 ng/µl after taking the individual number of methionine residues per protein into account. The translated proteins were either stored at -70 °C until further use or directly used in the appropriate assay.

4.5.2 Two-step *in vitro* translation

In vitro-translated wild type or mutated NR proteins were generated by two-step production procedure. The *in vitro* transcription was followed by translation using rabbit reticulocyte lysate as recommended by the supplier (Promega). The *in vitro* transcription reaction volume of 50 µl contained the following components:

3-5 µl	linearized DNA template (0.2-1 µg/µl)
5 µl	rNTPs (5 mM)
2 µl	T7 RNA-polymerase (20 U/µl, Fermentas)
1 µl	RNasin (40 U/µl, Fermentas)
10 µl	5x transcription buffer with $MgCl_2$

The reaction volume was adjusted to 50 µl by adding RNAse-free molecular biology grade water. The reaction mixture was incubated for 90 min at 37 °C. The yield and the quality of transcribed RNA was tested in 7 M urea containing PAGE, which was pre-run for 1 h at 200 V. To 5 µl of RNA mixture was added RNA loading

buffer, samples were ran in a gel, stained with ethidium bromide and visualized by UV trans-illuminator (260 nm). The synthesized RNA was stored at -20 °C, if not used immediately.

The *in vitro* translation reaction volume of 50 µl contained the following components:

35 µl	rabbit reticulocyte lysate, nuclease treated (Promega)
1 µl	amino acid mix (1 mM, Promega)
1 µl	RNasin (40 U/µl, Fermentas)
2-5 µl	transcribed RNA

The reaction volume was adjusted to 50 µl by adding RNAse-free molecular biology grade water. The reaction mixture was incubated for 90 min on 30 °C. Protein batches were quantified by test-translation in the presence of [^{35}S]-methionine. The specific concentration of the receptor proteins was adjusted to approximately 4 ng/µl after taking the individual number of methionine residues per protein into account. The translated proteins were either stored at -70 °C until further use or directly used in the appropriate assay.

4.6 Bacterial overexpression and purification of GST-fusion proteins

Fusion proteins, (GST-SRC1$^{596\text{-}790}$, GST-TIF2$^{646\text{-}926}$, GST-RAC3$^{673\text{-}1106}$ or GST alone (as a control)), were overexpressed in the bacterial system using *E.coli* BL21(DE3)pLysS strain (Stratagene) containing the respective expression plasmids. After the bacterial cultures reached an OD_{600} of 0.4-0.6 overexpression was stimulated with 0.25 mM isopropyl-β-D-thio-galactopyranoside for 3 h at 37 °C. The production of GST-NCoR$^{1679\text{-}2453}$ was stimulated with 1.25 mM isopropyl-β-D-thio-galactopyranoside for 5 h at 25 °C. The proteins were purified and immobilized on glutathione-Sepharose 4B beads (Amersham-Pharmacia) according to the manufacturer's protocol. GST-fusion proteins were then eluted in the presence of glutathione and concentrated using Millipore UFV5BGC00 centrifugal filter-tubes (Millipore Corporation). The required amount of GST-protein for the assays was defined empirically.

4.7 Limited protease digestion assay (LPD)

4.7.1 LPD of the VDR

In vitro-translated, [^{35}S]-labeled VDR protein (2.5 µl) was incubated with DMSO or ligand for 15 min at room temperature in 10 µl 50 mM Tris-HCl [pH 7.9]. Trypsin (Promega; final concentration 20 ng/µl) was then added and the mixtures were further incubated for 15 min at room temperature. The digestion reactions were stopped by adding 10 µl protein gel-loading buffer (0.25 M Tris, pH 6.8, 20 % glycerol, 5 % mercaptoethanol, 2 % SDS, 0.025 % bromophenol blue). The samples were denatured for 3 min at 95 °C and separated through 15 % SDS-polyacrylamide gels. The gels were dried, exposed to a Fuji MP2040S imager screen (Fuji) and monitored on a Fuji FLA3000 reader.

4.7.2 LPD of the PPARs and CAR

In vitro translated, [^{35}S]-labeled VDR, CAR, and PPARγ_2 (5 µl) were incubated with DMSO or ligand for 15 min at room temperature. Trypsin (Promega; final concentration 100 ng/µl) was then added and the mixtures were further incubated for 30 min at room temperature. The digestion reactions were stopped by adding 7.5 µl protein gel-loading buffer (0.25 M Tris, pH 6.8, 20 % glycerol, 5 % mercaptoethanol, 2 % SDS, 0.025 % bromophenol blue). The samples were denatured for 3 min at 95 °C and resolved through 15 % SDS-polyacrylamide gels. The gels were dried, exposed to a Fuji MP2040S imager screen and monitored on a Fuji FLA3000 reader.

4.8 Gel shift and supershift assays (EMSA)

For gelshift assays, *in vitro*-translated heterodimers were incubated with saturating concentrations of DMSO or receptor specific ligands for 15 min at room temperature in a total volume of 20 µl binding-buffer (10 mM Hepes [pH 7.9], 1 mM DTT, 0.2 µg/µl poly(dI-C) and 5 % glycerol). The concentration of the K^+ ions in the binding-buffer had been adjusted with KCl to 150 mM. In case of supershift assays 0.5-10 µg of bacterially expressed GST, GST-SRC1$^{597-791}$, GST-TIF2$^{646-926}$, GST-RAC3$^{673-1106}$ or GST-NCoR$^{1679-2453}$ protein and 1 ng (approximately 50000 cpm) of the [^{32}P]-labeled RE was added and incubation was continued for 15 min. Protein-DNA complexes were resolved through 8 % non-denaturing polyacrylamide gels in 0.5x TBE (45 mM Tris, 45 mM boric acid, 1 mM EDTA [pH 8.3]). The gels were dried, exposed to a Fuji MP2040S imager screen and monitored on a Fuji FLA3000 reader.

4.9 Cellular transfection and *luciferase* reporter gene assay

Human breast cancer (MCF-7) or human epithelial kidney (HEK293) cells were seeded onto 6-well plates (10^5 cells/ml) and grown overnight in phenol red-free Dulbecco's Modified Eagle Medium (DMEM) supplemented with 5 % charcoal-treated fetal bovine serum. DNA-DOTAP (N-[1-(2,3-dioleoyloxy)propyl]-N,N,N-trimethylammonium methylsulfate) liposomes were formed by incubating 1 μg of the reporter plasmid and in indicated cases 100 ng-1 μg of expression vector for the respective NR and/or cofactor or its mutants with 10 μg DOTAP (Roth) for 15 min at room temperature in a total volume of 100 μl. After dilution with 900 μl phenol red-free DMEM, the liposomes were added to the cells. Phenol red-free DMEM supplemented with 15 % charcoal-treated fetal bovine serum (500 μl) was then added 4 h after transfection. At this time, specific ligands were also added. The cells were lysed 16 h after onset of stimulation using the reporter gene lysis buffer (Roche Diagnostics) and the constant light signal *luciferase* reporter gene assay was performed as recommended by the supplier (Canberra-Packard). The *luciferase* activities were normalized with respect to protein concentration.

4.10 *In silico* methods

4.10.1 Structural analysis and visualizations of the protein structures

For visualization and structural analysis of crystal structures from the Protein Data Bank (PDB), MacPyMOL 0.98 and/or 0.99beta37 (DeLano Scientific LLC) and/or SwissPDB viewer (www.expasy.org/spdbv/) were used. The same software was used for the structures obtained from MD simulations.

4.10.2 Ligand-binding pocket volume calculations

For ligand-binding pocket calculations the Voidoo [Kleywegt *et al.*, 1994] software was used. The probe radius was set to 1.4 Å in the case of crystal structures obtained from the PDB databank or 1.9 Å in the case of structures obtained via MD simulations. For the mesh representation of the ligand-binding domains the grid value for plot files was set to 0.5 Å and for iso-surfaces to 0.2 Å. The obtained graphical representation EZD file output was converted with MAPMAN [Kleywegt *et al.*, 1996] to DSN6 FRODO format electron density maps. The maps were loaded, visualized and rendered in MacPyMOL 0.98 and/or 0.99beta37 (DeLano Scientific LLC).

4.10.3 Clustering of the amino acids using self-organizing maps (SOMs)

SOMs is an artificial neural network algorithm in the unsupervised learning category which is useful in the visualization and interpretation of large high-dimensional data sets [Kohonen, 1997]. A map consists of a regular grid of processing units, "neurons". A model of some multidimensional observation is first made, eventually a vector consisting of features, is associated with each unit. The map attempts to represent all the available observations with optimal accuracy using a restricted set of models. At the same time the models become ordered on the grid so that similar models move closer to each other and dissimilar models further from each other. In this study a version of the Visual Data software (Visipoint Oy), whose core is based on a variation of a self-organizing maps, called a tree-structured SOMs, was used [Koikkalainen, 1994]. The software implementation consists of several SOMs that are organized hierarchically in an inverted pyramid-like fashion in several layers. The number of neurons at a higher level is four times greater than the number found in the previous level. The data to which the SOMs was applied to consisted of a set with five variables, where to each single amino acid related 5 values representing a distance for 5 different ligands or conformations (MC1288, Gemini I and II, Ro43-83582 I and II) are assigned. All these values were used as the training pattern. At the beginning, each neuron of the SOM was randomly assigned a weight vector with five variables with a maximal starting resolution of 1024. The weight vectors of the best matching neuron and its neighbors are moved towards the values of the input vectors such that neurons come to represent a group of amino acids with similar dynamics. While the training proceeds, the adjustment of the weight vectors is diminished. Finally, each amino acid is placed into a neuron, which best describes its dynamic pattern and the value of the difference is displayed on each neuron as a bar graph. The resulting map with a matrix resolution 16x16 was then changed to 4x4 to exclude empty clusters from the matrix. Later a Sammon's mapping algorithm was applied to the matrix to visualize the clustered groups in 2D-space (see Section 4.10.4).

4.10.4 Visualization of the clustered SOMs using Sammon's mapping

The Sammon's mapping algorithm is part of the Visual Data software (Visipoint Oy). It is an iterative method based on a gradient search [Sammon, 1969]. The aim of the algorithm is to represent points in an n-dimensional space, usually in two-dimensions. The square neurons obtained after applying the SOM are replaced with round ones and located so that the distance between them represents the dissimilarity between them. The algorithm finds the location in the target space so that as much as possible of the original structure of the measurement vectors in the n-dimensional space is conserved.

Chapter 5

Results

5.1 Mechanism of the constitutive activity in human and mouse CAR and human PPARs (I and III)

5.1.1 Constitutive activity of NRs

Constitutive activity with regard to NRs is the ability to achieve the active state of the LBD without ligand-induced conformational changes. This conformation is then consequently allowing the receptor to interact with CoAs, which increases the expression of its target genes. This capability is not unknown among the members of the NR superfamily and phylogenic studies imply that ligand recognition of NRs may have been acquired later during the evolution [Escriva *et al.*, 1997]. Receptors having this property mainly belong to the group of nutritional and xenobiotic sensors and/or "real" orphan NRs such as CAR, HNF-4, RORs, PPARs, ERRs and the LRH-1.

5.1.2 Ligand-independent association of CAR with p160 CoAs

CAR is representing a NR with constitutive activity, based on the ability to associate ligand-independently with CoAs. Since at the time when this study was conducted no crystal structure was available, we addressed the molecular mechanism of this behavior in a series of functional and biochemical assays. Firstly, supershift assays were performed with the p160 CoA protein family members SRC-1, TIF2, and RAC3, in the absence or presence of the agonist. These were then assayed for interaction with the CAR-RXR and VDR-RXR-heterodimers, the latter serving as a negative control for constitutive activity. The substrate for DNA-binding was the DR4-type RE of the mouse *CYP2B10* PBREM (NR1) (**I**, Fig. 1D). Interestingly, all three CoAs interacted in an indistinguishable way with either CAR or VDR when

agonist was added to the receptors (**I**, Fig. 1D). Although CAR-RXR heterodimers interacted with all three CoAs in the absence of agonist and in the presence of agonist CITCO, the supershifts were found to be more prominent. In contrast, only in the presence of $1\alpha,25(OH)_2D_3$, did VDR-RXR heterodimers bind and supershift with SRC-1, TIF2 and RAC3, as was expected for a classical endocrine NR (**I**, Fig. 1D).

Secondly, for a direct comparison of the basal activity and ligand inducibility of human CAR and human VDR on different DR4-type REs (**I**, Fig. 1A) *luciferase* reporter gene assays were performed (**I**, Fig. 1B) in transiently transfected MCF-7 cells. In these assays reporter constructs with two copies of DR4 (T/T), two copies of NR1 or one copy of the PBREM from the mouse *CYP2B10* promoter fused with the *tk* promoter driving the *luciferase* gene co-expressed with human CAR or VDR in the absence or presence of agonist were used. In cells CAR showed high basal activity under conditions when the agonist was not present in contrast with VDR, which could be activated only under conditions when $1\alpha,25(OH)_2D_3$ was present. The difference in the ligand inducibility of the two receptors is primarily dependent on the level of ligand-independent basal activity, which suggests that VDR with a lower basal activity is capable of a higher fold induction level than CAR which has already high basal activity (**I**, Fig. 1B). In summary, the high basal activity of CAR in the absence of CITCO is a sign of agonist-independent CoA association.

5.1.3 Impact of helix 12 on the CoA recruitment of human CAR and VDR

In VDR, an effective contact with CoAs is achieved when the charge clamp formed by the positively charged K246 (K177 in human CAR) and the negatively charged E420 (E345 in human CAR) has an optimal distance of 19 Å [Väisänen *et al.*, 2002]. To investigate the impact of helix 12 and these homologous amino acids on the constitutive activity of human CAR, the respective amino acids were mutated to alanine. In a separate mutant, helix 12 was deleted.

The deletion of helix 12 completely abrogated the effect of CITCO on human CAR transactivation in MCF-7 cells (**I**, Fig. 2A). As expected both charge clamp amino acids (K177 and E345 in human CAR) contribute to the constitutive activity of this receptor by stabilizing the binding of CoAs to it in an agonist-independent fashion. However these interactions are of minor importance for the ligand-dependent transactivation of human CAR (**I**, Fig. 2C and D). In contrast to this, the homologous mutations in human VDR have a clear effect on the ligand-dependent transactivation of this NR (**I**, Fig. 2E and F).

Our previous findings concerning mouse CAR [Andersin *et al.*, 2003] had shown, that the interaction between Y336 (helix 11) and C357 (helix 12) has a critical impact on the stabilization of this receptor in the active conformation. To investigate the role of the residues Y326 and C347 in human CAR homologous Y336 and C357, respectively in mouse CAR, as well as the orthologues amino acids H397 and F422 in

VDR (**I**, Fig. 4A), the amino acid residues were mutated individually and the effects of these changes were assessed in reporter gene and supershift assays (**I**, Figs. 2C, D, E and F).

From this comparison it was proposed that in human CAR the impact of the Y326/C347 interaction is less crucial than the H397/F422 interaction in human VDR (**I**, Figs. 2C, D, E and F).

5.1.4 Stabilization of helix 12 in human CAR, mouse CAR and human VDR

To investigate the molecular mechanism of the stabilization of the helix 12 in these NRs, we first addressed the question whether the interaction of the negatively charged C-terminus of helix 12 with the positively charged K195 (human CAR) in helix 4 may contribute to the stabilization of helix 12 (**I**, Fig. 2B). Therefore the respective lysine of helix 4 in both human and mouse CAR was mutated into alanine. In addition, a separate mutant was created where helix 12 was extended by three amino acids. Taken together, the results indicate that for both CAR orthologues the interaction between the lysine of helix 4 and the C-terminal carboxy group is critical for the constitutive activity of the receptor (**I**, Figs. 3A-D).

A subsequent structural analysis of a human CAR model, based on the published PXR crystal structure, indicated an additional intra-molecular interaction for the stabilization of helix 12. This consisted of a possible interaction between I330 (helix 11) and L343 (helix 12) (**I**, Fig. 2B). These two amino acids as well as the orthologous amino acids L340 and L353 in mouse CAR (**I**, Fig. 4A) were then mutated to test this hypothesis. In human CAR L343A blunted the inducibility by CITCO and reduced the basal activity by 75 %. The other mutation, I330A showed a 1.9-fold higher response to ligand than wild type receptor and only a 50 % reduction of constitutive activity in MCF-7 cells (**I**, Fig. 3A). This observation is in accordance with the observed *in vitro* interaction of DNA-bound CAR-RXR heterodimers with TIF2, which is blunted irrespective to the presence of the agonist by the mutation L343A and abrogated only in the absence of CITCO with I330A (**I**, Fig. 3B). In mouse CAR the orthologus mutations showed a slightly different profile. Both L353A and L340A reduced but did not abrogate TCPOBOP-induced transactivation and reduced the constitutive activity of mouse CAR drastically (**I**, Fig. 3C, right panel). In supershift assays the mutants blunted both ligand-independent and ligand-dependent interaction of CAR-RXR heterodimers with CoA protein (**I**, Fig. 3D).

According to a structural alignment (**I**, Fig. 4A), the human VDR counterparts to I330 and L343 of human CAR are Y401 and V418, respectively. Both amino acids were mutated individually into alanine or into the amino acid residues present at the orthologues position in human CAR. Furthermore, the double mutant Y401I/V418L was created. All the VDR mutants were investigated by supershift assay (**I**, Fig. 3E). In the absence of ligand the mutants Y401I and V418L showed a weak supershift

with TIF2, while the double-mutant Y401I/V418L displayed a significant ligand-independent interaction with the CoA protein (**I**, Fig. 3E).

In summary, the I330-L343 and L340-L353 interactions of human and mouse CAR, respectively, had a significant contribution to the stabilization of helix 12 and the constitutive interaction of the receptor with CoA protein. However, I330A increased the ligand responsiveness of human CAR, while L340A decreased that of mouse CAR.

5.1.5 Ligand-independent association of human PPARs with p160 CoAs

A structural comparison of the helix 12 of apo-receptors, which display constitutive activity, such as LRH-1 and ERR3, with apo-PPARδ and γ (**III**, Fig. 1A) raised the possibility that in un-liganded PPAR LBDs the helix 12 can take the active conformation. Moreover, the superimposition of the apo- and holo-PPARγ structures suggested that it was possible for the apo-PPARγ to maintain the critical 19 Å inevitable for the charge clamp residues K329 and E499 required for the efficient CoA interaction (**III**, Fig. 1B and C).

To test this hypothesis we made supershift experiments where we tested all PPAR subtypes with the three members of the p160 CoAs. All three CoAs effectively interacted with PPARs in the absence of ligand (**III**, Fig. 2A), however RAC3 showed the best interaction in these assays. The addition of the ligand caused minor enhancement in the CoA interaction. We then made additional supershift experiments where we compared the CoA interaction profile on the chosen example of PPARγ with CAR and VDR. From these experiments PPARγ can be placed between CAR and VDR with its interaction profile resembling more the profile of CAR, which showed ligand-independent CoA association already under the lowest concentrations of RAC3. On the contrary, VDR was unable to interact with RAC3 in the absence of its natural ligand. This is in contrast to the situation in the presence of $1\alpha,25(OH)_2D_3$, where already the lowest concentration of CoA was enough for efficient interaction to occur.

In further studies we examined the basal activities and ligand inducibilities of the compared receptors in cell-based assays. We tested all three PPARs, CAR and VDR in *luciferase* reporter assays with constructs bearing four copies of DR1-type RE originated from human CPTI-β gene promoter, two copies of DR4-type RE from rat Pit-1 enhancer and four copies of DR3-type RE derived from the rat *atrial natriuretic factor* gene promoter, respectively (**III**, Fig. 3A-D). We investigated the basal activity and ligand inducibility in MCF-7 and HEK293 cells. In both cell lines CAR and PPARs showed in the absence of extraneous ligand high basal activity that clearly arose from CoA interaction. As expected, overexpressed VDR did not show high basal activity (**III**, Fig. 3A and C). In the next step we introduced to cells NR-specific ligands and we compared the ligand inducibilities of the NRs. VDR showed 36- and 74-fold increase in the activity in HEK293 and MCF-7 cells, respectively (**III**, Fig. 3B

and D). CITCO could not stimulate CAR more than 1.8 fold and PPAR-specific ligands reached 3.5 fold maximum in case of PPARδ specific agonist. To show that the used cell lines do not contain a high-affinity PPAR-specific agonists we overexpressed NCoR with all the PPARs, which resulted in a significant decrease of the basal activity. On the other hand a "strong" agonist, such as rosiglitazone, was able to restore the activity of PPARγ, even in the presence of NCoR.

Summing up, PPARs show ligand-independent CoAs association *in vitro* in gelshifts and within living cells as demonstrated by the *luciferase* experiments described above.

5.1.6 Structural basis of the constitutive activity of human PPARs

To further identify the structural determinants of the ligand-independent CoAs association, we prepared mutants of the candidate amino acids identified from the *in silico*-derived structural analysis of the apo- and holo-PPARs. We tested all the mutants in *luciferase* reporter gene assays and in supershift experiments (**III**, Fig. 4-6).

According to which type of stabilization is provided via candidate amino acids we assigned them to four groups that represent the backbone of the structural basis for ligand-independent CoA interaction. The common property for all the amino acids is that they are helping to stabilize the position of helix 12 and thereby influencing the effective CoA docking to the LBD. In the following chapters PPARγ_2 numbering is used for the residues.

The first group consists of residues K329 and E499 (**III**, Fig. 4A and B). These amino acids represent the stabilization, which can be either ligand-independent or -dependent. K329 and E499 create the earlier mentioned charge clamp, which is a critical requisite for CoA interaction. When either or both of these amino acids are mutated the ligand–independent and -dependent CoA interaction is abolished (**III**, Fig. 4C-E).

In the second group, there are K347 and D503, which display a mixture of direct and indirect stabilization of helix 12 by both interacting directly with each other and in addition contacting the CoA peptide. This amino acid pair is conserved in human CAR where K347's orthologue K195 and the C-terminus of the helix 12 make a ionic interaction. Identical stabilization is present in mouse CAR.

The residues of the third group, E352, D424, R425, R471 and Y505, are involved in a direct stabilization of helix 12 via ionic interactions and hydrogen bonds (**III**, Fig. 5A and B). These amino acids have an additional function since they are located in the heterodimerization interface with RXR. These mutants show basal activities from 45-80 % of the wild type and ligand inducibilities up to 260 % for R425A (**III**, Fig. 5C and D).

Although the last group represents amino acids, which contact the ligand, they form an extensive hydrogen bond network already in the absence of agonist. Amino acids H351, Y355, H477 and Y501 belong to this group. They are responsible for both

ligand-dependent and -independent stabilization of helix 12 (**III**, Fig. 6A and B). The mutants of these amino acids with only one exception, H477, do not have lower basal activities compared to wild type receptor. This observation is even more surprising in case of the mutant Y501A (**III**, Fig. 6C and D), because it disturbs the hydrogen bond network and thus partially destabilizes the helix 12. This amino acid is located in helix 12 and it is responsible for the direct ligand-helix 12 interaction. The mutant Y501A is unable to bind any intracellular ligands, which could directly stabilize the helix 12, and shows a clear evidence for the ligand-independent association with CoAs.

All the amino acids involved in the stabilization of the helix 12 in PPARγ are conserved in all three subtypes suggesting a very similar molecular mechanism also for PPARα and δ (**III**, Fig. 7B and C). When looking at the properties and functions of the LBD such as ligand-independent CoA association, ligand-inducibility or LBD dynamics, PPARs can be place between VDR and CAR (**III**, Fig. 7D) though closer to CAR and other NRs with constitutive activity.

In summary, at least four different groups of amino acids are responsible for the molecular basis of the ligand in-dependent CoA association and the stabilization of the helix 12.

5.2 A structural basis for the species-specific antagonism of 26,23-lactones on vitamin D signaling (II)

In order to investigate the species-specific differences, the functional profiles of the VDR antagonists ZK168281 and TEI-9647 (**II**, Fig. 1A) were compared in rat osteosarcoma (Ros17/2.8), human osteosarcoma (MG-63), rat epidermal keratinocytes (REK), human immortalized keratinocytes (HaCaT) and MCF-7 cells. In all cellular systems, ZK168281 had insignificant agonistic activity (**II**, Fig. 1B lanes 2, 8, 14, 20 and 26). In contrast, at the same concentration (1 μM) TEI-9647 showed significant residual agonistic activity (**II**, Fig. 1B lanes 3, 9, 15, 21 and 27), which was higher in rat than in human cells. Remarkably, the five cell lines differ in their relative basal activity and therefore in their maximal inducibility by $1\alpha,25(OH)_2D_3$. For example, in Ros17/2.8 cells (lane 6) the basal activity was more than two times higher than in MCF-7 cells (**II**, Fig. 1B lane 30).

The results suggest that the origin of the species-specific difference in the functional profile of TEI-9647 might be caused by amino acid differences in the VDR of rodent and human. We compared the amino acid sequences of human and rat VDR and found only two amino acids that are different and they are located in the region close to the ligand-binding pocket and helix 12. These differences occur at positions 403 and 410, respectively (**II**, Fig. 2A). The rodent receptors both carry a serine and an asparagine residue at these positions, whereas the human VDR has two cysteines at positions 403 and 410, respectively.

In order to test our hypothesis about the critical role of C403 and C410 in the function of TEI-9647 as a VDR antagonist, we made the mutants C403S, C410N and the double mutant C403S/C410N and we compared their antagonistic profiles of ZK168281 and TEI-9647 in MCF-7 cells with the wild type receptor (**II**, Fig. 3). The mutagenesis of VDR at positions 403 and 410 had virtually no effect on the antagonistic action of ZK168281 (**II**, Fig. 3A). In case of wild type and C403S VDR TEI-9647 still showed some partial antagonistic action, which was lost in C410N and C430S/C410N mutants (**II**, Fig. 3 lanes 17 and 23). Interestingly, the profile of C430S/C410N in human cell line MCF7 was found to be similar to that of the rat cell lines Ros17/2.8 and REK (**II**, Fig. 1).

To further understand the role of the positions 403 and 410 in the antagonistic versus the agonistic action of TEI-9647 we tested the wild type and mutated receptors in supershift experiments on DR3-type VDRE and with bacterially expressed CoA TIF2 (**II**, Fig. 4). 1α,25(OH)$_2$D$_3$ induced a supershift with wild type as well as with mutants, whereas in the presence of ZK168281 or solvent no CoA association was detectable. TEI-9647 did not induce a shift with wild type, only a very faint CoA complex with C403S, a slightly stronger interaction with C410N and a dominant shift with C430S/C410N (**II**, Fig. 4 lane 32) suggesting an agonistic profile of TEI-9647.

To follow up the loss of the antagonistic potential of TEI-9647 we performed limited protease digestion assays, which report on the flexibility of the C-terminal part of the VDR, with wild type, C403S, C410N and C430S/C410N (**II**, Fig. 5). With wild type both ZK168281 and TEI-9647 stabilize a subpopulation of all VDR molecules in the antagonist-specific conformation c2. However, the two antagonistic positions are different from each other. The conformation profile of C410N resembled that of wild type, where both TEI-9647 and ZK168281 acted as antagonists with this VDR mutant. In contrast, with C403S and C430S/C410N, only ZK168281 but not TEI-9647 was able to stabilize the antagonistic conformation c2.

In summary, the origin of the species-specific profiles observed in model cell lines is based on the sequence differences between rat and human VDR. In human receptor, the two key amino acids are at the positions 403 and 410.

5.2.1 Molecular determinants of species-specific antagonism

To further investigate the molecular basis of the species-specific anatgonism, 6 ns MD simulations were performed with wild type complexed with 1α,25(OH)$_2$D$_3$, ZK168281 and TEI-9647 and with C430S/C410N bound by TEI-9647 in order to understand the molecular basis of the effects of these ligands (**II**, Fig. 6). In the structure with ZK168281, the extended rigid side chain disturbs the interaction between H397 and F422 and thus the stable positioning of helix 12 (**II**, Fig. 6B). This blocks the ability to interact with CoA protein and explains the pure antagonistic profile of ZK168281. The lactone ring of TEI-9647 is more bulky than the end of the side chain of the 1α,25(OH)$_2$D$_3$ and cannot interact effectively with H305 and H397.

Moreover, the carbonyl group of the lactone ring cannot interact directly with F422. These observations indicate that steric hindrance plays a role in this ligand's antagonistic behavior. However, TEI-9647 lacks an extended side chain and disturbs helix 12 less than ZK168281 (**II**, Fig. 6C). In fact, the disturbance of helix 12 by TEI-9647 is so weak that it can be counterbalanced by backbone contacts of N410 in C430S/C410N with P408 and L404 (**II**, Fig. 6D). Therefore, in rodent VDRs the backbone contacts of their loop amino acid N410 stabilize the helix 11-helix 12 interaction (**II**, Fig. 6E), so that the LBD of rodent VDR binds CoA proteins even in the presence of TEI-9647. The differences in the structures of the complexes of wild type and C403S/C410N with TEI-9647 is better illustrated, when the variation of the backbone rmsd of amino acids 393 to 422 and the distance between the Cα-atoms of T415 and F422 are monitored over the whole MD simulation period of 6 ns (**II**, Fig. 7). The rmsd can be used to indicate the mobility of helices 11 and 12 and is inversely proportional to the stability of helix 12. After 2.5 ns of MD simulation the rmsd of the wild type VDR-TEI-9647 complex was significantly higher than that of the complexes of wild type with $1\alpha,25(OH)_2D_3$ and of C430S/C410N with $1\alpha,25(OH)_2D_3$ or TEI-9647 (**II**, Fig. 7A).

Interestingly, the latter three LBD-ligand complexes have the same average rmsd indicating their comparable ability to stabilize the interaction with CoA proteins. The peak after 4 ns of the simulation of wild type with $1\alpha,25(OH)_2D_3$ is due to a transient conformational change in the loop region (residues 407-414) between helices 11 and 12. The distance between the Cα-atoms of T415 and F422 measures the length of helix 12 (**II**, Fig. 7B). An increased length of helix 12 is a sign of greater flexibility and is inversely proportional to the probability of an interaction with CoA proteins. In this view of the structures, the wild type-TEI-9647 complex was shown after 2 ns of simulations to have significantly longer and more flexible helix 12 than the complexes of wild type with $1\alpha,25(OH)_2D_3$ and of C430S/C410N with $1\alpha,25(OH)_2D_3$ or TEI-9647. Again, the latter two LBD-ligand complexes appeared to be identical and had the same average length of helix 12 (10.7 to 10.9 Å, which is close to 10.8 Å in the X-ray crystal structure of the wild type-$1\alpha,25(OH)_2D_3$-complex).

Taken together, the structural basis for the species-specific action of TEI-9647 is directly connected with the ligand's chemical structure and the critical amino acids in helix 11 of rat and human VDR. In both receptors, the lactone ring of TEI-9647 does not effectively disturb the helix 12, but in rat VDR additional interactions can be established between the lactone ring and the residues in helix 11, which weakly stabilizes the receptor in active conformation. This is not possible in the human receptor that lacks these critical residues. The extended side chain of ZK168281 uses the same strategy of perturbing the position of helix 12 in both receptors, and thus there are no species-specific differences in the action of this antagonist.

5.3 Antagonist- and inverse-agonist triggered conformational changes in the LBD of human VDR, human and mouse CAR (IV)

The dynamic exchange of cofactors is usually connected with conformational changes mediated via ligands. While agonists change the receptors conformation in order to help CoAs establish efficient interaction on the other hand antagonists and inverse agonists shift the balance on CoRs' behalf. As it was already mentioned earlier, there is only one crystal structure with CoR peptide currently available, which is PPARα co-crystal with SMRT [Xu *et al.*, 2002]. This fact makes the study of CoR interaction rather difficult and laborious.

5.3.1 Ligand-dependent interactions of VDR and CAR with CoAs and CoRs

To examine the ligand-dependent interaction between the NRs human VDR, human and mouse CAR with the CoA TIF2 and the CoR NCoR supershift experiments were performed (**IV**, Fig. 2). In the absence of ligands, DNA-complexed VDR did not show any association with TIF2 or NCoR (**IV**, Fig. 2A lanes 4 and 8), however after introducing the natural agonist $1\alpha,25(OH)_2D_3$ VDR was able to interact with TIF2 (**IV**, Fig. 2A lane 5). The antagonist ZK168281 did not induce an interaction of VDR with CoA protein (**IV**, Fig. 2A lane 7) and the combination of agonist and antagonist resulted only in a very faint complex of VDR-RXR heterodimers with TIF2 (**IV**, Fig. 2A lane 6). Application of $1\alpha,25(OH)_2D_3$ did only induce residual interaction of VDR with NCoR (**IV**, Fig. 2A lane 9), whereas in the presence of ZK168281 VDR showed association with NCoR (**IV**, Fig. 2A lane 10). The combined application of agonist and antagonist resulted in the significant interaction of NCoR with VDR (**IV**, Fig. 2A lane 11).

On the contrary, human and mouse CAR showed significant interaction with TIF2 even in the absence of ligands (**IV**, Fig. 2B and C lane 4). Surprisingly, both receptors interacted ligand-independently also with NCoR (**IV**, Fig. 2B and C lane 7). As expected agonist CITCO increased the interaction of human CAR with CoA, however, it also induced a significant interaction of the receptor with NCoR (**IV**, Fig. 2B lanes 5 and 8). Inverse agonist clotrimazole blunted the ligand independent association of human CAR with TIF2 and also slightly reduced the interaction of the receptor with NCoR (**IV**, Fig. 2B lanes 6 and 9). In case of mouse CAR, the agonist TCPOBOP increased the interaction with CoA protein, but in contrast to CITCO it decreased the interaction of the receptor with CoR protein (**IV**, Fig. 2C lanes 5 and 8). Finally, androstanol behaved as expected from an inverse agonist and it decreased the interaction of mouse CAR with TIF2 and increased the association with NCoR (**IV**, Fig. 2 lanes 6 and 9).

In order to compare the functional profiles in the presence of agonist or antagonist/inverse agonist we tested the receptors in the transiently transfected model cell line MCF-7 (Fig. 3). The *luciferase* reporter gene assays were performed under conditions when CoA, CoR or empty plasmid was overexpressed. At endogenous cofactor levels the very low basal activity of VDR on the DR3-type RE (**IV**, Fig. 3A lane 1) was induced nearly 50-fold by 10 nM $1\alpha,25(OH)_2D_3$ (Fig. 3A lane 2), while 100-times higher concentrations of ZK168281 (1 μM) resulted only in less than a 4-fold induction (**IV**, Fig. 3A lane 4). The combined application of agonist and antagonist led to 16.7-fold induction (**IV**, Fig. 3A lane 3). The overexpression of TIF2 resulted in a significant increase of the basal level (3.8-fold, **IV**, Fig. 3A lane 5), but in a less prominent increase of agonist-stimulated values, so that only an approximately 15-fold induction was observed (**IV**, Fig. 3A lane 6). CoA overexpression increased the response in the presence of antagonist (4.9-fold, **IV**, Fig. 3A lane 8), but the combined application of agonist and antagonist did not provide significantly higher induction (6.5-fold, **IV**, Fig. 3A lane 7). The overexpression of NCoR reduced the basal activity to 60 % (**IV**, Fig. 3A lane 9), but also the effects of agonist and antagonist alone and in combination, so that only 34.3-, 3.5- and 2-fold inductions were observed (**IV**, Fig. 3A lanes 10, 11 and 12), respectively.

Human CAR showed high basal activity on the DR4-type RE (**IV**, Fig. 3B lane 1), which could only be induced 2.5-fold by CITCO (**IV**, Fig. 3B lane 2) and was reduced to 60 % by clotrimazole. TIF2 overexpression had only minor effects on the basal activity and ligand response of human CAR (**IV**, Fig. 3B lanes 4, 5 and 6). In contrast, NCoR overexpression clearly blunted the responsiveness of the receptor; the basal activity was significantly reduced to 30 % (**IV**, Fig. 3B lane 7), the induction by CITCO was only 1.6-fold (**IV**, Fig. 3B lane 8) and in the presence of clotrimazole still 90 % of the basal activity level was observed (**IV**, Fig. 3B lane 9). The induction profile of mouse CAR (**IV**, Fig. 3C) was similar to that of human CAR but the mouse-specific ligands had more prominent effects. Mouse CAR also showed high basal activity on the DR4-type RE (**IV**, Fig. 3C lane 1), which was induced three-fold by TCPOPOB (**IV**, Fig. 3C lane 2) and reduced to 30 % by androstanol (**IV**, Fig. 3C lane 3). CoA protein overexpression slightly increased the basal activity (1.4-fold, **IV**, Fig. 3C lane 4), reduced the response to the agonist (2.6-fold induction, **IV**, Fig. 3C lane 5) and to the antagonist (still 70 % of basal activity, **IV**, Fig. 3C lane 6). In case of NCoR overexpression the basal activity was reduced significantly to 50 % (**IV**, Fig. 3C lane 7), the response to TCPOBOP was lowered to a 2.2-fold induction (**IV**, Fig. 3C lane 8) and in the presence of androstanol it reached 40 % of the basal activity (**IV**, Fig. 3C lane 9).

In summary, these experiments showed that NR-specific agonists and antagonists/inverse agonists display distinct profiles in the presence of overexpressed CoAs and CoRs in cellular models.

5.3.2 Molecular basis of the VDR and CAR association with CoR

The acquired data suggested that CoR have a significant effect on the ligand response and basal activity of both endocrine and adopted orphan NRs, therefore we were interested in finding the molecular basis of the NR-CoR interaction. At the time when the study was conducted there was no CAR crystal structure available therefore molecular homology modeling was performed on the PPARα (1KKQ) crystal structure template. To these structures the antagonists clotrimazole and androstanol, respectively, were docked, whereas for the ZK168281-bound VDR-LBD a structure from a previous MD simulation study was available [Väisänen *et al.*, 2002]. To each of the three LBDs a peptide representing the amino acids 2265 to 2289 of the second RID of NCoR was docked and MD simulations were performed. Detailed views of the resulting structures indicate interactions of helices 3, 4 and 12 of the NR-LBDs with the CoR peptide (**IV**, Fig. 4).

The most remarkable and consistent observation of the three model structures was that helix 12 is not flexible, as the "mouse-trap" model suggests, but takes a fixed position, as does helix 12 of PPARα in the co-crystal with CoR peptide. In the VDR-LBD-ZK168281 complex V418 of helix 12 interacts with I2280 of NCoR and S427 of the C-terminus makes a backbone contact to F2289 of the CoR (**IV**, Fig. 4A). In a similar way, helix 12 of CAR is stabilized by an interaction between the positively charged K2283 of the CoR peptide and C347 as well as the negatively charged C-terminus in the human orthologue and C357, S358 and the C-terminus in the mouse receptor (**IV**, Fig. 4B and C). In addition, K264 of helix 4 in VDR and the homologous residues K195 and K205 in human and mouse CAR, respectively, form a salt bridge with E2278 of NCoR. Moreover, K246 of helix 3 in VDR and its homologue residues K177 and K187 in human and mouse CAR, respectively, contact the CoR peptide at the backbone of L2285. In addition, K246 also interacts with the backbone of A2284. Despite their rather divergent structure all three ligands contact the homologous amino acids H397, Y326 and Y336 in helix 11 of VDR, human and mouse CAR, respectively.

It is remarkable that both the antagonist ZK168281 and the two inverse agonists clotrimazole and androstanol stabilize their respective receptors in a very similar conformation. Interestingly, the long side chain of ZK168281 is directly contacting NCoR at position L2277 (**IV**, Fig. 4A). Such a contact is not observed with the smaller ligands clotrimazole and androstanol (**IV**, Fig. 4B and C). In order to challenge the models described above for each of the three receptors, a series of point mutants was created and the interactions were conformed in supershift experiments (**IV**, Fig. 5, 6) and *luciferase* reporter gene assays (**IV**, Table 1).

Taken together, the interactions between the RID of CoR and the LBDs of mouse CAR, human CAR and VDR are conserved. In addition, our models show that helix 12 is stabilized by CoR's RID in all three NRs.

5.4 Molecular basis of the agonists-induced selective modulation of the ligand-binding pocket volume in human VDR (V)

Although the natural ligand for VDR, 1α,25$(OH)_2D_3$, can inhibit the growth of various human cancers and can regulate the human immune system [Reichle *et al.*, 1989] when used at supraphysiological levels, this hormone can produce serious side effects such as severe hypercalcemia and soft tissue calcification [Vieth, 1990]. Therefore, the fundamental challenge to organic and medicinal chemists is to create new analogues, which are more safe and selective. Up to now there are more than 3000 synthetic analogues of 1α,25$(OH)_2D_3$ known [Carlberg, 2004] from which some have higher affinities than the natural hormone. These analogues referred as superagonist are significantly more transcriptionally potent or efficacious than the natural hormone. There have been suggestions that the better activity is based on the higher stability of these ligands. However, until now the molecular mechanism of the superagonism has not been investigated in detail.

5.4.1 Selective modulation of the ligand-binding pocket's volume by VDR agonists

The ligand-binding pocket of VDR consist of 40 amino acids (**V**, Table 2) which we defined using the Voidoo software. In order to find differences in the position of the side chains in the individually superimposed structures of MC1288, Gemini (conformation I and II) and Ro43-83582 (conformation I and II) with the 1α,25$(OH)_2D_3$-bound VDR, we measured for each of the 40 amino acid residues the distance between the respective most terminal atoms (excluding hydrogens). The obtained 200 values represent a five-dimensional data set (5 ligands or conformations x 40 amino acids). (**V**, Table 2). To group the amino acids with similar movement patterns we applied to the data set a data-mining clustering algorithm of SOMs and we visualized the data in two dimensions with Sammon's mapping (for details, see Section Material and methods in **V**). The amino acids with most profound dynamics are located in the groups I-X from the 16 clustered groups we obtained (**V**, Fig. 2A).

Next we were investigating the change of the volume of the ligand-binding pocket for different ligands and their conformations. We calculated the pocket volumes with the Voidoo software and the ligand volumes from Connolly's surfaces in the Sybyl software package (**V**, Table 3). The volume of MC1288 is 2.5 % less when compared to 1α,25$(OH)_2D_3$ even though the chemical structures of both ligands are highly alike and, surprisingly, there is a vivid decrease of 17.2 % in the pocket volume for MC1288. For Gemini and Ro43-83582, the ligand volume is 20 % and 25 % larger, respectively, when compared to the volume of 1α,25$(OH)_2D_3$, which is expectable since both contain an additional side chain. The pocket volume changes in case of Gemini and Ro43-83582 are dependent on the conformation of the ligands.

For Gemini I (inactive) (**V**, Fig. 1B) there is an increase of about 7.2 %, but for Gemini II (active) (**V**, Fig. 1B) it is already 18.5 %. The later suggests a directly proportional volume change since the ligand volume of Gemini II is also increased by about 19 %. In case of Ro43-83582 the accommodation of the pocket seems to have a different trend compared to that of Gemini. In both conformations, I and II, there is a small increase of the pocket volumes about 2.5 % and 9.5 %, respectively. The values for Ro43-83582 I suggest tighter packing of this conformation in the pocket. Hence, the ligand volume increase is 23.8 % but the ligand-binding pocket volume increase is only 2.5 %.

In addition, we calculated how much of the pocket volume is occupied by the respective ligand. While 1α,25$(OH)_2D_3$ occupies 55.9 % of the pocket, for MC1288 it is 66.5 %. Interestingly, Gemini I (62.8 %) fills up the pocket more than the active Gemini II (56.4 %). Ro43-83582 II and I occupy 63.7 % and 67.5 % volumes of the pocket, respectively.

In summary, the above-mentioned values allow the grouping of the ligands according to how much they fill the ligand-binding pocket of VDR. 1α,25$(OH)_2D_3$ is in one group with Gemini II. MC1288 is grouped with Ro43-83582 I, and Gemini I and Ro43-83582 II are between the two mentioned groups. MC1288 and Ro43-83582 I are close to each other in their functional properties and they represent the strong agonists with profound physiological effects.

5.4.2 Dynamics of the selective amino acids in the ligand-binding pocket

We chose representative amino acids from clustered groups I, V, IX and XIV in order to find out whether the transfer of the information from the ligand in the pocket to the surface requires these amino acids. We made the mutations of these amino acids F150A, Y295A, A303V, L309A, L309F, H397A, and F422A. We tested the ligand inducibilities of wild type and mutant receptors in *luciferase* reporter gene assays (**V**, Fig. 4A). Only L309F was showing values close to the inducibility of the wild type. Contrariwise mutants F150A, Y295A and F422A had inducibilities in the range of 11-26 % compared to wild type. Interestingly, mutants A303V, L309A and H397A showed agonist selective profiles. Remarkably the induction profile for A303V starts at 17 % for 1α,25$(OH)_2D_3$ and has a grading character with 53 % for MC1288, 83 % for Gemini and finally achieving 157 % in case of Ro43-83582. The mutation L309A is not well tolerated in case of agonists with one side chain although in case of MC1288 the inducibility is 2.1 times higher compared to 1α,25$(OH)_2D_3$. Although Gemini shows no change, Ro43-83582 has an increase of 30 % compared to 1α,25$(OH)_2D_3$. Introduction of a bulky phenylalanine at the same position surprisingly reverses the adverse effects of L309A. There is no perceptible difference in the induction of L309F compared to wild type.

To investigate the CoA interactions of the mutants, we carried out supershift experiments (**V**, Fig. 4C). The closest profile to that of the wild type (**V**,

Fig. 4C lanes 1-5) is L309F (**V**, Fig. 4C lanes 26-30) supporting the results from *luciferase* reporter gene assays. On the other hand, Y295A, H397A and F422A are not able to interact with CoA. Ro43-83582 can still induce the CoA interaction in case of mutants Y295A (**V**, Fig. 4C lane 15) and H397A (**V**, Fig. 4C lane 35), but not for F422A (**V**, Fig. 4C lane 40). Very surprising is the result for F150A in case of Gemini (**V**, Fig. 4C lane 9), which suggests that the mutation F150A abolishes the CoA interaction and is required for the efficient information transmission from the pocket to the surface. This mutation may stabilize the receptor in the inactive conformation and thereupon it is not able to interact with CoAs.

Taken together, the shrinking of the ligand-binding pocket in the complex with MC1288 as well as its expansion in order to accommodate the second side chain of Gemini or Ro43-83582 is the combined result of minor movements of multiple residues and major movements of a few critical amino acids.

5.4.3 Agonist-selective rearrangement of the hydrophobic residues in helices 6 and 7 and the loop between them

In the superimposed structures, the regions showing the biggest difference were helices 6 and 7. Since the amino acids A303 and L309 are located in this region we were interested in the detailed arrangement of their neighbor residues. We focused mainly on the amino acids with hydrophobic character since the mutants A303V, L309A and L309F represent interventions that may change the hydrophobicity of this region and may have an effect on interactions with other apolar residues. We identified four residues (V300, I310, L313 and L393) that may have an interaction with A303 or L309. In addition we considered the interaction of these residues with the groups located at the atoms C21, C26 and C31 in case of the ligands with two side chains. We visualized and measured the distances of the interacting hydrophobic amino acids for this region of the LBD (**V**, Fig. 5). The detailed structures show visible movements and agonist-selective rearrangements of the picked hydrophobic amino acids that may be the origin of the ligands' selectivity. Particularly interesting is the preference of the agonists for the use of amino acids to fix their aliphatic side chains through anchoring hydroxyl groups. The only exception is MC1288, for which the distances between the ligand's hydroxyl groups and the contact residues H397 and H305 are identical to those found in $1\alpha,25(OH)_2D_3$. However, the selectivity for MC1288 can be found elsewhere and it has its origin most likely in the rearrangement of the specific hydrophobic residues. Five residues show smaller deviations in their positions compared to $1\alpha,25(OH)_2D_3$. Surprisingly, the distance between A303 and C26 is 4.3 Å while in case of $1\alpha,25(OH)_2D_3$ it is 5.6 Å. This may explain also the 2.1 times higher inducibility for A303V where a more hydrophobic valine was introduced. In case of Gemini and Ro43-83582, the situation is conformation-specific and they both use different stabilization of the side chains. Paradoxical is the case of Ro43-83582 I, which does not require the residue H397 for its stabilization. Instead, it uses alternatively the carbonyl backbone group of L309.

This observation is consistently confirmed by experimental data (**V**, Fig. 4A and C lane 35). Although Gemini I implies the same model, it has to be noted that in this case F422 is repositioned (**V**, Fig. 3), and therefore the active conformation cannot be achieved. On the contrary, this residue takes practically an identical position in Ro43-83582- and $1\alpha,25(OH)_2D_3$-bound structures.

In summary, the flexible region of helices 6 and 7 shows agonist-specific rearrangement of the residues forming a hydrophobic core. In addition, the utilization of the anchoring hydroxyl groups by different ligands is also shown to be ligand-specific. This finding is consistent with the mutational analysis in *in vitro* experiments and the visualized conformation-specific stabilization of the two side chains of Gemini and Ro43-83582.

Chapter 6

Discussion

6.1 Mechanism of the constitutive activity in human and mouse CAR and human PPARs (I and III)

6.1.1 Constitutive activity of NRs

The comparison of the crystal structures of apo-RXR [Bourguet *et al.*, 1995] and holo-RAR [Renaud *et al.*, 1995] led to the formulation of the "mouse-trap" model [Moras *et al.*, 1998], in which helix 12 acts as a lid to the ligand-binding pocket of the LBD. However, the movement of the helix 12 from apo-states to agonist conformations in orphan receptors such as PPARs questioned this model because the dynamics of the helix 12 is not so prominent [Nolte *et al.*, 1998].

An elegant model has been developed to explain the activation of classical endocrine NRs, but no uniform mechanism has been suggested for the structural basis of the modulation of activity and stabilization of the apo-receptors for adopted orphan and orphan NRs [Steinmetz *et al.*, 2001]. CAR, LRH-1, SF-1, ERR3, RORs, and HNF-4 are NRs, which display vivid constitutive activity, notwithstanding the fact that some of them, such as RORs, were co-crystallized with cholesterol sulfate [Kallen *et al.*, 2002] and retinoic acid [Stehlin-Gaon *et al.*, 2003], respectively. Others, such as HNF-4α and γ have a constitutively bound lipid in their ligand-binding pockets [Wisely *et al.*, 2002]. The recent finding that phosphatidylinositols are ligands for SF-1 and LRH-1 enlarged the group of NRs that exhibit constitutive activity and could be modulated by ligands [Krylova *et al.*, 2005]. To date, there are no high affinity natural agonists identified for human and mouse CAR, but the possibility of binding xenobiotics such as TCPOBOP and CITCO suggests that CAR did not loose during the evolution its ability to bind ligands despite its high constitutive activity [Baes *et al.*, 1994]. All these results suggest that the constitutive activity is not in contradiction to the ability to bind ligands. For these receptors the conditional

induction after ligand binding may represent an additional way by which they modulate their activity.

The results presented in this thesis demonstrate that CAR and PPARs display high constitutive activity in the absence of agonists, which is due to ligand independent CoA association. The molecular basis of this behavior is the stabilization of the helix 12 in the active conformation via inter- and extra-molecular interactions.

6.1.2 Mechanism of the constitutive activity in human and mouse CAR

In case of CAR, the helix 12 is stabilized by at least three different direct contacts with the partner amino acids from helices 4 and 11. In detail, these contacts are in human CAR L343-I330, C347-Y326 and K195 with the oxygen from the C-terminal carboxy group of C347. In mouse CAR, these stabilizations are analogous [Frank *et al.*, 2004]. The interaction between the C-terminus and K205 in mouse CAR was previously reported by Dussault *et al.* [Dussault *et al.*, 2002] and we confirmed this interaction for human CAR. This interaction seems to restrict the mobility of the short helix 12, which becomes effectively fixed and rigid in the active conformation.

We obtained all our data at the time when crystal structures for human and mouse CAR were still unavailable. Despite of this we identified the residues L343 and I330 as critical for the constitutive activity [Frank *et al.*, 2004]. Later, the human CAR LBD homology models suggested that even without ligand, helix 12 adopts the active conformation because of hydrophobic interactions of L343 with LBD residues Y326 and I330, and of I346 with residue V199 [Jyrkkärinne *et al.*, 2005]. The recently published crystal structures for human and mouse CAR [Shan *et al.*, 2004; Suino *et al.*, 2004; Xu *et al.*, 2004] brought important insights into the molecular basis of the structural features that underline the constitutive activity of this receptor. L343 and I330 with other apolar amino acids are part of the hydrophobic core, which is between helices 11-12 and helices 3 and 4-5. This hydrophobic core is conserved in other NRs such as PPARs [Molnár, unpublished results] and probably its primary role is helping in protein-folding and in the stabilization of the protein scaffold. Although the other interaction C347-Y326 was not observed in the structures, Y336 in mouse CAR has a critical role in the TCPOBOP-induced activation where it makes hydrogen bonds with N175 to strengthen the rigidity of the region where helices 11 and 12 are located. Furthermore, this residue is rather critical in the dynamics of inactivation of the receptor by androstanol.

In addition to these specific interactions and the presence of the hydrophobic core there are other structural elements that stabilize the helix 12 in the active conformation in the absence of a ligand. One of them is the presence of the shortest linker helix known amongst the NRs, between helices 11 and 12. The stability of this linker region has been shown to affect the active position of helix 12 [Ueda *et al.*, 2002].

6.1.3 Structural basis of the constitutive activity of human PPARs

It has been earlier shown that for active VDR the distance between the residues forming the charge clamp E420-K246 is 19 Å [Väisänen *et al.*, 2002]. Interestingly, this distance in the adopted orphan NRs such as ERR3 (19.36 Å), mouse LRH-1 (19.63 Å) and CAR (18.3 Å) is maintained suggesting that the one requirement for the active state of a receptor is the distance between the charge clamp residues. We found that for the apo-PPARγ, this distance is 19.9 Å. This shows that the receptor is able to achieve the active conformation even in the absence of agonist. Furthermore, *in vitro*, in gelshift and *luciferase* reporter gene assays this receptor showed a ligand-independent CoA association, which has its origin in the ligand-independent stabilization of the helix 12. These findings represent a paradox since PPARs are sensors for fatty acids and some endogenous ligands have been identified for them [Forman *et al.*, 1995; Fu *et al.*, 2003].

The overexpression of CoRs such as NCoR, in model cell lines, led to a significant reduction of the basal activity. This means that a massive increase of CoRs in relation to endogenous CoA proteins apparently leads to an exchange of CoAs against CoRs as PPAR-associated proteins and the basal activity is reduced as a result. Interestingly, this process may happen in the presence of endogenous fatty acids within the ligand-binding pocket of the PPARs, however it is not largely influenced by it. We showed that only a high affinity agonist such as rosiglitazone is able to reverse this state. This suggests that only a specific ligand has the potency to overcome repression caused by high amounts of CoR, whereas endogenous fatty acid ligands are unable to do so. Another argument showing the minor influence of the endogenous ligands comes from the mutant Y501A. This residue is essential for agonists in order to activate the receptor and induce the active conformation [Gampe *et al.*, 2000], since it is a direct ligand contact point in helix 12. Hence results from our study indicate that the mutant Y501A has blunted ligand inducibility in the presence of rosiglitazone but its basal activity is not reduced compared to the native receptor. This suggests that endogenous ligands cannot influence the basal activity of PPARs effectively, however they can modulate their inducibility.

From the obtained data, we suggested that the helix 12 region contributes 75% to the basal activity of PPAR, but the remaining 25% of the activity might come from the interaction of the AF-1 domain with other CoAs, since many investigators have shown that this region contribute to the basal activity of the receptor [Castillo *et al.*, 1999; Gelman *et al.*, 1999; Juge-Aubry *et al.*, 1999]. Although there might be a direct link between the two domains in the ligand-independent activation, we focused our studies mainly on the mechanisms that involve ligand-independent stabilization of helix 12.

6.1.4 Molecular mechanism of ligand-independent stabilization of the helix 12 in human PPARs

As described above, the origin of the ligand-independent CoA association appears to be the stabilization of the helix 12 in the apo-PPARs. This is achieved by at least four groups of amino acids. These amino acid groups represent interactions with distinct character.

In the first group, there are residues K329 and E499 that form the charge clamp, which is essential for CoA docking [Heery *et al.*, 1997]. This interaction is rather well conserved in the NR superfamily except for Nurr-1, which has a reversed charged clamp E422 (helix 3) and K590 (helix 12). Interestingly, no known CoA motif has been found to interact with its LBD [Wang *et al.*, 2003c].

The second group includes K347 and D503, residues that interact together and additionally contact the CoA motif. This interaction is also conserved in both human and mouse CAR and was discussed earlier (for details, see Chapter 6.1.2) [Dussault *et al.*, 2002; Frank *et al.*, 2004; Suino *et al.*, 2004; Xu *et al.*, 2004].

The third group represents the charged amino acids E352, D424 R425 and R471, which form a hydrogen bond interaction network with Y505 (helix 12). Y505 is the very last residue in the helix 12 and it is conserved between all the subtypes. This interaction is receptor-specific since an analogous interaction in other receptors would require a helix 12 whose length would be 11 amino acids and the last one has to be an amino acid with a long side chain capable of making hydrogen bonds. The residue R425, from the loop between helices 8 and 9, has a naturally occurring mutation R425C that results in familial partial lipodystrophy [Agarwal *et al.*, 2002]. The R425C mutation disables the stabilization of helix 12 and in addition affects the overall stability of the LBD. However, a high affinity PPAR-specific ligand such as rosiglitazone would increase the stability of helix 12 and may be effective in overcoming the effect of the mutation.

In the fourth group amino acids H351, H477, Y355 and Y501 are included. Although some of these amino acids make contact with rosiglitazone [Gampe *et al.*, 2000], there is a network of hydrogen bonds formed between these residues even in the absence of this ligand. In addition, there is a stacking interaction between the two phenyl groups of the tyrosines. When rosiglitazone is bound to the ligand-binding pocket, it expands this network and makes the stabilization of the helix 12 stronger. This is the molecular mechanism of the ligand-dependent stabilization of the active conformation.

6.2 A structural basis for the species-specific antagonism of 26,23-lactone analogs on vitamin D signaling (II)

6.2.1 Species-specific affinity of the ligands

The observation that some ligands have different affinities for rodent and human receptors is not unique. A good example is the aryl hydrocarbon receptor, which in humans shows lower affinity for its ligands than the murine receptor. This difference is due to the variation of one amino acid at position 301. In the human protein it is a valine residue whereas in the murine orthologue it is an alanine [Ema *et al.*, 1994]. Another example is the xenobiotic receptor PXR for which it was shown that some receptor agonists are mouse and others human specific. SR12813 is a human PXR specific agonist that cannot activate the mouse orthologue. The mutation of four residues in mouse PXR can "humanize" the previously insensitive receptor, which results in an activation by SR12813. Finally, residue L308 is responsible for the rifampicin sensitivity of the human PXR. The mutation of this residue to phenylalanine, a residue found in rat PXR, reduces the apparent affinity of this receptor to rifampicin induction [Tirona *et al.*, 2004].

6.2.2 Molecular mechanisms for the species-specific differential profiles of ligands

The observation that the same ligand shows opposite profiles when bound to human and rodent receptors is rather rare. One example is for CAR, which can bind a large variety of compounds. Meclizine, an antiemetic drug, shows in case of mouse CAR an agonistic profile and at the same time it is an inverse agonists for human CAR. However, the molecular mechanism of this species-specific ligand profile was not fully investigated [Huang *et al.*, 2004].

TEI-9647, the 26,23-lactone derivate of $1\alpha,25(OH)_2D_3$, shows very similar profile to that of meclizine. In respect to mouse CAR, we showed that TEI-9647 displays species-specific profiles for VDR, where in rat cells it acts as an agonists but in human cells it acts as an antagonist. The molecular basis of this species-specific effect is the different binding mode of TEI-9647 in rat and human VDRs. For agonistic action in rat VDR it requires two residues S403 and N410 from the loop region between helices 11 and 12, which are not present in human VDR. Although it can bind to the human receptor, the lactone ring of TEI-9647 is not efficient in forming the critical interaction H397-ligand-F422 [Rochel *et al.*, 2000], which would require the aliphatic chain present in $1\alpha,25(OH)_2D_3$. The bulky lactone ring of TEI-9647 disturbs the exact positioning of helix 12, which results in a decreased interaction with CoA proteins. The displacement of helix 12 by TEI-9647 is much weaker than that by the pure antagonist ZK168281, so that only the 26,23-lactone but not the

25-carboxylic ester is affected by the increased interaction potential of S403 and N410 in rodent VDR.

ZK168281 and TEI-9647 represent the two different groups of antagonists for VDR. ZK168281 shows a functional affinity towards VDR that is comparable to that of $1\alpha,25(OH)_2D_3$, while that of TEI-9647 is at least 10-fold lower . With wild type VDR, both ZK168281 and TEI-9647 stabilize a subpopulation of all VDR molecules in the antagonist-specific conformation. However, it has been previously established that each of them stabilize the LBD in slightly different antagonistic conformations [Toell *et al.*, 2001].

Selective antagonism as exhibited by TEI-9647 appears to be a complex phenomenon that arises through the interplay of a number of factors, such as differential ligand effects on the transactivation of the NR, the type of cofactor recruited as well as cell and promoter contexts. So far, the partial antagonism of TEI-9647 has been explained by a reduced interaction of VDR with RXR and/or the CoA SRC-1 [Ozono *et al.*, 1999]. An alternative explanation involving covalent binding of this ligand to VDR has been excluded in a separate study [Bula *et al.*, 2000]. This antagonism displays species-specific differences and was shown to be more potent in human osteosarcoma and promyelocytic leukemia cells [Miura *et al.*, 1999a; Miura *et al.*, 1999b; Ozono *et al.*, 1999]. In contrast to this, in a rat *in vivo* model, the action of TEI-9647 could not convincingly be distinguished from that of a weak VDR agonist [Ishizuka *et al.*, 2001].

6.3 Antagonist- and inverse-agonist triggered conformational changes in the LBD of human VDR, human and mouse CAR (IV)

6.3.1 Unified classification of antagonists and inverse agonists

We demonstrated that ZK168281, clotrimazole and androstanol, despite of their divergent chemical structures, do have comparable effects on the CoR recruitment of VDR and human and mouse CAR, respectively. This led us to the conclusion that antagonists of endocrine NRs and inverse agonists of adopted orphan NRs may be considered as one class of ligand. The primary function of the inverse agonists seems to be to lower the ligand-independent constitutive activity in case of some adopted orphan NRs like CAR and PPARs, while antagonists show their potential mostly in cases, where they are present together with an agonist. The joint class of antagonists and inverse agonists is clearly distinguishable from the class of agonists, even if the functional profile of CITCO suggests some overlap between them. The dualistic profile of CITCO is not unique since there has been identified other compounds, such as estrogens, for CAR with similar effects [Mäkinen *et al.*, 2003].

Agonists and antagonists/inverse agonists compete at the same time for the binding to the ligand-binding pocket and thus the effective agonist-antagonist or agonist-inverse agonist ligand couples should have comparable range of affinities for the NR LBD. The VDR antagonist ZK168281 has the same affinity (K_d = 0.1 nM) for VDR as the natural agonist 1α,25$(OH)_2D_3$ [Bury *et al.*, 2000], but its extended side chain pushes helix 12 from its agonistic position [Väisänen *et al.*, 2002] and directly contacts and stabilizes CoR's RID. These properties make ZK168281 a more potent regulator of the cofactor exchange than the inverse agonists clotrimazole and androstanol.

6.3.2 Why is it difficult to classify ligands?

The molecular mechanism common to both antagonists and inverse agonists is the promotion of NR's interaction with CoRs and the disabling of its contacts with CoAs. In contrast, NR agonists have an opposite action since they favor CoA interaction and prevent CoR association. The ligands in this study demonstrate that there are intersections in the profiles between these adjacent states. The potential of the ligand to show one and/or another profile is receptor specific. A good example of this is clotrimazole, which prevents CoA association with human CAR but only weakly recruits CoRs. On the contrary CITCO, the human CAR agonist, supports interactions with both CoAs and CoRs. In particular the latter example raises the question, whether the simplistic view that one ligand can recruit only one type and at the same time disable the interaction with cofactor of the opposite class is valid for all compounds. An alternative explanation may be that the larger ligand-binding pocket of adopted orphan receptors allows the binding of a relatively small ligand, such as CITCO, without inducing major changes in their conformation. Human and mouse CARs are able to bind in their apo-states both CoA and CoR proteins. This suggests that the ratio between CoA and CoR proteins *in vivo* may be a critical parameter in determining the active and inactive state of the receptor and the ligand serves as a lock to further stabilize it.

6.3.3 The mechanism of ligand antagonism or inverse agonism

Although it is very difficult to characterize the ligands according to their physiological properties, it is rather simple to summarize the mechanism of ligand antagonism and inverse agonism. Antagonists and inverse agonists can be classified into groups based on the structural changes they induce. Most of them induce a major change in the position of the helix 12, which is subsequently displaced from its active position. The ligands, which are able to initiate this process, contain either long aliphatic chains or bulky moieties like the antagonists ZK168281 and GW6471 [Xu *et al.*, 2002]. This part of the ligand is then perturbing to the space where the active helix 12 is located and thus it has to move away. A different way of repositioning the helix 12 is to use the rigid part of the molecule, initiate there a conformational change

and start a cascade of structural changes, which will then lead to a rearrangement of the position of helix 12. The classical example of this mechanism is androstanol, which induces a change between the helices 10 and 11 of mouse CAR, which then finally influences the dynamics of helix 12 [Shan *et al.*, 2004]. The next group of antagonists has completely different mechanism of action. Good examples are the peptide antagonists of AR and ER that contain LXXLL motifs. They can effectively block androgen or estrogen signaling by preventing the association of these NRs with required coactivators [Chang *et al.*, 2005; Hall *et al.*, 2000]. Theoretically, there might be possibilities for the ligands to influence the heterodimerization or DNA-binding as well.

6.3.4 Similarities in the interactions of CoAs and CoRs with NRs

According to the "mouse-trap" model, helix 12 has a central role in determining the agonist-triggered interaction of NR-LBDs with CoA proteins [Moras *et al.*, 1998] and this has been proven extensively in many studies. For apo-NRs, which should be able to interact with CoR proteins, the model suggests free movement of helix 12 as observed in the RXR-LBD crystal structure [Bourguet *et al.*, 1995]. Amino acids that were identified in this study as being important for CoR interaction, such as the conserved lysines in helices 3 and 4, have already been described to be critical for the CoA contacts of the respective receptors [Frank *et al.*, 2004].

There is a conjuction of the surfaces on the outer area of LBDs which is used for interactions by CoA and CoR RIDs, respectively [Li *et al.*, 2003]. The difference between the two RIDs is that the LXXLL CoA motif adopts a two-turn α-helix while the LXXXIXXXL/I CoR motif adopts a three-turn α-helix instead [Li *et al.*, 2003]. The longer CoR motif would make a steric clash with the helix 12, which in order to allow the interaction with CoR has to change its position. Many critical hydrophobic interactions are required for the stabilization of both motifs. We did not directly address the question of these apolar interactions, but we confirmed that CoA and CoR proteins use an overlapping region on the surface of NR LBDs for their binding.

6.3.5 A model for the fixed helix 12 by a CoR RID

It has been shown in *in vitro* studies that NRs lacking their helix 12 interact the most efficiently with CoRs [Zamir *et al.*, 1996]. However, the truncation of the helix 12 occurs rarely *in vivo* in NRs and thus they have to deal with its presence when CoRs are bound. We proposed a model of a fixed helix 12 via CoR, which is an energetically more favorable state for the receptor than a free-floating helix proposed by the "mouse-trap" model. Although this stabilization is favorable for the NR, it has no advantage for the CoR interaction. This model would explain why the mutants of the contact points between helix 12 and the NCoR RID show only minor effects, if any at all, on CoR association when compared with the mutants of the salt bridge

between the conserved lysine in helix 4 and E2278 in the NCoR RID. For CoR-NR LBD interactions, the latter salt bridge seems to have the same critical impact than the charge clamp between the conserved lysine in helix 3 and the glutamate in helix 12 has for CoA interactions. It is remarkable that the glutamate in helix 12 is changing its spatial position upon binding to CoA or CoR while the positions of the two lysines in helices 3 and 4 are ligand-independent and stay fixed. This would partially explain why endocrine NRs favor CoR interactions in the absence of ligands. This seems not to be the case of adopted orphan NRs such as CAR and PPARs, which display constitutive activity, since the ligand-independent stabilization of their helix 12 prevents their association with CoR RIDs [Frank *et al.*, 2004; Molnár *et al.*, 2005]. However, this behavior can be observed in cellular systems only under normal physiological ratios of CoRs and CoAs.

6.4 Molecular basis for the agonist-induced selective modulation of the ligand-binding pocket volume in the human VDR (V)

6.4.1 Molecular mechanism of MC1288-induced conformational changes

Biochemical analysis suggested that the binding of 20-epi analogs such as MC1288 and KH1060 [Binderup *et al.*, 1991] to VDR's ligand-binding pocket induces conformations distinct from that induced by the natural hormone [Peleg *et al.*, 1995]. This model additionally proposed that the contact points used by 20-epi analogs with VDR are different from those used by $1\alpha,25(OH)_2D_3$. However, the model was not supported by the crystal structures [Tocchini-Valentini *et al.*, 2001] and the results presented in this thesis. We tried to provide an explanation for the molecular origin of the agonist-specific action. The structural comparison of the $1\alpha,25(OH)_2D_3$- and MC1288-bound structures revealed a region between helices 6 and 7, which shows the highest differences. This region is opposite to helix 12 and both regions serve as a cap for the ligand-binding pocket. In the region between helices 6 and 7, we identified four hydrophobic residues V300, I310, L313 and L393 that may interact with A303 and L309, the critical residues showing agonist-specific profiles. In addition, we considered the interaction of these residues with the groups located at the atoms C21, C26 and C31 in case of the ligands with two side chains. The determined distances showed that five of the nine measured distances are shorter in MC1288 than in $1\alpha,25(OH)_2D_3$-bound structures suggesting the tighter packing of this region with stronger hydrophobic core. Although these differences are not visible in the crystallized structures [Rochel *et al.*, 2000; Tocchini-Valentini *et al.*, 2001] we created our structural models in the presence of CoA peptide, which may help to stabilize the LBDs in a more natural state and thus emphasize the differences between the two structures.

6.4.2 Molecular mechanism of Gemini- and Ro43-83582-induced conformational changes in the LBD

Gemini and its derivates represent, from a mechanistic point of view, the most interesting analogs of $1\alpha,25(OH)_2D_3$ since they carry two side chains [Herdick *et al.*, 2000; Norman *et al.*, 2000; Uskokovic *et al.*, 1997]. In this study, the superimposed Gemini, Ro43-83582 and $1\alpha,25(OH)_2D_3$ structures showed the very same region of difference as in case of MC1288, the region between helices 6 and 7. This region of differences was in agreement with the partial results available from the zebra fish crystal structure bound Gemini, when compared to $1\alpha,25(OH)_2D_3$ [Ciesielski *et al.*, 2004]. We looked at the earlier described hydrophobic core (for details see chapter 6.4.1) and found similar changes like in case of MC1288 that seems to be the molecular mechanisms for superagonist-specific actions of these analogs.

6.4.3 Selective modulation of the ligand-binding pocket volume

In the currently crystallized structures, the size of the ligand-binding pocket range from ≈ 0 Å^3 in case of Nurr-1 to ≈ 1400 Å^3 for PPARγ LBDs [Benoit *et al.*, 2004; Li *et al.*, 2003]. However, the present understanding of the ligand-binding pocket changes is rather static since not many extensive studies have been conducted to investigate the pocket volume dynamics in the presence of different ligands. We showed that in the presence of MC1288 the pocket is shrinking by 17.2 %, but on the contrary, Gemini and its derivatives expand the pocket 7-19 %. This increase is understandable since the volume of these ligands is 20-25 % bigger than the volume of $1\alpha,25(OH)_2D_3$. However, the change in the pocket volume is not proportional to the increase of the ligand's volume.

Beside this, we also calculated how much of the pocket volume is occupied by $1\alpha,25(OH)_2D_3$, MC1288, Gemini I and II, and Ro43-83582 I and II. From these data, we propose that the superagonistic action of the ligands may be a function of the occupied volume in the pocket. We grouped the ligands according to this parameter into two groups. In the first group there is $1\alpha,25(OH)_2D_3$ together with Gemini II and they fill up 56 % of the pocket. The second group includes MC1288 and Ro43-83582 I and they are occupying 67-68 % of the pocket. Gemini I (62.8 %) and Ro43-83582 II (63.7 %) represent the junction between these two groups.

The "pocket-filling" feature of ligands may be of valuable importance in judging the potential of the agonists' actions. However, it has to be noted that it is necessary in the process of ligand evaluation to calculate the pocket and the ligand volumes for respective compounds individually, since the use of "default" volume from the $1\alpha,25(OH)_2D_3$–bound structure would give biased information. We suggested that superagonistic action of the ligands might be the function of the occupied volume in the pocket. However, it is always advisable to look at the same time for additional changes or deformations caused by the evaluated ligand in the pocket like repositioning of critical residues.

6.4.4 Ligand-binding pocket volume calculations

For the calculation of the ligand-binding pocket volumes in VDR we used Voidoo software (for details, see Section Material and Methods 4.10.2). In many recent crystal structure publications it is unfortunate that the authors did not mention the software or algorithms and parameters used in these calculations. Depending on which algorithms and parameters are used in the calculations, the obtained results may vary. Because of this it is not advisable to compare the absolute volumes of the cavities obtained from different sources and studies. The only possible way is to apply the same calculation method for all the evaluated NR structures and then make a comparison.

A good example of this paradox is the determined ligand-binding pocket volume of VDR by Rochel *el al.* [Rochel *et al.*, 2000], algorithm used for PDBSum database [Laskowski, 2001; Laskowski *et al.*, 1996] and my own calculation where the values were 697 $Å^3$, 940 $Å^3$ and 776 $Å^3$, respectively. The largest difference between the calculated pockets is 26 %. Even though Rochel *et al.* and I used the same software, the results differ by 10 % from each other. This is probably due to the different probe radius and grid plot set used in the calculations. Rochel *et al.* used the software with its default parameters (probe radius=1.4 and grid plot=0.7) while I had user-defined parameters (probe radius=1.9 and grid plot=0.5). My results may be closer to the real volume of the pocket since bigger volumes represent more accurate results [Xu HE, personal communication] and the smaller grid plot makes more meshes in the curvature of the calculated surface and therefore the calculated volumes are bigger.

Despite of this, the differences are only present in the absolute calculated volumes. For comparative purposes we suggest to use relative volumes where one of the pocket volumes is set to 100 % and the others are compared to it. The relative volumes show minor changes, if any, when different parameters are used for the calculations of the same set of structures.

6.4.5 Energy transmission in the LBD of NRs

Allosteric energy transmission is fundamental for many biologic processes like activation of G-coupled proteins via ligands [Menon *et al.*, 2001], regulation of the catalytic activity of tyrosine kinases [Young *et al.*, 2001] and ligand-dependent activation of NRs [Mangelsdorf *et al.*, 1995]. In all cases, the functional output of the protein depends on independent activity of the functional surfaces, but the efficient coupling and transmission from one surface to the other determines the final response [Shulman *et al.*, 2004]. The LBD of NRs contains four structurally distinct but functionally linked surfaces: (1) ligand-binding pocket, (2) cofactor binding surface, (3) helix 12 and (4) heterodimerization surface.

In case of VDR, one of the long-range energy interactions transmits the information from the ligand-binding pocket out to the surface of the protein influencing directly the function of the receptor. Although I presented in this thesis

the data that investigated whether the transmission of the information from the ligand-binding pocket to the surface requires amino acids F150, Y295, A303, L309, H397 and F422, the characteristics of the energy architecture that connects these residues with other functional surfaces remain still unknown. Unfortunately, crystal structures provide a limited view of protein energetics, and traditional structure-function studies cannot always identify the functional coupling of the residues. Although MD simulations may partially help to overcome these problems, the task to identify a set of residues involved in the energetic architecture of the NR LBD remains a challenging problem and awaits further investigation.

Chapter 7

Summary and Conclusions

In conclusion, the five scientific papers, on which this thesis is based, represent a detailed investigation of the structural basis of the dynamic properties of the LBDs of CAR, VDR and the PPARs. We made a systematic examination of the ligand-protein interactions, cofactor-LBD interactions and functional properties of NRs such as constitutive activity. Our studies were primarily directed towards molecular understanding of the mechanisms of these processes.

Mechanism for the constitutive activity of human and mouse CAR (I)

This study indicated that the constitutive activity of the adopted orphan NR human CAR is mediated by at least four contacts. In detail, there is a direct interaction between amino acids L343-I330, C347-Y326, K195-C-terminus and an indirect interaction between K177-E345 creating the charge clamp. Mouse CAR uses orthologous amino acid contacts for the same purpose, but the relative impact of each of the interactions is species-specific. The later interaction, the glutamate-lysine charge clamp, is rather conserved throughout the NR superfamily. The hydrophobic interaction between a pair of large non-polar amino acids in helices 11 and 12 was shown to be the structural basis of the ligand-independent activity of constitutively active NRs and is not used by the endocrine members of the NR superfamily. Three out of four contacts identified in our study were confirmed by recently published crystal structures.

Specific ligand selective conformational changes in human and rat VDR leading to an explanation of species-specific antagonism (II)

In this study, we aimed to reveal the specific mechanism of TEI-9647 action by using species-specific differences. We found that the bulky lactone ring of this compound disturbs the exact positioning of helix 12 and therefore blocks the

interaction with CoA proteins. Furthermore, in rat cells, we found that the residual agonistic activity of TEI-9647 was higher than that observed in human cells. We found that this is because the rodent-specific amino acids S403 and N410 display more and stronger interactions with TEI-9647 than C403 and C410 in humans. This results in the loss of the antagonist function of TEI-9647 in rodents.

Mechanism for ligand independent CoA interaction in the human PPARs leading to recognition of their constitutive activity (III)

Here we demonstrated that human PPARs show ligand-independent CoA association comparable with the NR CAR. Using PPARγ as an example, we found that four different amino acid groups contribute to the ligand independent stabilization of helix 12 of the PPAR LBD. These are: (I) K329-E499, mediating a charge clamp-type stabilization of helix 12 via a CoA bridge; (II) E352, D424, R425, R471 and Y505, directly stabilizing the helix 12 via salt bridges and hydrogen bonds; (III) K347-D503, interacting with each other as well as contacting the CoA; and (IV) H351, Y355, H477 and Y501, forming a hydrogen bond network. These amino acids are conserved within the PPAR subfamily, suggesting that the same mechanism applies for all three PPARs. Taken together, the ligand independent tight control of the position of the PPAR helix 12 provides an effective alternative for establishing an interaction with CoA proteins. Therefore, PPARs more likely should be considered as active NRs in the absence of agonist, and their functional profile should class them close to the group of NRs with constitutive activity, such as CAR, RORs and LRH-1. The recognition of the constitutive activity of PPARs provides an additional view on PPAR signaling.

The antagonist and inverse agonist-triggered conformational changes in the LBD of human and mouse CAR and VDR (IV)

The ligand-triggered dynamic exchange of CoA and CoR proteins bound to NRs is the molecular basis of the action of agonists, inverse agonists, and antagonists. The structural determinants of the antagonist and inverse agonist-triggered interaction VDR and human and mouse CAR with the second RID of NCoR led to the main conclusion of this study that antagonists of endocrine NRs and inverse agonists of adopted NRs have a comparable functional profile. The second important finding of this study is the stabilization of helix 12 in all three receptors by direct contacts with residues of the CoR. However, in contrast to the CoA interaction, which is dependent on a fixed position of helix 12, this helix is not needed for CoR interaction. In fact, helix 12 has to move from its position in the agonistic LBD conformation to a perpendicular position, where it does not disturb the contact between the LBD and the CoR. Therefore, fixation of the helix 12's position in the antagonistic/inverse agonistic conformation is only energetically favorable but of no specific function. The molecular mechanisms that explain the comparable functional profile of antagonist

and inverse agonists are likely to be extended from VDR and CAR to other members of the NR superfamily and may lead to the design of even more effective ligands.

Mechanism of agonism of the ligands with high affinity for human VDR (V)

I presented in this thesis the data, which showed that the ligand-binding pocket of VDR consists of 40 residues from which some are modulated by agonists. We proposed here a dynamic model of the ligand-binding pocket that can change in volume by 380 $Å^3$. We identified the amino acids A303, L309 and H397 that can accommodate their position in an agonist-specific manner. They are located in helices 6 and 7 in the region opposite to helix 12. These two regions create the lid for the ligand-binding pocket. Moreover, in this region, we identified a hydrophobic core consisting of nine apolar residues that interact between themselves as well as with the hydrophobic parts of the ligands such as the methyl groups on C21, C26 and C31. The changes in this hydrophobic core are probably one of the mechanisms of the agonist-specific actions. Furthermore, we suggested that the ligand's superagonistic profile is dependent on the "pocket-filling" feature of the agonist. This may be a valuable indicator when judging the potential of the agonists' actions.

Chapter 8

Future Aspects

In the last decades structural biology has been proven to be important to the NR research field. Although to date most of the NR LBDs have been crystallized, there are still challenging tasks left concerning the group of "real orphans" that in many cases have brought surprising observations. Many of the "real orphans" are still to be crystallized and hopefully in the near future we will have a complete set of human NRs protein structures. We are still missing the structure of a whole NR, which would provide valuable information and extend our view on the structure-function relationships in this protein family.

All the crystal structures available in the database have been helpful for a "smart drug design" approach and the collaborative efforts of structural biologists, cheminformaticians, structural bioinfomaticians and medicinal chemists have shown that there are many possible routes to find new compounds as ligands for NRs. In the near future many non-traditional ligands are expected to be taken into practice such as two-side chain analogs for VDR, and ligands with profiles leading to the recruitment of specific cofactors in specific tissues. New inverse agonists and partial agonists may represent the next wave of modulators for changing the properties of the constitutively active receptors. In addition, the dynamic attributes of NRs such as cavity modulation, information flow to the surface of the receptor and dynamic exchange of cofactors should be taken into account when new ligands are being designed.

In general, the crystal structures have provided valuable information, but in the past few years, structural bioinformatics has contributed as an important complement to the research field of NRs. Nowadays, many papers contain MD simulations. However, laymen are accepting the new methods and their results with particular skepticism. Nevertheless, these approaches have proven to provide realistic data and particularly they have been shown to be useful when investigating the dynamic properties of NRs. These methods are entirely dependent on the computational power and thus the introduction of new computational algorithms

and progress on the hardware will help to their further development. In the near future the numbers of structural bioinformatics applications are expected to increase, which may help in the investigation of bigger protein complexes.

References

Adams, M. D., Celniker, S. E., Holt, R. A., Evans, C. A., Gocayne, J. D., Amanatides, P. G., Scherer, S. E., Li, P. W., Hoskins, R. A., Galle, R. F., *et al.* (2000). The genome sequence of *Drosophila melanogaster*. Science *287*, 2185-2195.

Agarwal, A. K., and Garg, A. (2002). A novel heterozygous mutation in *peroxisome proliferator-activated receptor-γ* gene in a patient with familial partial lipodystrophy. J Clin Endocrinol Metab *87*, 408-411.

Alen, P., Claessens, F., Verhoeven, G., Rombauts, W., and Peeters, B. (1999). The androgen receptor amino-terminal domain plays a key role in p160 coactivator-stimulated gene transcription. Mol Cell Biol *19*, 6085-6097.

Andersin, T., Väisänen, S., and Carlberg, C. (2003). The critical role of carboxy-terminal amino acids in ligand-dependent and -independent transactivation of the constitutive androstane receptor. Mol Endocrinol *17*, 234-246.

Anzick, S. L., Kononen, J., Walker, R. L., Azorsa, D. O., Tanner, M. M., Guan, X. Y., Sauter, G., Kallioniemi, O. P., Trent, J. M., and Meltzer, P. S. (1997). AIB1, a steroid receptor coactivator amplified in breast and ovarian cancer. Science *277*, 965-968.

Baek, S. H., Ohgi, K. A., Rose, D. W., Koo, E. H., Glass, C. K., and Rosenfeld, M. G. (2002). Exchange of N-CoR corepressor and Tip60 coactivator complexes links gene expression by NF-κB and β-amyloid precursor protein. Cell *110*, 55-67.

Baes, M., Gulick, T., Choi, H. S., Martinoli, M. G., Simha, D., and Moore, D. D. (1994). A new orphan member of the nuclear hormone receptor superfamily that interacts with a subset of retinoic acid response elements. Mol Cell Biol *14*, 1544-1552.

Baker, A. R., McDonnell, D. P., Hughes, M., Crisp, T. M., Mangelsdorf, D. J., Haussler, M. R., Pike, J. W., Shine, J., and O'Malley, B. W. (1988). Cloning and expression of full-length cDNA encoding human vitamin D receptor. Proc Natl Acad Sci U S A *85*, 3294-3298.

Barak, Y., Liao, D., He, W., Ong, E. S., Nelson, M. C., Olefsky, J. M., Boland, R., and Evans, R. M. (2002). Effects of peroxisome proliferator-activated receptor δ on placentation, adiposity, and colorectal cancer. Proc Natl Acad Sci U S A *99*, 303-308.

Barak, Y., Nelson, M. C., Ong, E. S., Jones, Y. Z., Ruiz-Lozano, P., Chien, K. R., Koder, A., and Evans, R. M. (1999). PPAR γ is required for placental, cardiac, and adipose tissue development. Mol Cell *4*, 585-595.

Benoit, G., Malewicz, M., and Perlmann, T. (2004). Digging deep into the pockets of orphan nuclear receptors: insights from structural studies. Trends Cell Biol *14*, 369-376.

Bevan, C. L., Hoare, S., Claessens, F., Heery, D. M., and Parker, M. G. (1999). The AF1 and AF2 domains of the androgen receptor interact with distinct regions of SRC1. Mol Cell Biol *19*, 8383-8392.

Binderup, L., Latini, S., Binderup, E., Bretting, C., Calverley, M., and Hansen, K. (1991). 20-epi-vitamin D_3 analogues: a novel class of potent regulators of cell growth and immune responses. Biochem Pharmacol *42*, 1569-1575.

Bouillon, R., Okamura, W. H., and Norman, A. W. (1995). Structure-function relationships in the vitamin D endocrine system. Endocr Rev *16*, 200-257.

Bourguet, W., Ruff, M., Chambon, P., Gronemeyer, H., and Moras, D. (1995). Crystal structure of the ligand-binding domain of the human nuclear receptor RXRα. Nature *375*, 377-382.

Brzozowski, A. M., Pike, A. C., Dauter, Z., Hubbard, R. E., Bonn, T., Engström, O., Öhman, L., Greene, G. L., Gustafsson, J. Å., and Carlquist, M. (1997). Molecular basis of agonism and antagonism in the oestrogen receptor. Nature *389*, 753-758.

Bula, C. M., Bishop, J. E., Ishizuka, S., and Norman, A. W. (2000). 25-dehydro-1α-hydroxyvitamin D_3- 26,23S-lactone antagonizes the nuclear vitamin D receptor by mediating a unique noncovalent conformational change. Mol Endocrinol *14*, 1788-1796.

Burmester, J. K., Maeda, N., and DeLuca, H. F. (1988a). Isolation and expression of rat 1,25-dihydroxyvitamin D_3 receptor cDNA. Proc Natl Acad Sci U S A *85*, 1005-1009.

Burmester, J. K., Wiese, R. J., Maeda, N., and DeLuca, H. F. (1988b). Structure and regulation of the rat 1,25-dihydroxyvitamin D_3 receptor. Proc Natl Acad Sci U S A *85*, 9499-9502.

Bury, Y., Steinmeyer, A., and Carlberg, C. (2000). Structure activity relationship of carboxylic ester antagonists of the vitamin D_3 receptor. Mol Pharmacol *58*, 1067-1074.

Carlberg, C. (2004). Ligand-mediated conformational changes of the VDR are required for gene transactivation. J Steroid Biochem Mol Biol *89-90*, 227-232.

Carlberg, C., Bendik, I., Wyss, A., Meier, E., Sturzenbecker, L. J., Grippo, J. F., and Hunziker, W. (1993). Two nuclear signalling pathways for vitamin D. Nature *361*, 657-660.

Castillo, G., Brun, R. P., Rosenfield, J. K., Hauser, S., Park, C. W., Troy, A. E., Wright, M. E., and Spiegelman, B. M. (1999). An adipogenic cofactor bound by the differentiation domain of PPARγ. Embo J *18*, 3676-3687.

Cavailles, V., Dauvois, S., L'Horset, F., Lopez, G., Hoare, S., Kushner, P. J., and Parker, M. G. (1995). Nuclear factor RIP140 modulates transcriptional activation by the estrogen receptor. Embo J *14*, 3741-3751.

Chang, C., Abdo, J., Hartney, T., and McDonnell, D. P. (2005). Development of peptide antagonists for the androgen receptor using combinatorial peptide phage display. Mol Endocrinol *19*, 2478-2490.

Chawla, A., Repa, J. J., Evans, R. M., and Mangelsdorf, D. J. (2001). Nuclear receptors and lipid physiology: opening the X-files. Science *294*, 1866-1870.

Chen, H., Lin, R. J., Schiltz, R. L., Chakravarti, D., Nash, A., Nagy, L., Privalsky, M. L., Nakatani, Y., and Evans, R. M. (1997). Nuclear receptor coactivator ACTR is a novel histone acetyltransferase and forms a multimeric activation complex with P/CAF and CBP/p300. Cell *90*, 569-580.

Chen, J. D., and Evans, R. M. (1995). A transcriptional co-repressor that interacts with nuclear hormone receptors. Nature *377*, 454-457.

Chen, Y., Ferguson, S. S., Negishi, M., and Goldstein, J. A. (2003). Identification of constitutive androstane receptor and glucocorticoid receptor binding sites in the *CYP2C19* promoter. Mol Pharmacol *64*, 316-324.

Choi, H. S., Chung, M., Tzameli, I., Simha, D., Lee, Y. K., Seol, W., and Moore, D. D. (1997). Differential transactivation by two isoforms of the orphan nuclear hormone receptor CAR. J Biol Chem *272*, 23565-23571.

Chou, C. J., Haluzik, M., Gregory, C., Dietz, K. R., Vinson, C., Gavrilova, O., and Reitman, M. L. (2002). WY14,643, a peroxisome proliferator-activated receptor α (PPARα) agonist, improves hepatic and muscle steatosis and reverses insulin resistance in lipoatrophic A-ZIP/F-1 mice. J Biol Chem *277*, 24484-24489.

Ciesielski, F., Rochel, N., Mitschler, A., Kouzmenko, A., and Moras, D. (2004). Structural investigation of the ligand binding domain of the zebrafish VDR in complexes with 1α,25$(OH)_2D_3$ and Gemini: purification, crystallization and preliminary X-ray diffraction analysis. J Steroid Biochem Mol Biol *89-90*, 55-59.

Craig, D., Howell, M. T., Gibbs, C. L., Hunt, T., and Jackson, R. J. (1992). Plasmid cDNA-directed protein synthesis in a coupled eukaryotic in vitro transcription-translation system. Nucleic Acids Res *20*, 4987-4995.

Cronet, P., Petersen, J. F., Folmer, R., Blomberg, N., Sjoblom, K., Karlsson, U., Lindstedt, E. L., and Bamberg, K. (2001). Structure of the PPARα and -γ ligand binding domain in complex with AZ 242; ligand selectivity and agonist activation in the PPAR family. Structure (Camb) *9*, 699-706.

Darimont, B. D., Wagner, R. L., Apriletti, J. W., Stallcup, M. R., Kushner, P. J., Baxter, J. D., Fletterick, R. J., and Yamamoto, K. R. (1998). Structure and specificity of nuclear receptor-coactivator interactions. Genes Dev *12*, 3343-3356.

Desvergne, B., and Wahli, W. (1999). Peroxisome proliferator-activated receptors: nuclear control of metabolism. Endocr Rev *20*, 649-688.

Ding, X. F., Anderson, C. M., Ma, H., Hong, H., Uht, R. M., Kushner, P. J., and Stallcup, M. R. (1998). Nuclear receptor-binding sites of coactivators glucocorticoid receptor interacting protein 1 (GRIP1) and steroid receptor coactivator 1 (SRC-1): multiple motifs with different binding specificities. Mol Endocrinol *12*, 302-313.

Dressel, U., Thormeyer, D., Altincicek, B., Paululat, A., Eggert, M., Schneider, S., Tenbaum, S. P., Renkawitz, R., and Baniahmad, A. (1999). Alien, a highly conserved protein with characteristics of a corepressor for members of the nuclear hormone receptor superfamily. Mol Cell Biol *19*, 3383-3394.

Dreyer, C., Krey, G., Keller, H., Givel, F., Helftenbein, G., and Wahli, W. (1992). Control of the peroxisomal β-oxidation pathway by a novel family of nuclear hormone receptors. Cell *68*, 879-887.

Dussault, I., Lin, M., Hollister, K., Fan, M., Termini, J., Sherman, M. A., and Forman, B. M. (2002). A structural model of the constitutive androstane receptor defines novel interactions that mediate ligand-independent activity. Mol Cell Biol *22*, 5270-5280.

Ebdrup, S., Pettersson, I., Rasmussen, H. B., Deussen, H. J., Frost Jensen, A., Mortensen, S. B., Fleckner, J., Pridal, L., Nygaard, L., and Sauerberg, P. (2003). Synthesis and biological and structural characterization of the dual-acting peroxisome proliferator-activated receptor α/γ agonist ragaglitazar. J Med Chem *46*, 1306-1317.

Eelen, G., Verlinden, L., Rochel, N., Claessens, F., De Clercq, P., Vandewalle, M., Tocchini-Valentini, G., Moras, D., Bouillon, R., and Verstuyf, A. (2005). Superagonistic action of 14-epi-analogs of 1,25-dihydroxyvitamin D explained by vitamin D receptor-coactivator interaction. Mol Pharmacol *67*, 1566-1573.

Ema, M., Ohe, N., Suzuki, M., Mimura, J., Sogawa, K., Ikawa, S., and Fujii-Kuriyama, Y. (1994). Dioxin binding activities of polymorphic forms of mouse and human arylhydrocarbon receptors. J Biol Chem *269*, 27337-27343.

Escriva, H., Safi, R., Hanni, C., Langlois, M. C., Saumitou-Laprade, P., Stehelin, D., Capron, A., Pierce, R., and Laudet, V. (1997). Ligand binding was acquired during evolution of nuclear receptors. Proc Natl Acad Sci U S A *94*, 6803-6808.

Evans, R. M., Barish, G. D., and Wang, Y. X. (2004). PPARs and the complex journey to obesity. Nat Med *10*, 355-361.

Feldman, D., Chen, T., Hirst, M., Colston, K., Karasek, M., and Cone, C. (1980). Demonstration of 1,25-dihydroxyvitamin D_3 receptors in human skin biopsies. J Clin Endocrinol Metab *51*, 1463-1465.

Feng, W., Ribeiro, R. C., Wagner, R. L., Nguyen, H., Apriletti, J. W., Fletterick, R. J., Baxter, J. D., Kushner, P. J., and West, B. L. (1998). Hormone-dependent coactivator binding to a hydrophobic cleft on nuclear receptors. Science *280*, 1747-1749.

Ferguson, S. S., LeCluyse, E. L., Negishi, M., and Goldstein, J. A. (2002). Regulation of human *CYP2C9* by the constitutive androstane receptor: discovery of a new distal binding site. Mol Pharmacol *62*, 737-746.

Forman, B. M., Tontonoz, P., Chen, J., Brun, R. P., Spiegelman, B. M., and Evans, R. M. (1995). 15-Deoxy-$\Delta^{12,14}$-prostaglandin J_2 is a ligand for the adipocyte determination factor PPAR γ. Cell *83*, 803-812.

Frank, C., Molnár, F., Matilainen, M., Lempiäinen, H., and Carlberg, C. (2004). Agonist-dependent and agonist-independent transactivations of the human constitutive androstane receptor are modulated by specific amino acid pairs. J Biol Chem *279*, 33558-33566.

Fu, J., Gaetani, S., Oveisi, F., Lo Verme, J., Serrano, A., Rodriguez De Fonseca, F., Rosengarth, A., Luecke, H., Di Giacomo, B., Tarzia, G., and Piomelli, D. (2003). Oleylethanolamide regulates feeding and body weight through activation of the nuclear receptor PPAR-α. Nature *425*, 90-93.

Fujishima, T., Liu, Z., Miura, D., Chokki, M., Ishizuka, S., Konno, K., and Takayama, H. (1998). Synthesis and biological activity of 2-methyl-20-epi analogues of 1α,25-dihydroxyvitamin D_3. Bioorg Med Chem Lett *8*, 2145-2148.

Gampe, R. T., Jr., Montana, V. G., Lambert, M. H., Miller, A. B., Bledsoe, R. K., Milburn, M. V., Kliewer, S. A., Willson, T. M., and Xu, H. E. (2000). Asymmetry in the PPARγ/RXRα crystal structure reveals the molecular basis of heterodimerization among nuclear receptors. Mol Cell *5*, 545-555.

Gelman, L., Zhou, G., Fajas, L., Raspe, E., Fruchart, J. C., and Auwerx, J. (1999). p300 interacts with the N- and C-terminal part of $PPAR_{\gamma 2}$ in a ligand-independent and -dependent manner, respectively. J Biol Chem *274*, 7681-7688.

Gelmetti, V., Zhang, J., Fanelli, M., Minucci, S., Pelicci, P. G., and Lazar, M. A. (1998). Aberrant recruitment of the nuclear receptor corepressor-histone deacetylase complex by the acute myeloid leukemia fusion partner ETO. Mol Cell Biol *18*, 7185-7191.

Gerbal-Chaloin, S., Daujat, M., Pascussi, J. M., Pichard-Garcia, L., Vilarem, M. J., and Maurel, P. (2002). Transcriptional regulation of *CYP2C9* gene. Role of glucocorticoid receptor and constitutive androstane receptor. J Biol Chem *277*, 209-217.

Glass, C. K., and Rosenfeld, M. G. (2000). The coregulator exchange in transcriptional functions of nuclear receptors. Genes Dev *14*, 121-141.

Grignani, F., De Matteis, S., Nervi, C., Tomassoni, L., Gelmetti, V., Cioce, M., Fanelli, M., Ruthardt, M., Ferrara, F. F., Zamir, I., *et al.* (1998). Fusion proteins of the retinoic

acid receptor-α recruit histone deacetylase in promyelocytic leukaemia. Nature *391*, 815-818.

Guan, H. P., Li, Y., Jensen, M. V., Newgard, C. B., Steppan, C. M., and Lazar, M. A. (2002). A futile metabolic cycle activated in adipocytes by antidiabetic agents. Nat Med *8*, 1122-1128.

Guerre-Millo, M., Gervois, P., Raspe, E., Madsen, L., Poulain, P., Derudas, B., Herbert, J. M., Winegar, D. A., Willson, T. M., Fruchart, J. C., *et al.* (2000). Peroxisome proliferator-activated receptor α activators improve insulin sensitivity and reduce adiposity. J Biol Chem *275*, 16638-16642.

Guidez, F., Ivins, S., Zhu, J., Soderstrom, M., Waxman, S., and Zelent, A. (1998). Reduced retinoic acid-sensitivities of nuclear receptor corepressor binding to PML- and PLZF-RARα underlie molecular pathogenesis and treatment of acute promyelocytic leukemia. Blood *91*, 2634-2642.

Gurnell, M., Wentworth, J. M., Agostini, M., Adams, M., Collingwood, T. N., Provenzano, C., Browne, P. O., Rajanayagam, O., Burris, T. P., Schwabe, J. W., *et al.* (2000). A dominant-negative peroxisome proliferator-activated receptor γ (PPARγ) mutant is a constitutive repressor and inhibits PPARγ-mediated adipogenesis. J Biol Chem *275*, 5754-5759.

Haffner, C. D., Lenhard, J. M., Miller, A. B., McDougald, D. L., Dwornik, K., Ittoop, O. R., Gampe, R. T., Jr., Xu, H. E., Blanchard, S., Montana, V. G., *et al.* (2004). Structure-based design of potent retinoid X receptor α agonists. J Med Chem *47*, 2010-2029.

Hall, J. M., Chang, C., and McDonnell, D. P. (2000). Development of peptide antagonists that target estrogen receptor β-coactivator interactions. Mol Endocrinol *14*, 2010-2023.

Haussler, M. R., and Norman, A. W. (1969). Chromosomal receptor for a vitamin D metabolite. Proc Natl Acad Sci U S A *62*, 155-162.

He, L. Z., Guidez, F., Tribioli, C., Peruzzi, D., Ruthardt, M., Zelent, A., and Pandolfi, P. P. (1998). Distinct interactions of PML-RARα and PLZF-RARα with co-repressors determine differential responses to RA in APL. Nat Genet *18*, 126-135.

Heery, D. M., Kalkhoven, E., Hoare, S., and Parker, M. G. (1997). A signature motif in transcriptional co-activators mediates binding to nuclear receptors. Nature *387*, 733-736.

Herdick, M., and Carlberg, C. (2000). Agonist-triggered modulation of the activated and silent state of the vitamin D_3 receptor by interaction with co-repressors and co-activators. J Mol Biol *304*, 793-801.

Hong, H., Kohli, K., Trivedi, A., Johnson, D. L., and Stallcup, M. R. (1996). GRIP1, a novel mouse protein that serves as a transcriptional coactivator in yeast for the

hormone binding domains of steroid receptors. Proc Natl Acad Sci U S A *93*, 4948-4952.

Hong, S. H., Yang, Z., and Privalsky, M. L. (2001). Arsenic trioxide is a potent inhibitor of the interaction of SMRT corepressor with its transcription factor partners, including the PML-retinoic acid receptor α oncoprotein found in human acute promyelocytic leukemia. Mol Cell Biol *21*, 7172-7182.

Honkakoski, P., and Negishi, M. (1998a). Regulatory DNA elements of phenobarbital-responsive cytochrome P450 *CYP2B* genes. J Biochem Mol Toxicol *12*, 3-9.

Honkakoski, P., Sueyoshi, T., and Negishi, M. (2003). Drug-activated nuclear receptors CAR and PXR. Ann Med *35*, 172-182.

Honkakoski, P., Zelko, I., Sueyoshi, T., and Negishi, M. (1998b). The nuclear orphan receptor CAR-retinoid X receptor heterodimer activates the phenobarbital-responsive enhancer module of the *CYP2B* gene. Mol Cell Biol *18*, 5652-5658.

Hu, X., Li, Y., and Lazar, M. A. (2001). Determinants of CoRNR-dependent repression complex assembly on nuclear hormone receptors. Mol Cell Biol *21*, 1747-1758.

Huang, W., Zhang, J., Wei, P., Schrader, W. T., and Moore, D. D. (2004). Meclizine is an agonist ligand for mouse constitutive androstane receptor (CAR) and an inverse agonist for human CAR. Mol Endocrinol *18*, 2402-2408.

Hörlein, A. J., Näär, A. M., Heinzel, T., Torchia, J., Gloss, B., Kurokawa, R., Ryan, A., Kamei, Y., Soderström, M., Glass, C. K., and et al. (1995). Ligand-independent repression by the thyroid hormone receptor mediated by a nuclear receptor co-repressor. Nature *377*, 397-404.

Ikeda, M., Kawaguchi, A., Takeshita, A., Chin, W. W., Endo, T., and Onaya, T. (1999). CBP-dependent and independent enhancing activity of steroid receptor coactivator-1 in thyroid hormone receptor-mediated transactivation. Mol Cell Endocrinol *147*, 103-112.

Ishizuka, S., Miura, D., Ozono, K., Chokki, M., Mimura, H., and Norman, A. W. (2001). Antagonistic actions *in vivo* of (23S)-25-dehydro-1α-hydroxyvitamin D_3 26,23-lactone on calcium metabolism induced by 1α,25-dihydroxyvitamin D_3. Endocrinology *142*, 59-67.

Ishizuka, T., and Lazar, M. A. (2003). The N-CoR/histone deacetylase 3 complex is required for repression by thyroid hormone receptor. Mol Cell Biol *23*, 5122-5131.

Issemann, I., and Green, S. (1990). Activation of a member of the steroid hormone receptor superfamily by peroxisome proliferators. Nature *347*, 645-650.

Jepsen, K., Hermanson, O., Onami, T. M., Gleiberman, A. S., Lunyak, V., McEvilly, R. J., Kurokawa, R., Kumar, V., Liu, F., Seto, E., *et al.* (2000). Combinatorial roles of the nuclear receptor corepressor in transcription and development. Cell *102*, 753-763.

Juge-Aubry, C. E., Hammar, E., Siegrist-Kaiser, C., Pernin, A., Takeshita, A., Chin, W. W., Burger, A. G., and Meier, C. A. (1999). Regulation of the transcriptional activity of the peroxisome proliferator-activated receptor α by phosphorylation of a ligand-independent trans-activating domain. J Biol Chem *274*, 10505-10510.

Jyrkkärinne, J., Windshügel, B., Mäkinen, J., Ylisirniö, M., Peräkylä, M., Poso, A., Sippl, W., and Honkakoski, P. (2005). Amino acids important for ligand specificity of the human constitutive androstane receptor. J Biol Chem *280*, 5960-5971.

Kallen, J. A., Schlaeppi, J. M., Bitsch, F., Geisse, S., Geiser, M., Delhon, I., and Fournier, B. (2002). X-ray structure of the hRORα LBD at 1.63 A: structural and functional data that cholesterol or a cholesterol derivative is the natural ligand of RORα. Structure (Camb) *10*, 1697-1707.

Kast, H. R., Goodwin, B., Tarr, P. T., Jones, S. A., Anisfeld, A. M., Stoltz, C. M., Tontonoz, P., Kliewer, S., Willson, T. M., and Edwards, P. A. (2002). Regulation of multidrug resistance-associated protein 2 (ABCC2) by the nuclear receptors pregnane X receptor, farnesoid X-activated receptor, and constitutive androstane receptor. J Biol Chem *277*, 2908-2915.

Kato, S., Endoh, H., Masuhiro, Y., Kitamoto, T., Uchiyama, S., Sasaki, H., Masushige, S., Gotoh, Y., Nishida, E., Kawashima, H., *et al.* (1995). Activation of the estrogen receptor through phosphorylation by mitogen-activated protein kinase. Science *270*, 1491-1494.

Kerry, D. M., Dwivedi, P. P., Hahn, C. N., Morris, H. A., Omdahl, J. L., and May, B. K. (1996). Transcriptional synergism between vitamin D-responsive elements in the rat 25-hydroxyvitamin D_3 *24-hydroxylase* (*CYP24*) promoter. J Biol Chem *271*, 29715-29721.

Kersten, S., Seydoux, J., Peters, J. M., Gonzalez, F. J., Desvergne, B., and Wahli, W. (1999). Peroxisome proliferator-activated receptor α mediates the adaptive response to fasting. J Clin Invest *103*, 1489-1498.

Kim, H., Haluzik, M., Asghar, Z., Yau, D., Joseph, J. W., Fernandez, A. M., Reitman, M. L., Yakar, S., Stannard, B., Heron-Milhavet, L., *et al.* (2003). Peroxisome proliferator-activated receptor-α agonist treatment in a transgenic model of type 2 diabetes reverses the lipotoxic state and improves glucose homeostasis. Diabetes *52*, 1770-1778.

Klaholz, B. P., Renaud, J. P., Mitschler, A., Zusi, C., Chambon, P., Gronemeyer, H., and Moras, D. (1998). Conformational adaptation of agonists to the human nuclear receptor RAR γ. Nat Struct Biol *5*, 199-202.

Kleywegt, G. J., and Jones, T. A. (1994). Detection, delineation, measurement and display of cavities in macromolecular structures. Acta Crystallogr D Biol Crystallogr *50*, 178-185.

Kleywegt, G. J., and Jones, T. A. (1996). xdlMAPMAN and xdlDATAMAN - programs for reformatting, analysis and manipulation of biomacromolecular electron-density maps and reflection data sets. Acta Crystallogr D Biol Crystallogr *52*, 826-828.

Kliewer, S. A., Forman, B. M., Blumberg, B., Ong, E. S., Borgmeyer, U., Mangelsdorf, D. J., Umesono, K., and Evans, R. M. (1994). Differential expression and activation of a family of murine peroxisome proliferator-activated receptors. Proc Natl Acad Sci U S A *91*, 7355-7359.

Kohonen, T. (1997). Self-Organizing Maps, In Series in Information Sciences (Heidelberg: Springer).

Koikkalainen, P. (1994). Progress with the tree-structured self-organizing map, In Proceedings of the 11th European Conference on Artificial Intelligence, European Committee for Artificial Intelligence (ECCAI), A. G. Cohn, ed. (New York: Wiley and Sons).

Krylova, I. N., Sablin, E. P., Moore, J., Xu, R. X., Waitt, G. M., MacKay, J. A., Juzumiene, D., Bynum, J. M., Madauss, K., Montana, V., *et al.* (2005). Structural analyses reveal phosphatidyl inositols as ligands for the NR5 orphan receptors SF-1 and LRH-1. Cell *120*, 343-355.

Kubota, N., Terauchi, Y., Miki, H., Tamemoto, H., Yamauchi, T., Komeda, K., Satoh, S., Nakano, R., Ishii, C., Sugiyama, T., *et al.* (1999). PPAR γ mediates high-fat diet-induced adipocyte hypertrophy and insulin resistance. Mol Cell 4, 597-609.

Laskowski, R. A. (2001). PDBsum: summaries and analyses of PDB structures. Nucleic Acids Res *29*, 221-222.

Laskowski, R. A., Luscombe, N. M., Swindells, M. B., and Thornton, J. M. (1996). Protein clefts in molecular recognition and function. Protein Sci *5*, 2438-2452.

Lavinsky, R. M., Jepsen, K., Heinzel, T., Torchia, J., Mullen, T. M., Schiff, R., Del-Rio, A. L., Ricote, M., Ngo, S., Gemsch, J., *et al.* (1998). Diverse signaling pathways modulate nuclear receptor recruitment of N-CoR and SMRT complexes. Proc Natl Acad Sci U S A *95*, 2920-2925.

Lee, S. K., Kim, H. J., Na, S. Y., Kim, T. S., Choi, H. S., Im, S. Y., and Lee, J. W. (1998). Steroid receptor coactivator-1 coactivates activating protein-1-mediated transactivations through interaction with the c-Jun and c-Fos subunits. J Biol Chem *273*, 16651-16654.

Leers, J., Treuter, E., and Gustafsson, J. Å. (1998). Mechanistic principles in NR box-dependent interaction between nuclear hormone receptors and the coactivator TIF2. Mol Cell Biol *18*, 6001-6013.

Lehmann, J. M., Moore, L. B., Smith-Oliver, T. A., Wilkison, W. O., Willson, T. M., and Kliewer, S. A. (1995). An antidiabetic thiazolidinedione is a high affinity ligand for peroxisome proliferator-activated receptor γ (PPAR γ). J Biol Chem *270*, 12953-12956.

Lempiäinen, H., Molnár, F., Macias Gonzalez, M., Peräkylä, M., and Carlberg, C. (2005). Antagonist- and inverse agonist-driven interactions of the vitamin D receptor and the constitutive androstane receptor with corepressor protein. Mol Endocrinol *19*, 2258-2272.

Li, H., and Chen, J. D. (1998). The receptor-associated coactivator 3 activates transcription through CREB-binding protein recruitment and autoregulation. J Biol Chem *273*, 5948-5954.

Li, H., Gomes, P. J., and Chen, J. D. (1997). RAC3, a steroid/nuclear receptor-associated coactivator that is related to SRC-1 and TIF2. Proc Natl Acad Sci U S A *94*, 8479-8484.

Li, Y., Lambert, M. H., and Xu, H. E. (2003). Activation of nuclear receptors: a perspective from structural genomics. Structure (Camb) *11*, 741-746.

Luisi, B. F., Xu, W. X., Otwinowski, Z., Freedman, L. P., Yamamoto, K. R., and Sigler, P. B. (1991). Crystallographic analysis of the interaction of the glucocorticoid receptor with DNA. Nature *352*, 497-505.

Lutterbach, B., Westendorf, J. J., Linggi, B., Patten, A., Moniwa, M., Davie, J. R., Huynh, K. D., Bardwell, V. J., Lavinsky, R. M., Rosenfeld, M. G., *et al.* (1998). ETO, a target of t(8;21) in acute leukemia, interacts with the N-CoR and mSin3 corepressors. Mol Cell Biol *18*, 7176-7184.

Ma, H., Hong, H., Huang, S. M., Irvine, R. A., Webb, P., Kushner, P. J., Coetzee, G. A., and Stallcup, M. R. (1999). Multiple signal input and output domains of the 160-kilodalton nuclear receptor coactivator proteins. Mol Cell Biol *19*, 6164-6173.

Maglich, J. M., Parks, D. J., Moore, L. B., Collins, J. L., Goodwin, B., Billin, A. N., Stoltz, C. A., Kliewer, S. A., Lambert, M. H., Willson, T. M., and Moore, J. T. (2003). Identification of a novel human constitutive androstane receptor (CAR) agonist and its use in the identification of CAR target genes. J Biol Chem *278*, 17277-17283.

Maglich, J. M., Stoltz, C. M., Goodwin, B., Hawkins-Brown, D., Moore, J. T., and Kliewer, S. A. (2002). Nuclear pregnane x receptor and constitutive androstane receptor regulate overlapping but distinct sets of genes involved in xenobiotic detoxification. Mol Pharmacol *62*, 638-646.

Makowski, A., Brzostek, S., Cohen, R. N., and Hollenberg, A. N. (2003). Determination of nuclear receptor corepressor interactions with the thyroid hormone receptor. Mol Endocrinol *17*, 273-286.

Mangelsdorf, D. J., and Evans, R. M. (1995). The RXR heterodimers and orphan receptors. Cell *83*, 841-850.

Mangelsdorf, D. J., Ong, E. S., Dyck, J. A., and Evans, R. M. (1990). Nuclear receptor that identifies a novel retinoic acid response pathway. Nature *345*, 224-229.

McInerney, E. M., Rose, D. W., Flynn, S. E., Westin, S., Mullen, T. M., Krones, A., Inostroza, J., Torchia, J., Nolte, R. T., Assa-Munt, N., *et al.* (1998). Determinants of coactivator LXXLL motif specificity in nuclear receptor transcriptional activation. Genes Dev *12*, 3357-3368.

McKenna, N. J., Lanz, R. B., and O'Malley, B. W. (1999). Nuclear receptor coregulators: cellular and molecular biology. Endocr Rev *20*, 321-344.

Menon, S. T., Han, M., and Sakmar, T. P. (2001). Rhodopsin: structural basis of molecular physiology. Physiol Rev *81*, 1659-1688.

Mi, L. Z., Devarakonda, S., Harp, J. M., Han, Q., Pellicciari, R., Willson, T. M., Khorasanizadeh, S., and Rastinejad, F. (2003). Structural basis for bile acid binding and activation of the nuclear receptor FXR. Mol Cell *11*, 1093-1100.

Misiti, S., Schomburg, L., Yen, P. M., and Chin, W. W. (1998). Expression and hormonal regulation of coactivator and corepressor genes. Endocrinology *139*, 2493-2500.

Miura, D., Manabe, K., Gao, Q., Norman, A. W., and Ishizuka, S. (1999a). 1α,25-dihydroxyvitamin D_3-26,23-lactone analogs antagonize differentiation of human leukemia cells (HL-60 cells) but not of human acute promyelocytic leukemia cells (NB4 cells). FEBS Lett *460*, 297-302.

Miura, D., Manabe, K., Ozono, K., Saito, M., Gao, Q., Norman, A. W., and Ishizuka, S. (1999b). Antagonistic Action of Novel 1α,25-Dihydroxyvitamin D_3-26,23-lactone Analogs on Differentiation of Human Leukemia Cells (HL-60) Induced by 1α,25-Dihydroxyvitamin D_3. J Biol Chem *274*, 16392-16399.

Molnár, F., Matilainen, M., and Carlberg, C. (2005). Structural determinants of the agonist-independent association of human peroxisome proliferator-activated receptors with coactivators. J Biol Chem *280*, 26543-26556.

Moras, D., and Gronemeyer, H. (1998). The nuclear receptor ligand-binding domain: structure and function. Curr Opin Cell Biol *10*, 384-391.

Mäkinen, J., Reinisalo, M., Niemi, K., Viitala, P., Jyrkkarinne, J., Chung, H., Pelkonen, O., and Honkakoski, P. (2003). Dual action of oestrogens on the mouse constitutive androstane receptor. Biochem J *376*, 465-472.

Na, S. Y., Lee, S. K., Han, S. J., Choi, H. S., Im, S. Y., and Lee, J. W. (1998). Steroid receptor coactivator-1 interacts with the p50 subunit and coactivates nuclear factor κB-mediated transactivations. J Biol Chem *273*, 10831-10834.

Nagpal, S., Lu, J., and Boehm, M. F. (2001). Vitamin D analogs: mechanism of action and therapeutic applications. Curr Med Chem *8*, 1661-1679.

Nagy, L., and Schwabe, J. W. (2004). Mechanism of the nuclear receptor molecular switch. Trends Biochem Sci *29*, 317-324.

Nolte, R. T., Wisely, G. B., Westin, S., Cobb, J. E., Lambert, M. H., Kurokawa, R., Rosenfeld, M. G., Willson, T. M., Glass, C. K., and Milburn, M. V. (1998). Ligand binding and co-activator assembly of the peroxisome proliferator- activated receptor-γ. Nature *395*, 137-143.

Norman, A. W., Manchand, P. S., Uskokovic, M. R., Okamura, W. H., Takeuchi, J. A., Bishop, J. E., Hisatake, J. I., Koeffler, H. P., and Peleg, S. (2000). Characterization of a novel analogue of 1α,25(OH)$_2$-vitamin D$_3$ with two side chains: interaction with its nuclear receptor and cellular actions. J Med Chem *43*, 2719-2730.

Oberfield, J. L., Collins, J. L., Holmes, C. P., Goreham, D. M., Cooper, J. P., Cobb, J. E., Lenhard, J. M., Hull-Ryde, E. A., Mohr, C. P., Blanchard, S. G., *et al.* (1999). A peroxisome proliferator-activated receptor γ ligand inhibits adipocyte differentiation. Proc Natl Acad Sci U S A *96*, 6102-6106.

Oliver, W. R., Jr., Shenk, J. L., Snaith, M. R., Russell, C. S., Plunket, K. D., Bodkin, N. L., Lewis, M. C., Winegar, D. A., Sznaidman, M. L., Lambert, M. H., *et al.* (2001). A selective peroxisome proliferator-activated receptor δ agonist promotes reverse cholesterol transport. Proc Natl Acad Sci U S A *98*, 5306-5311.

Ostberg, T., Svensson, S., Selen, G., Uppenberg, J., Thor, M., Sundbom, M., Sydow-Backman, M., Gustavsson, A. L., and Jendeberg, L. (2004). A new class of peroxisome proliferator-activated receptor agonists with a novel binding epitope shows antidiabetic effects. J Biol Chem *279*, 41124-41130.

Ozono, K., Saito, M., Miura, D., Michigami, T., Nakajima, S., and Ishizuka, S. (1999). Analysis of the molecular mechanism for the antagonistic action of a novel 1α,25-dihydroxyvitamin D$_3$ analogue toward vitamin D receptor function. J Biol Chem *274*, 32376-32381.

Oñate, S. A., Tsai, S. Y., Tsai, M. J., and O'Malley, B. W. (1995). Sequence and characterization of a coactivator for the steroid hormone receptor superfamily. Science *270*, 1354-1357.

Paquet, Y., Trottier, E., Beaudet, M. J., and Anderson, A. (2000). Mutational analysis of the *CYP2B2* phenobarbital response unit and inhibitory effect of the constitutive androstane receptor on phenobarbital responsiveness. J Biol Chem *275*, 38427-38436.

Patrone, C., Ma, Z. Q., Pollio, G., Agrati, P., Parker, M. G., and Maggi, A. (1996). Cross-coupling between insulin and estrogen receptor in human neuroblastoma cells. Mol Endocrinol *10*, 499-507.

Peleg, S., Sastry, M., Collins, E. D., Bishop, J. E., and Norman, A. W. (1995). Distinct conformational changes induced by 20-epi analogues of 1 α,25-dihydroxyvitamin D$_3$ are associated with enhanced activation of the vitamin D receptor. J Biol Chem *270*, 10551-10558.

Peraldi, P., Xu, M., and Spiegelman, B. M. (1997). Thiazolidinediones block tumor necrosis factor-α-induced inhibition of insulin signaling. J Clin Invest *100*, 1863-1869.

Perissi, V., Staszewski, L. M., McInerney, E. M., Kurokawa, R., Krones, A., Rose, D. W., Lambert, M. H., Milburn, M. V., Glass, C. K., and Rosenfeld, M. G. (1999). Molecular determinants of nuclear receptor-corepressor interaction. Genes Dev *13*, 3198-3208.

Peräkylä, M., Molnár, F., and Carlberg, C. (2004). A structural basis for the species-specific antagonism of 26,23-lactones on vitamin D signaling. Chem Biol *11*, 1147-1156.

Peters, J. M., Lee, S. S., Li, W., Ward, J. M., Gavrilova, O., Everett, C., Reitman, M. L., Hudson, L. D., and Gonzalez, F. J. (2000). Growth, adipose, brain, and skin alterations resulting from targeted disruption of the mouse peroxisome proliferator-activated receptor β(δ). Mol Cell Biol *20*, 5119-5128.

Petkovich, M., Brand, N. J., Krust, A., and Chambon, P. (1987). A human retinoic acid receptor which belongs to the family of nuclear receptors. Nature *330*, 444-450.

Pike, J. W., and Haussler, M. R. (1980). Characteristics and purification of the intestinal receptor for 1,25-dihydroxyvitamin D. Methods Enzymol *67*, 508-522.

Potter, G. B., Beaudoin, G. M., III, DeRenzo, C. L., Zarach, J. M., Chen, S. H., and Thompson, C. C. (2001). The *hairless* gene mutated in congenital hair loss disorders encodes a novel nuclear receptor corepressor. Genes Dev *15*, 2687-2701.

Rachez, C., Suldan, Z., Ward, J., Chang, C. P., Burakov, D., Erdjument-Bromage, H., Tempst, P., and Freedman, L. P. (1998). A novel protein complex that interacts with the vitamin D_3 receptor in a ligand-dependent manner and enhances VDR transactivation in a cell-free system. Genes Dev *12*, 1787-1800.

Rajala, M. W., Obici, S., Scherer, P. E., and Rossetti, L. (2003). Adipose-derived resistin and gut-derived resistin-like molecule-β selectively impair insulin action on glucose production. J Clin Invest *111*, 225-230.

Reddy, J. K., and Hashimoto, T. (2001). Peroxisomal β-oxidation and peroxisome proliferator-activated receptor α: an adaptive metabolic system. Annu Rev Nutr *21*, 193-230.

Reichle, H., Pfeiffer, U., Wendt, P., and Blumel, G. (1989). Chemiluminescence-inducing radicals in experimental porcine septic shock lung. Prog Clin Biol Res *308*, 339-344.

Renaud, J. P., Rochel, N., Ruff, M., Vivat, V., Chambon, P., Gronemeyer, H., and Moras, D. (1995). Crystal structure of the RAR-γ ligand-binding domain bound to all-trans retinoic acid. Nature *378*, 681-689.

Repa, J. J., and Mangelsdorf, D. J. (2000). The role of orphan nuclear receptors in the regulation of cholesterol homeostasis. Annu Rev Cell Dev Biol *16*, 459-481.

Robinson-Rechavi, M., Carpentier, A. S., Duffraisse, M., and Laudet, V. (2001). How many nuclear hormone receptors are there in the human genome? Trends Genet *17*, 554-556.

Rochel, N., Wurtz, J. M., Mitschler, A., Klaholz, B., and Moras, D. (2000). The crystal structure of the nuclear receptor for vitamin D bound to its natural ligand. Mol Cell *5*, 173-179.

Rochette-Egly, C., Adam, S., Rossignol, M., Egly, J. M., and Chambon, P. (1997). Stimulation of RAR α activation function AF-1 through binding to the general transcription factor TFIIH and phosphorylation by CDK7. Cell *90*, 97-107.

Rochette-Egly, C., Gaub, M. P., Lutz, Y., Ali, S., Scheuer, I., and Chambon, P. (1992). Retinoic acid receptor-β: immunodetection and phosphorylation on tyrosine residues. Mol Endocrinol *6*, 2197-2209.

Rosen, E. D., Sarraf, P., Troy, A. E., Bradwin, G., Moore, K., Milstone, D. S., Spiegelman, B. M., and Mortensen, R. M. (1999). PPARγ is required for the differentiation of adipose tissue *in vivo* and *in vitro*. Mol Cell *4*, 611-617.

Rosen, E. D., Walkey, C. J., Puigserver, P., and Spiegelman, B. M. (2000). Transcriptional regulation of adipogenesis. Genes Dev *14*, 1293-1307.

Sammon, J. W. (1969). A nonlinear mapping for data structure analysis. IEEE Transactions on Computers *C-18*, 401-409.

Sanger, F., Nicklen, S., and Coulson, A. R. (1977). DNA sequencing with chain-terminating inhibitors. Proc Natl Acad Sci U S A *74*, 5463-5467.

Sap, J., Munoz, A., Damm, K., Goldberg, Y., Ghysdael, J., Leutz, A., Beug, H., and Vennstrom, B. (1986). The c-erb-A protein is a high-affinity receptor for thyroid hormone. Nature *324*, 635-640.

Sauerberg, P., Pettersson, I., Jeppesen, L., Bury, P. S., Mogensen, J. P., Wassermann, K., Brand, C. L., Sturis, J., Woldike, H. F., Fleckner, J., *et al.* (2002). Novel tricyclic-α-alkyloxyphenylpropionic acids: dual PPARα/γ agonists with hypolipidemic and antidiabetic activity. J Med Chem *45*, 789-804.

Schmidt, A., Endo, N., Rutledge, S. J., Vogel, R., Shinar, D., and Rodan, G. A. (1992). Identification of a new member of the steroid hormone receptor superfamily that is activated by a peroxisome proliferator and fatty acids. Mol Endocrinol *6*, 1634-1641.

Schwabe, J. W., Chapman, L., Finch, J. T., and Rhodes, D. (1993). The crystal structure of the estrogen receptor DNA-binding domain bound to DNA: how receptors discriminate between their response elements. Cell *75*, 567-578.

Shaffer, P. L., and Gewirth, D. T. (2002). Structural basis of VDR-DNA interactions on direct repeat response elements. Embo J *21*, 2242-2252.

Shan, L., Vincent, J., Brunzelle, J. S., Dussault, I., Lin, M., Ianculescu, I., Sherman, M. A., Forman, B. M., and Fernandez, E. J. (2004). Structure of the murine constitutive androstane receptor complexed to androstenol: a molecular basis for inverse agonism. Mol Cell *16*, 907-917.

Shao, D., Rangwala, S. M., Bailey, S. T., Krakow, S. L., Reginato, M. J., and Lazar, M. A. (1998). Interdomain communication regulating ligand binding by PPAR-γ. Nature *396*, 377-380.

Sher, T., Yi, H. F., McBride, O. W., and Gonzalez, F. J. (1993). cDNA cloning, chromosomal mapping, and functional characterization of the human peroxisome proliferator activated receptor. Biochemistry *32*, 5598-5604.

Shiau, A. K., Barstad, D., Loria, P. M., Cheng, L., Kushner, P. J., Agard, D. A., and Greene, G. L. (1998). The structural basis of estrogen receptor/coactivator recognition and the antagonism of this interaction by tamoxifen. Cell *95*, 927-937.

Shulman, A. I., Larson, C., Mangelsdorf, D. J., and Ranganathan, R. (2004). Structural determinants of allosteric ligand activation in RXR heterodimers. Cell *116*, 417-429.

Sluder, A. E., and Maina, C. V. (2001). Nuclear receptors in nematodes: themes and variations. Trends Genet *17*, 206-213.

Stehlin, C., Wurtz, J. M., Steinmetz, A., Greiner, E., Schüle, R., Moras, D., and Renaud, J. P. (2001). X-ray structure of the orphan nuclear receptor RORβ ligand-binding domain in the active conformation. Embo J *20*, 5822-5831.

Stehlin-Gaon, C., Willmann, D., Zeyer, D., Sanglier, S., Van Dorsselaer, A., Renaud, J. P., Moras, D., and Schüle, R. (2003). All-trans retinoic acid is a ligand for the orphan nuclear receptor RORβ. Nat Struct Biol *10*, 820-825.

Steinmetz, A. C., Renaud, J. P., and Moras, D. (2001). Binding of ligands and activation of transcription by nuclear receptors. Annu Rev Biophys Biomol Struct *30*, 329-359.

Steppan, C. M., Bailey, S. T., Bhat, S., Brown, E. J., Banerjee, R. R., Wright, C. M., Patel, H. R., Ahima, R. S., and Lazar, M. A. (2001). The hormone resistin links obesity to diabetes. Nature *409*, 307-312.

Sueyoshi, T., Kawamoto, T., Zelko, I., Honkakoski, P., and Negishi, M. (1999). The repressed nuclear receptor CAR responds to phenobarbital in activating the human *CYP2B6* gene. J Biol Chem *274*, 6043-6046.

Sueyoshi, T., and Negishi, M. (2001). Phenobarbital response elements of cytochrome P450 genes and nuclear receptors. Annu Rev Pharmacol Toxicol *41*, 123-143.

Sugatani, J., Kojima, H., Ueda, A., Kakizaki, S., Yoshinari, K., Gong, Q. H., Owens, I. S., Negishi, M., and Sueyoshi, T. (2001). The phenobarbital response enhancer module in the human bilirubin *UDP-glucuronosyltransferase UGT1A1* gene and regulation by the nuclear receptor CAR. Hepatology *33*, 1232-1238.

Suino, K., Peng, L., Reynolds, R., Li, Y., Cha, J. Y., Repa, J. J., Kliewer, S. A., and Xu, H. E. (2004). The nuclear xenobiotic receptor CAR: structural determinants of constitutive activation and heterodimerization. Mol Cell *16*, 893-905.

Tagami, T., Madison, L. D., Nagaya, T., and Jameson, J. L. (1997). Nuclear receptor corepressors activate rather than suppress basal transcription of genes that are negatively regulated by thyroid hormone. Mol Cell Biol *17*, 2642-2648.

Takada, I., Yu, R. T., Xu, H. E., Lambert, M. H., Montana, V. G., Kliewer, S. A., Evans, R. M., and Umesono, K. (2000). Alteration of a single amino acid in peroxisome proliferator-activated receptor-α (PPARα) generates a PPARδ phenotype. Mol Endocrinol *14*, 733-740.

Takeshita, A., Yen, P. M., Misiti, S., Cardona, G. R., Liu, Y., and Chin, W. W. (1996). Molecular cloning and properties of a full-length putative thyroid hormone receptor coactivator. Endocrinology *137*, 3594-3597.

Takeyama, K., Masuhiro, Y., Fuse, H., Endoh, H., Murayama, A., Kitanaka, S., Suzawa, M., Yanagisawa, J., and Kato, S. (1999). Selective interaction of vitamin D receptor with transcriptional coactivators by a vitamin D analog. Mol Cell Biol *19*, 1049-1055.

Taneja, R., Rochette-Egly, C., Plassat, J. L., Penna, L., Gaub, M. P., and Chambon, P. (1997). Phosphorylation of activation functions AF-1 and AF-2 of RARα and RARγ is indispensable for differentiation of F9 cells upon retinoic acid and cAMP treatment. Embo J *16*, 6452-6465.

The NR nomenclature committee (1999). A unified nomenclature system for the nuclear receptor superfamily. Cell *97*, 161-163.

Tirona, R. G., Leake, B. F., Podust, L. M., and Kim, R. B. (2004). Identification of amino acids in rat pregnane X receptor that determine species-specific activation. Mol Pharmacol *65*, 36-44.

Tocchini-Valentini, G., Rochel, N., Wurtz, J. M., Mitschler, A., and Moras, D. (2001). Crystal structures of the vitamin D receptor complexed to superagonist 20-epi ligands. Proc Natl Acad Sci U S A *98*, 5491-5496.

Tocchini-Valentini, G., Rochel, N., Wurtz, J. M., and Moras, D. (2004). Crystal structures of the vitamin D nuclear receptor liganded with the vitamin D side chain analogues calcipotriol and seocalcitol, receptor agonists of clinical importance. Insights into a structural basis for the switching of calcipotriol to a receptor antagonist by further side chain modification. J Med Chem *47*, 1956-1961.

Toell, A., Gonzalez, M. M., Ruf, D., Steinmeyer, A., Ishizuka, S., and Carlberg, C. (2001). Different molecular mechanisms of vitamin D_3 receptor antagonists. Mol Pharmacol *59*, 1478-1485.

Tontonoz, P., Hu, E., and Spiegelman, B. M. (1994). Stimulation of adipogenesis in fibroblasts by PPARγ_2, a lipid-activated transcription factor. Cell *79*, 1147-1156.

Torchia, J., Rose, D. W., Inostroza, J., Kamei, Y., Westin, S., Glass, C. K., and Rosenfeld, M. G. (1997). The transcriptional co-activator p/CIP binds CBP and mediates nuclear-receptor function. Nature *387*, 677-684.

Tsai, C. C., Kao, H. Y., Yao, T. P., McKeown, M., and Evans, R. M. (1999). SMRTER, a *Drosophila* nuclear receptor coregulator, reveals that EcR-mediated repression is critical for development. Mol Cell *4*, 175-186.

Ueda, A., Kakizaki, S., Negishi, M., and Sueyoshi, T. (2002). Residue threonine 350 confers steroid hormone responsiveness to the mouse nuclear orphan receptor CAR. Mol Pharmacol *61*, 1284-1288.

Umesono, K., Murakami, K. K., Thompson, C. C., and Evans, R. M. (1991). Direct repeats as selective response elements for the thyroid hormone, retinoic acid, and vitamin D_3 receptors. Cell *65*, 1255-1266.

Uppenberg, J., Svensson, C., Jaki, M., Bertilsson, G., Jendeberg, L., and Berkenstam, A. (1998). Crystal structure of the ligand binding domain of the human nuclear receptor PPARγ. J Biol Chem *273*, 31108-31112.

Uskokovic, M. R., Manchand, P. S., Peleg, S., and Norman, A. W. (1997). Synthesis and preliminary evaluation of the biological properties of a 1α,25-dihydroxyvitamin D_3 analog with two side-chains. Proceedings of the 10th International Vitamin D Workshop *May 24*, 19–21.

Vieth, R. (1990). The mechanisms of vitamin D toxicity. Bone Miner *11*, 267-272.

Voegel, J. J., Heine, M. J., Zechel, C., Chambon, P., and Gronemeyer, H. (1996). TIF2, a 160 kDa transcriptional mediator for the ligand-dependent activation function AF-2 of nuclear receptors. Embo J *15*, 3667-3675.

Väisänen, S., Peräkylä, M., Kärkkäinen, J. I., Steinmeyer, A., and Carlberg, C. (2002). Critical role of helix 12 of the vitamin D_3 receptor for the partial agonism of carboxylic ester antagonists. J Mol Biol *315*, 229-238.

Wang, H., Faucette, S., Sueyoshi, T., Moore, R., Ferguson, S., Negishi, M., and LeCluyse, E. L. (2003a). A novel distal enhancer module regulated by pregnane X receptor/constitutive androstane receptor is essential for the maximal induction of *CYP2B6* gene expression. J Biol Chem *278*, 14146-14152.

Wang, J., Hoshino, T., Redner, R. L., Kajigaya, S., and Liu, J. M. (1998). ETO, fusion partner in t(8;21) acute myeloid leukemia, represses transcription by interaction with the human N-CoR/mSin3/HDAC1 complex. Proc Natl Acad Sci U S A *95*, 10860-10865.

Wang, Y. X., Lee, C. H., Tiep, S., Yu, R. T., Ham, J., Kang, H., and Evans, R. M. (2003b). Peroxisome-proliferator-activated receptor δ activates fat metabolism to prevent obesity. Cell *113*, 159-170.

Wang, Z., Benoit, G., Liu, J., Prasad, S., Aarnisalo, P., Liu, X., Xu, H., Walker, N. P., and Perlmann, T. (2003c). Structure and function of Nurr1 identifies a class of ligand-independent nuclear receptors. Nature *423*, 555-560.

Weatherman, R. V., Fletterick, R. J., and Scanlan, T. S. (1999). Nuclear-receptor ligands and ligand-binding domains. Annu Rev Biochem *68*, 559-581.

Webb, P., Anderson, C. M., Valentine, C., Nguyen, P., Marimuthu, A., West, B. L., Baxter, J. D., and Kushner, P. J. (2000). The nuclear receptor corepressor (N-CoR) contains three isoleucine motifs (I/LXXII) that serve as receptor interaction domains (IDs). Mol Endocrinol *14*, 1976-1985.

Webb, P., Nguyen, P., Shinsako, J., Anderson, C., Feng, W., Nguyen, M. P., Chen, D., Huang, S. M., Subramanian, S., McKinerney, E., *et al.* (1998). Estrogen receptor activation function 1 works by binding p160 coactivator proteins. Mol Endocrinol *12*, 1605-1618.

Wei, P., Zhang, J., Egan-Hafley, M., Liang, S., and Moore, D. D. (2000). The nuclear receptor CAR mediates specific xenobiotic induction of drug metabolism. Nature *407*, 920-923.

Weinberger, C., Thompson, C. C., Ong, E. S., Lebo, R., Gruol, D. J., and Evans, R. M. (1986). The *c-erb-A* gene encodes a thyroid hormone receptor. Nature *324*, 641-646.

Wisely, G. B., Miller, A. B., Davis, R. G., Thornquest, A. D., Jr., Johnson, R., Spitzer, T., Sefler, A., Shearer, B., Moore, J. T., Miller, A. B., *et al.* (2002). Hepatocyte nuclear factor 4 is a transcription factor that constitutively binds fatty acids. Structure (Camb) *10*, 1225-1234.

Wärnmark, A., Treuter, E., Wright, A. P., and Gustafsson, J. Å. (2003). Activation functions 1 and 2 of nuclear receptors: molecular strategies for transcriptional activation. Mol Endocrinol *17*, 1901-1909.

Xu, H. E., Lambert, M. H., Montana, V. G., Parks, D. J., Blanchard, S. G., Brown, P. J., Sternbach, D. D., Lehmann, J. M., Wisely, G. B., Willson, T. M., *et al.* (1999). Molecular recognition of fatty acids by peroxisome proliferator- activated receptors. Mol Cell *3*, 397-403.

Xu, H. E., Lambert, M. H., Montana, V. G., Plunket, K. D., Moore, L. B., Collins, J. L., Oplinger, J. A., Kliewer, S. A., Gampe, R. T., Jr., McKee, D. D., *et al.* (2001). Structural determinants of ligand binding selectivity between the peroxisome proliferator-activated receptors. Proc Natl Acad Sci U S A *98*, 13919-13924.

Xu, H. E., Stanley, T. B., Montana, V. G., Lambert, M. H., Shearer, B. G., Cobb, J. E., McKee, D. D., Galardi, C. M., Plunket, K. D., Nolte, R. T., *et al.* (2002). Structural basis for antagonist-mediated recruitment of nuclear co-repressors by PPARα. Nature *415*, 813-817.

Xu, L., Lavinsky, R. M., Dasen, J. S., Flynn, S. E., McInerney, E. M., Mullen, T. M., Heinzel, T., Szeto, D., Korzus, E., Kurokawa, R., *et al.* (1998). Signal-specific co-activator domain requirements for Pit-1 activation. Nature *395*, 301-306.

Xu, R. X., Lambert, M. H., Wisely, B. B., Warren, E. N., Weinert, E. E., Waitt, G. M., Williams, J. D., Collins, J. L., Moore, L. B., Willson, T. M., and Moore, J. T. (2004). A structural basis for constitutive activity in the human CAR/RXRα heterodimer. Mol Cell *16*, 919-928.

Yamauchi, T., Kamon, J., Waki, H., Murakami, K., Motojima, K., Komeda, K., Ide, T., Kubota, N., Terauchi, Y., Tobe, K., *et al.* (2001). The mechanisms by which both heterozygous peroxisome proliferator-activated receptor γ (PPARγ) deficiency and PPARγ agonist improve insulin resistance. J Biol Chem *276*, 41245-41254.

Yanagisawa, J., Yanagi, Y., Masuhiro, Y., Suzawa, M., Watanabe, M., Kashiwagi, K., Toriyabe, T., Kawabata, M., Miyazono, K., and Kato, S. (1999). Convergence of transforming growth factor-β and vitamin D signaling pathways on SMAD transcriptional coactivators. Science *283*, 1317-1321.

Yoh, S. M., Chatterjee, V. K., and Privalsky, M. L. (1997). Thyroid hormone resistance syndrome manifests as an aberrant interaction between mutant T_3 receptors and transcriptional corepressors. Mol Endocrinol *11*, 470-480.

Young, M. A., Gonfloni, S., Superti-Furga, G., Roux, B., and Kuriyan, J. (2001). Dynamic coupling between the SH2 and SH3 domains of c-Src and Hck underlies their inactivation by C-terminal tyrosine phosphorylation. Cell *105*, 115-126.

Zamir, I., Dawson, J., Lavinsky, R. M., Glass, C. K., Rosenfeld, M. G., and Lazar, M. A. (1997). Cloning and characterization of a corepressor and potential component of the nuclear hormone receptor repression complex. Proc Natl Acad Sci U S A *94*, 14400-14405.

Zamir, I., Harding, H. P., Atkins, G. B., Hörlein, A., Glass, C. K., Rosenfeld, M. G., and Lazar, M. A. (1996). A nuclear hormone receptor corepressor mediates transcriptional silencing by receptors with distinct repression domains. Mol Cell Biol *16*, 5458-5465.

Zierold, C., Darwish, H. M., and DeLuca, H. F. (1995). Two vitamin D response elements function in the rat 1,25-dihydroxyvitamin D *24-hydroxylase* promoter. J Biol Chem *270*, 1675-1678.

Appendix: Original publications

Kuopio University Publications C. Natural and Environmental Sciences

C 173. Tarvainen, Mika. Estimation Methods for Nonstationary Biosignals.
2004. 138 p. Acad. Diss.

C 174. Yppärilä, Heidi. Depth of sedation in intensive care patients. A neuropsysiological study.
2004. 104 p. Acad. Diss.

C 175. Sohlberg, Antti. Molecular small animal imaging with pinhole single-photon emission computed tomography.
2004. 104 p. Acad. Diss.

C 176. Kumlin, Timo. Studies on cancer-related effects of 50 Hz magnetic fields.
2004. 64 p. Acad. Diss.

C 177. Seppänen, Kari. Does mercury promote lipid peroxidation?: in vivo and in vitro studies concerning mercury and selenium in lipid peroxidation and coronary heart disease.
2004. 49 p. Acad. Diss.

C 178. Riikonen, Johanna. Modification of the growth, photosynthesis and leaf structure of silver birch by elevated CO2 and O3.
2004. 126 p. Acad. Diss.

C 179. Frank, Christian. Functional profiling of the xenobiotic nuclear receptors CAR and PXR.
2004. 87 p. Acad. Diss.

C 180. Rytkönen, Esko. High-frequency vibration and noise in dentistry.
2005. 80 p. Acad. Diss.

C 181. Seppänen, Aku. State estimation in process tomography.
2005. 117 p. Acad. Diss.

C 182. Ibrahim, Mohamed Ahmed. Plant essential oils as plant protectants and growth activators.
2005. 143 p. Acad. Diss.

C 183. Vuorinen, Terhi. Induced volatile emissions of plants under elevated carbon dioxide and ozone concentrations, and impacts on indirect antiherbivore defence.
2005. 98 p. Acad. Diss.

C 184. Savinainen, Juha. Optimized methods to determine ligand activities at the cannabinoid CB1 and CB2 receptors.
2005. 83 p. Acad. Diss.

C 185. Luomala, Eeva-Maria. Photosynthesis, chemical composition and anatomy of Scots pine and Norway spruce needles under elevated atmospheric CO2 concentration and temperature.
2005. 137 p. Acad. Diss.

C 186. Heikkinen, Lasse M. Statistical estimation methods for electrical pricess tomography.
2005. 147 p. Acad. Diss.

C 187. Riihinen, Kaisu. Phenolic compounds in berries.
2005. 97 p. Acad. Diss.